

AD-A100 028

UTAH UNIV SALT LAKE CITY
BEHAVIORAL AND BIOLOGICAL EFFECTS OF RESONANT ELECTROMAGNETIC A-ETC(U)
NOV 76 O P GANDHI, J. A D'ANDREA, M J HAGMANN DAMD17-74-C-8092

NL

UNCLASSIFIED

1 of 2
AD-A10028



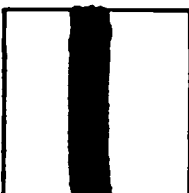
AD A100028

DTIC ACCESSION NUMBER



LEVEL

UTAH UNIV., SALT LAKE CITY



INVENTORY

BEHAVIORAL AND BIOLOGICAL EFFECTS OF RESONANT ELECTROMAGNETIC
ABSORPTION IN RATS. ANNUAL PROGRESS REPT. NO. 2.1974 - 1976.
NOV. 76 CONTRACT DAMD17-74-C-4092 ✓

DOCUMENT IDENTIFICATION

DISTRIBUTION STATEMENT A

Approved for public release
Distribution Unlimited

DISTRIBUTION STATEMENT

ACCESSION FOR

NTIS GRA&I

DTIC TAB

UNANNOUNCED

JUSTIFICATION



BY

**DISTRIBUTION /
AVAILABILITY CODES**

DIST

AVAIL AND/OR SPECIAL

A

DISTRIBUTION STAMP

DTIC
ELECTED
S JUN 10 1981 D
D

DATE ACCESSIONED

DATE RECEIVED IN DTIC

PHOTOGRAPH THIS SHEET AND RETURN TO DTIC-DDA-2

AD A100028

AD

BEHAVIORAL AND BIOLOGICAL EFFECTS OF RESONANT
ELECTROMAGNETIC ABSORPTION IN RATS

ANNUAL REPORT NO. 2

Om P. Gandhi
John A. D'Andrea
Mark J. Hagmann
James L. Lords
Kazem Sedigh

November 1976

Supported by
U. S. Army Medical Research and Development Command
Washington, D. C. 20314

Contract No. DAMD 17-74-C-4092

University of Utah
Salt Lake City, Utah 84112

DDC DISTRIBUTION STATEMENT

Approved for public release; distribution unlimited.

The findings in this report are not to be construed as
an official Department of the Army position unless so
designated by other authorized documents.

81 6 05 019

SECURITY CLASSIFICATION OF THIS PAGE (When Data Entered)

REPORT DOCUMENTATION PAGE		READ INSTRUCTIONS BEFORE COMPLETING FORM
1. REPORT NUMBER	2. GOVT ACCESSION NO.	3. RECIPIENT'S CATALOG NUMBER
4. TITLE (and Subtitle) Behavioral and Biological Effects of Resonant Electromagnetic Absorption in Rats		5. TYPE OF REPORT & PERIOD COVERED Annual Progress Report 1974-1976
7. AUTHOR(S) Om P. Gandhi, John A. D'Andrea, Mark J. Hagmann, James L. Lords, Kazem Sedigh		6. PERFORMING ORG. REPORT NUMBER DAMD 17-74-C-4092
9. PERFORMING ORGANIZATION NAME AND ADDRESS University of Utah Salt Lake City, Utah 84112		10. PROGRAM ELEMENT, PROJECT, TASK AREA & WORK UNIT NUMBERS 62758A 3A762758A824.02.012
11. CONTROLLING OFFICE NAME AND ADDRESS U.S. Army Medical Research and Development Command, Washington, D. C. 20314		12. REPORT DATE November 1976
14. MONITORING AGENCY NAME & ADDRESS (If different from Controlling Office)		13. NUMBER OF PAGES 146 15. SECURITY CLASS. (of this report) Unclassified 15a. DECLASSIFICATION/DOWNGRADING SCHEDULE
16. DISTRIBUTION STATEMENT (of this Report) Approved for public release; distribution unlimited.		
17. DISTRIBUTION STATEMENT (of the abstract entered in Block 20, If different from Report)		
18. SUPPLEMENTARY NOTES		
19. KEY WORDS (Continue on reverse side if necessary and identify by block number) Electromagnetic deposition and its distribution for man, free space irradiation, ground and reflector effects, peak absorption frequencies, simulation of man for 23-550 MHz, biological phantom materials to simulate tissue properties, monopole-above-ground radiation chamber, design of a waveguide slot array for constant radiation intensity, behavioral experiments with		
20. ABSTRACT (Continue on reverse side if necessary and identify by block number) Past experiments of this project utilizing three separate and distinct radiation facilities have determined the whole body and distribution within the body of resonant electromagnetic power absorption for both man models and laboratory rodents. The absorption of such energy is reliably determined by both the frequency of radiation and the orientation of the model or rodent in electromagnetic energy fields. For an ungrounded 1.75 m tall man, power absorption has been determined for $E \parallel L$, using scaled-down models, for the 23 to 570 MHz band with resonant power absorption at 62-68 MHz. Power absorption		

19. (continued)

laboratory rats, time to work stoppage at different frequencies.

20. (continued)

for the laboratory rat has been determined for the 300-800 MHz band with resonant absorption being at 600 MHz for the $E \parallel \hat{L}$ orientation. At respective resonance frequencies in the $E \parallel \hat{L}$ orientation for both man and laboratory rodent, maximum power absorption is found in the neck region of the body. For a grounded 1.75 m tall man, the resonance region shifts to approximately one-half the free space resonance or 30-34 MHz. Man models or laboratory rats placed in proximity of metallic reflecting surfaces experience considerably enhanced electromagnetic energy depositions. Behavioral experiments with laboratory rats have shown that frequency of radiation and animal orientation in the fields are highly significant parameters in determining electromagnetic energy absorption and consequential disruption of behavioral performance.

FOREWORD

In conducting the research described in this report, the investigators adhered to the "Guide of Laboratory Animal Facilities and Care" as promulgated by the Committee on the Guide for Laboratory Animal Resources, National Academy of Sciences, National Research Council.

TABLE OF CONTENTS

	<u>Page</u>
Foreword	ii
List of Figures and Tables	iv
Abstract	1
Objective	2
Highlights of the Work Done During the Last Year	2
Papers Published or Presented, Meetings Attended	53
Papers in Preparation	54
References	56
Appendix A: "Biological Phantom Materials for Simulating Man at Different Frequencies"	
Appendix B: "Distribution of Electromagnetic Energy Deposition in Models of Man with Frequencies Near Resonance"	
Appendix C: "Electromagnetic Power Deposition in Man and Animals with and without Ground and Reflector Effects"	
Appendix D: "Radiators for Microwave Biological Effects Research -- Waveguide Slot Array with constant Radiation Intensity"	
Appendix E: "Upper Bound on Cell Size for Moment-Method Solutions of Dielectric Scatterers"	
Appendix F: "Procedures for Improving Convergence of Moment-Method Solutions in Electromagnetics"	
Appendix G: "Behavioral Effects of Resonant Electromagnetic Power Absorption in Rats"	

LIST OF FIGURES AND TABLES

<u>Figure</u>	<u>Page</u>
1 A photograph of the monopole-above-ground radiation chamber	4
2 Calculated pattern of a monopole-above-ground radiator in a 45° corner reflector for $h/\lambda = 0.25$, $d/\lambda = 0.675$.	7
3 (a) Measured field variation in the E-plane at 350 MHz. $P = 50$ W, $h/\lambda = 0.25$, $d/\lambda = 0.675$, $Z = 2.15$ m (fields normalized relative to 11.0 mW/cm 2)	10
(b) Measured field variation in the H-plane at 350 MHz. $P = 50$ W, $h/\lambda = 0.25$, $d/\lambda = 0.675$, $Z = 2.15$ m (fields normalized relative to 11.0 mW/cm 2)	11
4 (a) Measured field variation in the H-plane at 600 MHz. $P = 50$ W, $h/\lambda = 0.25$, $d/\lambda = 0.675$, $Z = 2.15$ m (fields normalized relative to 10.6 mW/cm 2)	12
(b) Measured field variation in the H-plane at 600 MHz. $P = 50$ W, $h/\lambda = 0.25$, $d/\lambda = 0.675$, $Z = 2.15$ m (fields normalized relative to 10.6 mW/cm 2)	13
5 Whole body absorbed power density and relative absorption coefficient S for humans for electric field polarized along the major length L of the body ($\vec{E} \parallel \hat{L}$ orientation)	15
6 Whole body absorbed power density for humans for $\vec{H} \parallel \hat{L}$ and $\vec{k} \parallel \hat{L}$ orientations. Free space radiation (no ground effects)	16
7 Projected values of whole body absorbed power density for different size rats and mice without ground effects ($L/2b = 3.25$ where $2\pi b$ is the "average" circumference of the animals)	20
8 Projected SAR in a human of height L_m (in meters) with feet touching ground. (For each of the points shown on the graph, three measurements were taken. The average of nine measurements gives the peak value for the 8" size at $L/\lambda = 0.2$.)	21
9 Time to convulsion of 400 gm rats for 10 and 20 mW/cm 2 incident fields at different frequencies. (Animals placed $d = 0.4 \lambda$ from a 90° corner of reflecting surfaces.)	27

FigurePage

10	Time to rise in temperature of 100 gm rats at 400 MHz (10 mW/cm ²)	28
11	Photographs of two rat holders	30
12	Photographs of two rat holders that should be "relatively transparent" to microwaves of $\vec{E} \parallel \hat{L}$ polarization.	37
13	Plexiglas rat holder	38
14	Plexiglas rat holder with response lever and pellet tube	39
15	Rat colonic temperature rise during irradiation at 400, 500, 600, and 700 MHz (10 mW/cm ²)	42
16	T_4 levels of control and UHF radiated rats	46
17	Thyroxine (T_4) response to 600 MHz radiation. (Standard deviations are not shown overlapping.)	48
18	Thyroxine (T_4) response to 600 MHz radiation. (Standard deviations are not shown overlapping.)	51

Table

1	Forty-five degree corner reflector monopole-above-ground antenna	5
2	Monopole-above-ground radiator in a 45° corner reflector. Angular widths for different values of field deviation relative to maximum	8
3	Some measured parameters of the man models used for experiments	14
4	Total power deposited in man and animals at 10 mW/cm ²	24
5	Comparison of the whole-body-average "ungrounded" SAR at resonance with and without reflectors	31
6	Comparison of the whole-body-average "grounded" SAR at resonance with and without reflectors	32
7	Energy absorption in 400-gram Long Evans rats	41

<u>Table</u>		<u>Page</u>
8	Average weekly temperature rise during irradiation and sham irradiation	44
9	Average colonic temperature rise during radiation and sham irradiation	49
10	Average colonic temperature rise during radiation and sham irradiation	49

BEHAVIORAL AND BIOLOGICAL EFFECTS OF RESONANT
ELECTROMAGNETIC POWER ABSORPTION IN RATS

Abstract

Past experiments of this project utilizing three separate and distinct radiation facilities have determined the whole body and distribution within the body of resonant electromagnetic power absorption for both man models and laboratory rodents. The absorption of such energy is reliably determined by both the frequency of radiation and the orientation of the model or rodent in electromagnetic energy fields. For an ungrounded 1.75 m tall man, power absorption has been determined for $\vec{E} \parallel \hat{L}$, using scaled-down models, for the 23 to 570 MHz band with resonant power absorption at 62-68 MHz. Power absorption for the laboratory rat has been determined for the 300-800 MHz band with resonant absorption being at 600 MHz for the $\vec{E} \parallel \hat{L}$ orientation. At respective resonance frequencies in the $\vec{E} \parallel \hat{L}$ orientation for both man and laboratory rodent, maximum power absorption is found in the neck region of the body. For a grounded 1.75 m tall man, the resonance region shifts to approximately one-half the free space resonance or 30-34 MHz. Man models or laboratory rats placed in proximity of metallic reflecting surfaces experience considerably enhanced electromagnetic energy depositions. Behavioral experiments with laboratory rats have shown that frequency of radiation and animal orientation in the fields are highly significant parameters in determining electromagnetic energy absorption and consequential disruption of behavioral performance.

Objective

The objectives of the project are:

- a. To quantify the electromagnetic power absorption and its distribution for man when subjected to radiation at different frequencies and under various exposure conditions.
- b. To verify the important observations of (a) by exposure of living organisms.

The experiments for man are performed with reduced scale models filled with biological-phantom materials which simulate the electromagnetic properties of human tissue. The animal experiments consist of behavioral and biological effects of electromagnetic power absorption in rats.

The purpose of the project is to develop an understanding that would lead to projections for humans.

Highlights of the Work Done During the Last Year

1. The parallel plate radiation chamber was used to determine the distribution of energy deposition for various parts of the body for different sizes of biological phantom figurines. This work is detailed in Quarterly Report No. 4. The highlights of the results are:

- a. Maximum rate of energy deposition is observed for the neck for $\vec{E} \parallel \vec{L}$ resonance and near-resonance conditions. For this region, an energy deposition of nearly 12 times the whole body average is observed. The pattern of energy

deposition is very similar to that obtained from free space irradiation experiments. The higher rate of energy deposition of 28 times the whole body average observed for the neck region for free space experiments is ascribed to the larger power densities of 100 mW/cm^2 used there as compared to a maximum field intensity of 26.5 mW/cm^2 available in the parallel plate radiation chamber. The lower field intensity needs a longer exposure time, which results in the heat being carried away from the "hot" neck region to the cooler torso and head regions of the body.

- b. For $\vec{E} \parallel \vec{L}$ orientation, a detailed examination of the leg shows a higher rate of energy deposition in the knee and ankle regions. A power deposition varying as $(\text{cross-sectional area})^{-1}$ is observed. A similar result is observed for the arm where the maximum rate of deposition is for the elbow region.
- c. For $\vec{k} \parallel \vec{L}$ orientation (power propagating from head to toe; \vec{E} from arm to arm), the maximum rate of energy deposition is observed for the elbow region. The second highest absorption rate is measured for the neck region.

2. The monopole-above-ground chamber was designed and installed (Fig. 1). A new computer program was written to extend the field intensity calculations to the near field region. This is necessitated by the fact that high field intensities are generally needed for modeling, animal heating and lethality experiments. This may therefore require that the working

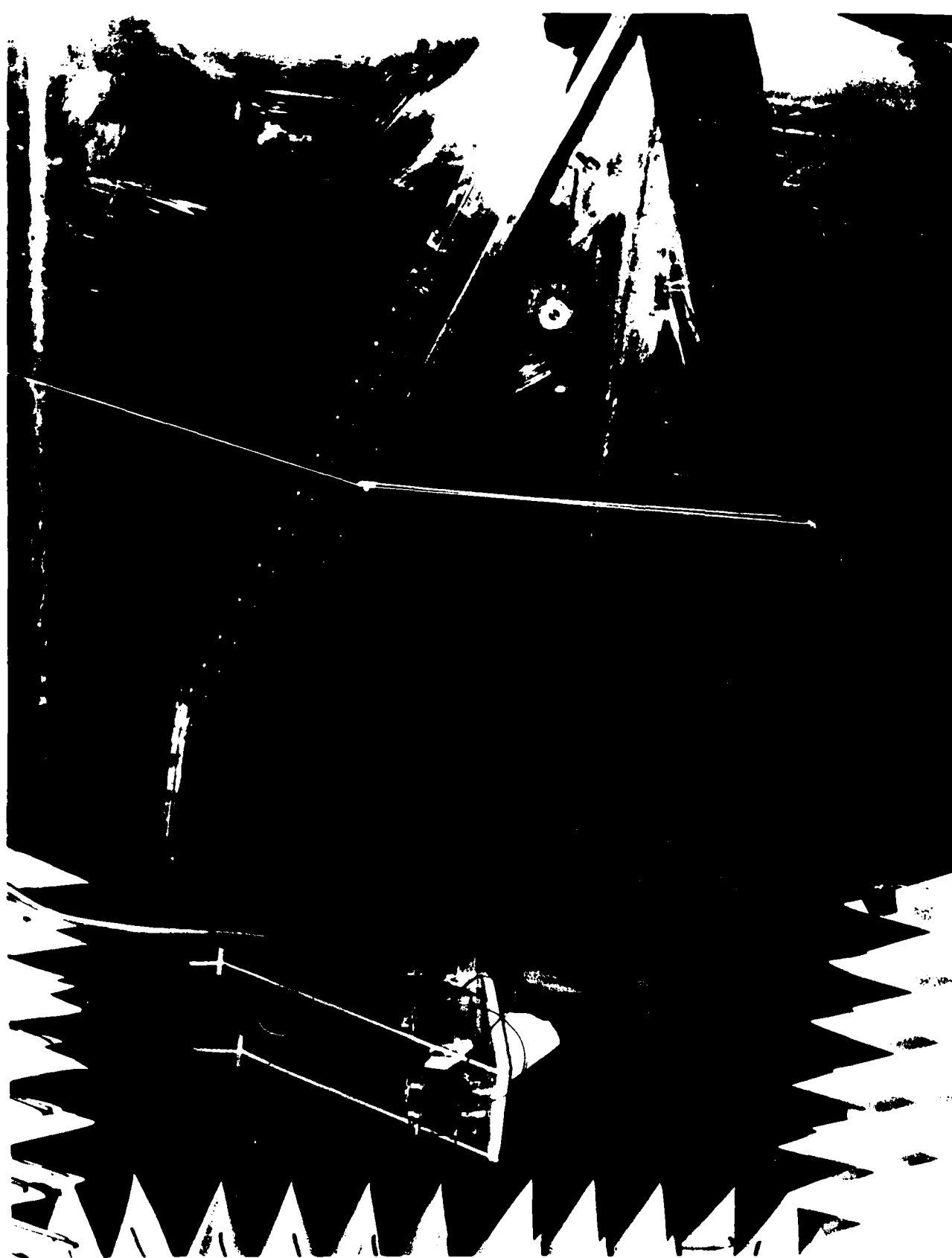


Fig. 1. A photograph of the monopole-above-ground radiation chamber.

region be located no more than a few wavelengths from the antenna. The computer program calculates the vector sum of near fields due to the dipole and its images (in assumed infinite reflectors). In order to apply the results to the case of the monopole-above-ground, the field components calculated for the half-space above ground are used (because of their physical realizability).

The field intensities calculated at various distances Z from the corner of the reflectors for some values of the spacing d of the monopole from the corner are given in Table 1.

Table 1. Forty-five degree corner reflector monopole-above-ground antenna.

Power input = 100 W
 Distance d = 33.75 cm
 Ground plane field intensity in mW/cm^2

Distance Z in meters	400 MHz $d/\lambda = 0.45$	500 MHz 0.56	600 MHz 0.675	700 MHz 0.788
1.5	26.0	26.1	28.3	24.7
2.0	14.7	14.7	15.8	13.8
2.5	9.5	9.4	10.1	8.8
3.0	6.6	6.5	7.0	6.1
4.0	3.7	3.7	3.9	3.4

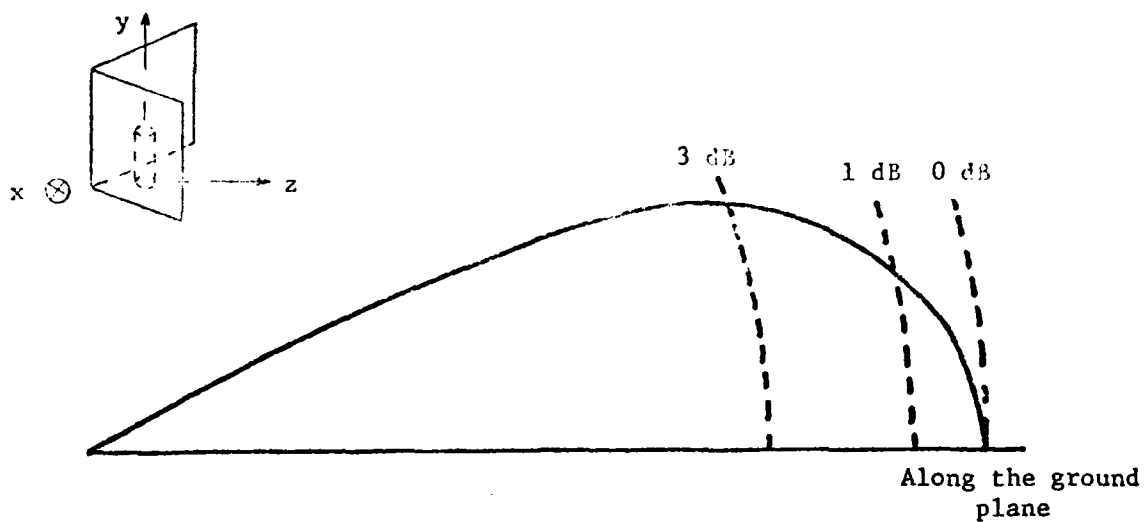
In each case a transmitted power of 100 watts is assumed. A point to note is that for distances beyond 2 meters, the

fields already satisfy the $1/r^2$ dependence that is characteristic of far-fields. This is ascribed to the fact that for this antenna, the $2D^2/\lambda$ condition for far-fields is satisfied for distances on the order of $z(2d)^2/\lambda$ or 1.5-2.0 m for most of the operating band.

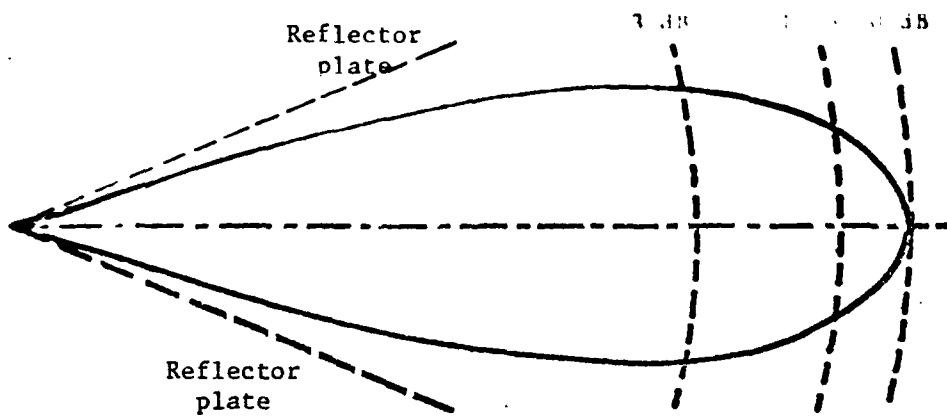
The calculated radiation patterns of the antenna in the $yz(E)$ - and $xz(H)$ -planes are shown in Fig. 2 for $d/\lambda = 0.675$. This value of $d/\lambda = 0.675$ is selected to obtain optimum input impedance and gain characteristics² of the radiator. The 1 dB beam widths in the yz (the E -plane) and xz (the H -plane or the plane of the ground) planes are on the order of 13.08° and $\pm 6.54^\circ$, respectively. The targets occupying these regions are consequently exposed to power densities varying by no more than ± 10 percent.

The radiation pattern of the corner reflector antenna is relatively insensitive to small changes in d/λ and monopole lengths h/λ . Table 2 gives the beam widths for various values of d/λ and h/λ . On account of a nearly 50Ω input impedance of $d/\lambda \approx 0.675$ quarter wave monopole antenna, this value of corner to antenna spacing is used, as far as possible, for convenience of matching over the frequency range.

Two input ports to which the monopole radiators may be screwed are provided. The corner reflector plates are movable back and forth in the xz -plane. The spacing $d/\lambda = 0.675$ at each of the measurement positions is fixed.



(a) Field pattern in the yz (E-plane)



(b) Field pattern in the xz or the plane of the ground

Fig. 2. Calculated pattern of a monopole-above-ground radiator in a 45° corner reflector for $h/\lambda = 0.25$, $d/\lambda = 0.675$.

Table 2. Monopole-above-ground radiator in a 45° corner reflector. Angular widths for different values of field deviation relative to maximum.

h/λ^1	0.20	0.30	0.25	0.35	0.40
d/λ^2	0.675	0.675	0.675	0.675	0.675
H-plane: -0.					
-0.5 dB	$\pm 6.54^\circ$				
-1.0 dB	$\pm 7.96^\circ$	$\pm 7.96^\circ$	$\pm 7.96^\circ$	$\pm 7.97^\circ$	$\pm 7.96^\circ$
-2.0 dB	$\pm 9.11^\circ$	$\pm 9.11^\circ$	$\pm 9.12^\circ$	$\pm 9.11^\circ$	$\pm 9.11^\circ$
-2.5 dB	$\pm 10.10^\circ$	$\pm 10.10^\circ$	$\pm 10.20^\circ$	$\pm 10.09^\circ$	$\pm 10.10^\circ$
-3.0 dB	$\pm 10.96^\circ$	$\pm 10.96^\circ$	$\pm 10.97^\circ$	$\pm 10.96^\circ$	$\pm 10.96^\circ$
E-plane: -0.5 dB					
-0.5 dB	9.49	9.03	8.77	10.67	9.71
-1.0 dB	13.36	12.74	12.39	14.14	13.08
-1.5 dB	16.27	15.55	15.13	17.18	16.70
-2.0 dB	18.69	17.89	17.45	19.68	18.34
-2.5 dB	20.79	19.91	19.41	21.84	20.40
-3.0 dB	22.66	21.73	21.19	23.76	22.25

¹ h/λ = height of monopole in terms of wavelength.

² d/λ = spacing to the corner of the reflectors in wavelengths.

The man-shaped phantom has been calibrated using the General Micro-wave Corporation field intensity probe Raham model 1 (300 to 18000 MHz). The measured field intensities in the E- and H- planes at a couple of representative frequencies are shown in Figs. 3 and 4. Measurements confirm the similarity of patterns at other frequencies.

3. Proportionately scaled man-shaped cavities of height 3, 4, 5, 6, 8, 10, 13, and 16 inches were made in polyurethane. Starting with wire frames, sculptured figurines were made of clay in roughly the same proportions as those given in reference 3. Each clay model was then molded of Silastic RTV silicone rubber (Dow Corning type 3110). The reusable molds so formed were used to cast epoxy figures. The epoxy figures were subsequently cast in polyurethane blocks. After polyurethane had been formed, the epoxy castings were cut in half around the central frontal plane for their easy removal. Two cavities, one resealed for filling with saline and the other for stuffing with biological phantom materials, were formed for each of the eight sizes.

The weights of the epoxy figures and the volume of the final polyurethane cavities are given in Table 3. The volume varies approximately as (height)³, which demonstrates the near proportionality of these figurines.

4. Biological phantom materials were developed for simulating man over the frequency range 13-230 MHz (including the important

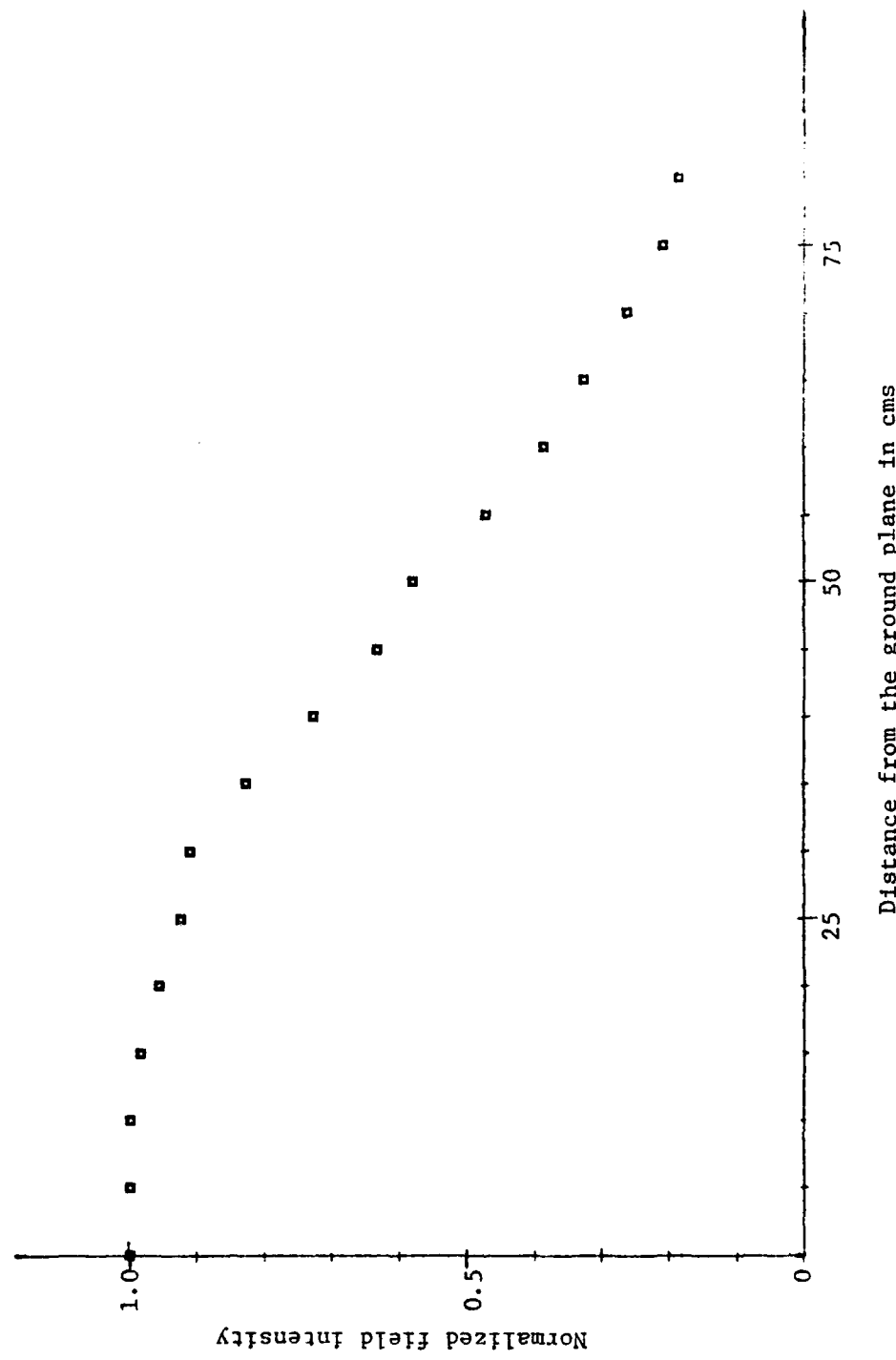


Fig. 3 (a). Measured field variation in the E-plane at 350 MHz. $P = 50$ W, $h/\lambda = 0.25$, $d/\lambda = 0.675$, $Z = 2.15$ m (fields normalized relative to 11.0 mW/cm 2).

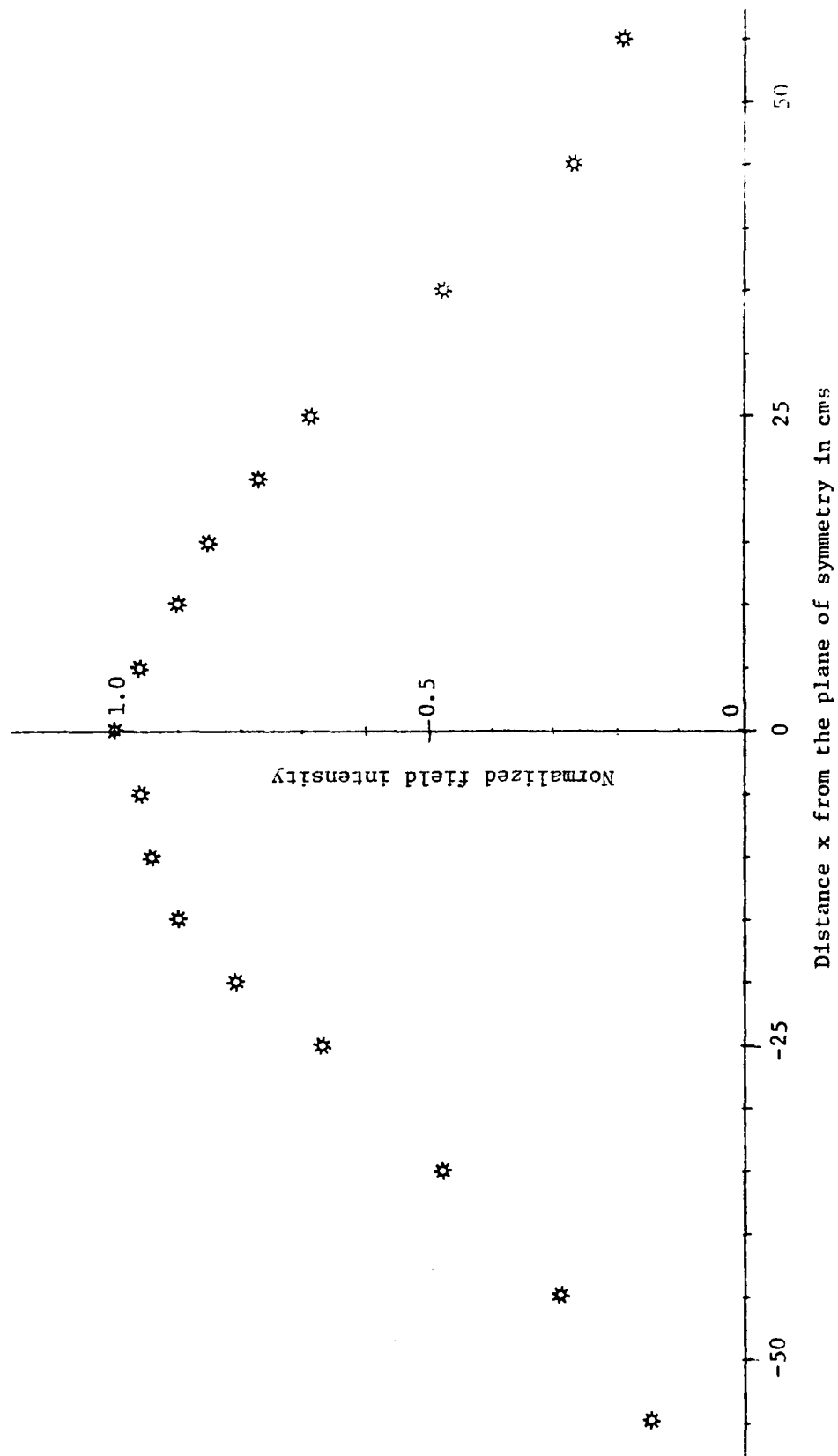


Fig. 3 (b). Measured field variation in the H-plane at 350 MHz. $P = 50$ W, $h/\lambda = 0.25$, $d/\lambda = 0.675$, $Z = 2.15$ m (fields normalized relative to 11.0 mW/cm 2).

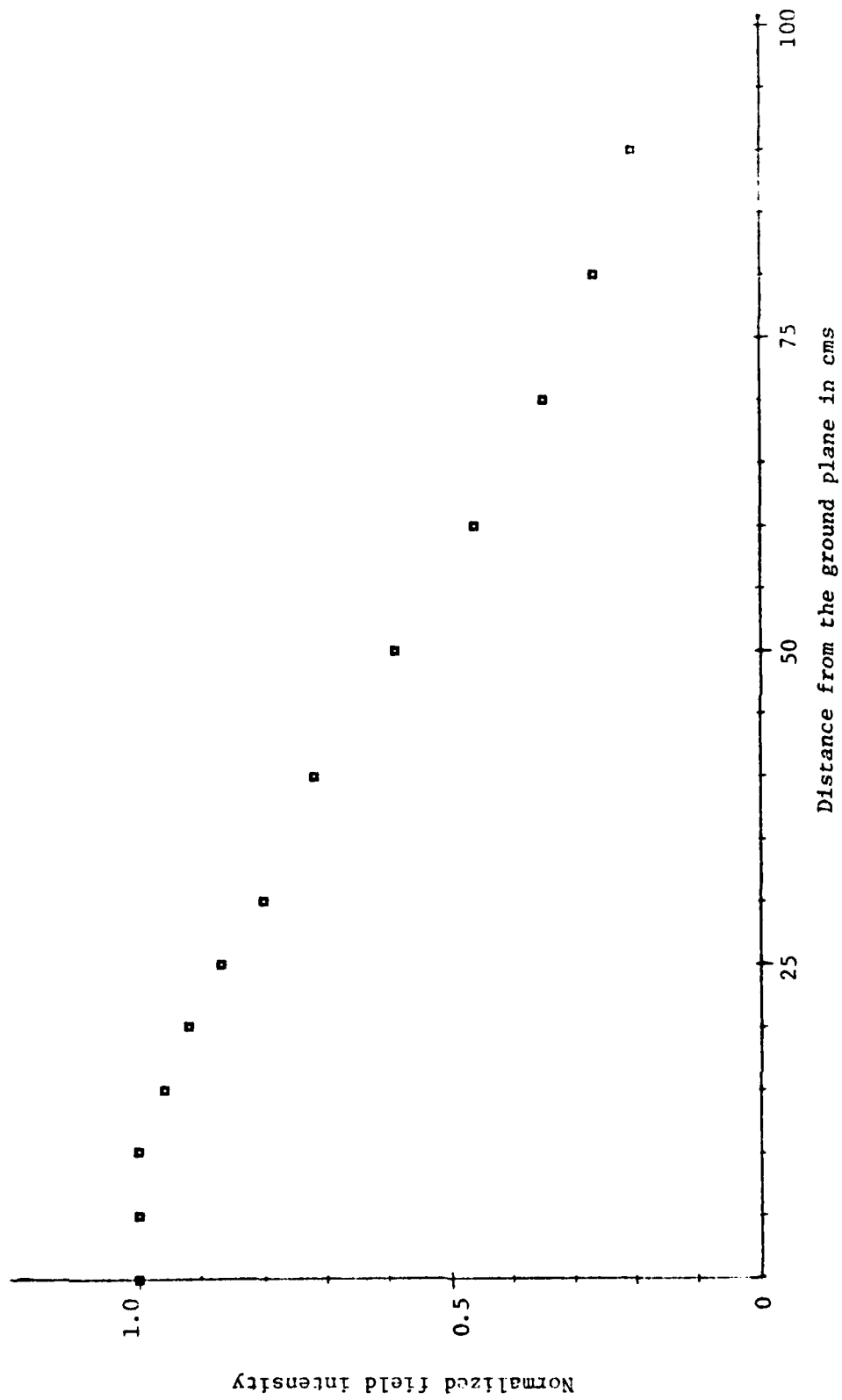


Fig. 4 (a). Measured field variation in the E-plane at 600 MHz. $P = 50$ W, $h/\lambda = 0.25$, $d/\lambda = 0.675$, $Z = 2.15$ m (fields normalized relative to 10.6 mW/cm^2).

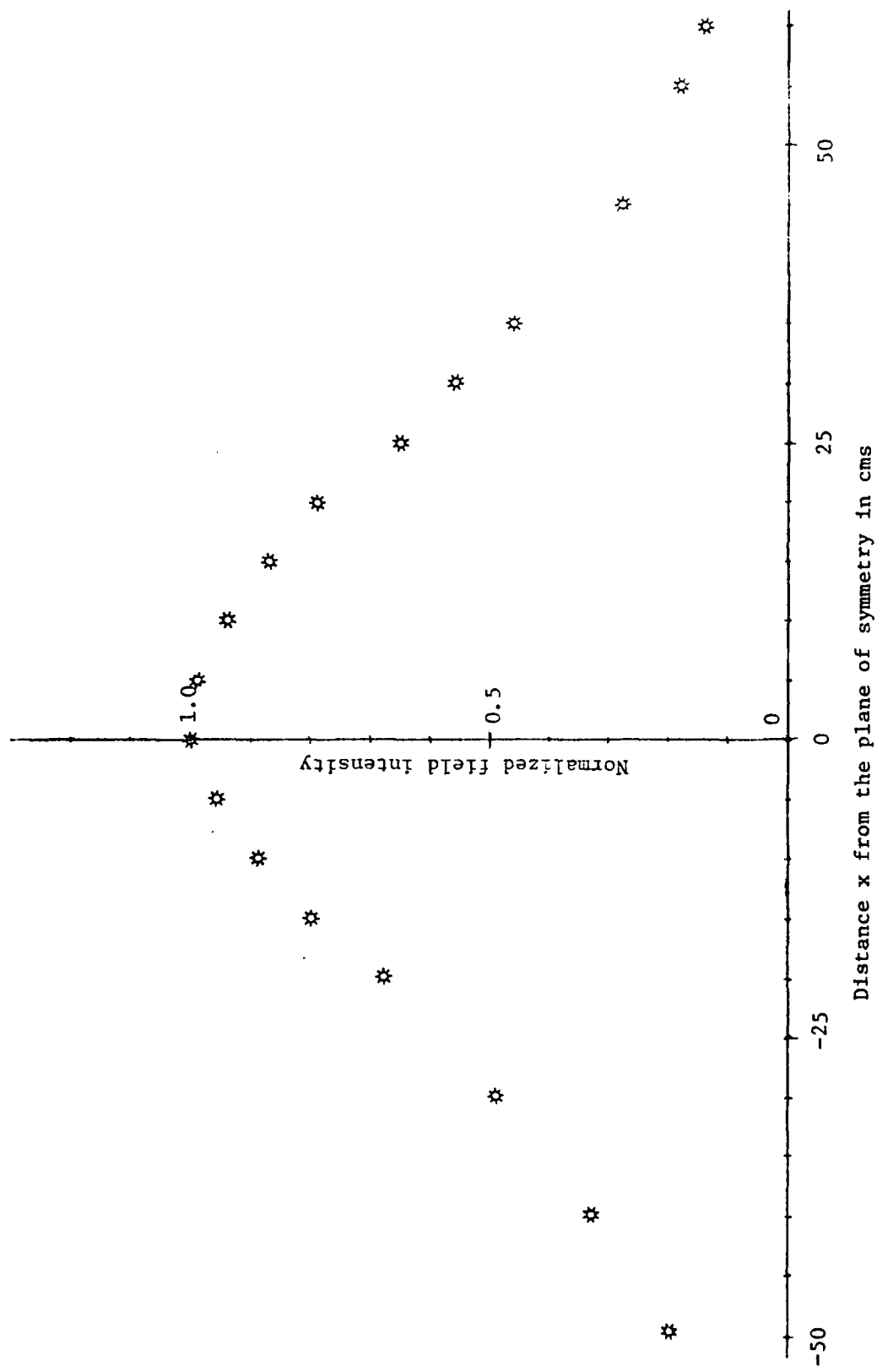


Fig. 4 (b). Measured field variation in the H-plane at 600 MHz. $P = 50$ W, $h/\lambda = 0.25$, $d/\lambda = 0.675$, $z = 2.15$ m (fields normalized relative to 10.6 mW/cm²).

Table 3. Some measured parameters of the man models used for experiments.

Height of the figurine inches	Weight of the epoxy mold gms	Volume of the polyurethane cavity cm ³
4"	21.7	15.0
5"	45.7	33.2
6"	59.3	50.0
8"	139.5	111.4
10"	267.5	208.5
13"	548.5	410.5
16"	1063.0	842.0

resonance regions of 33 and 65 MHz). These materials are to be used to fill the eight proportionately scaled figurines for dosimetric measurements at 300, 400, 600, 915, and 985 MHz. The compositions and their measured properties were described in a paper presented at the 1976 USNC/URSI meeting, and a copy of the same is attached here as Appendix A.

5. As a result of our extensive experiments spanning a period of almost two years, the curves giving the whole body absorption for man exposed to free space electromagnetic radiation have been generated and are sketched in Figs. 5 and 6. For each of the indicated polarizations, the orientation^{4*} of maximum

* A copy of this paper (Reference 4) is attached here as Appendix B for ready reference.

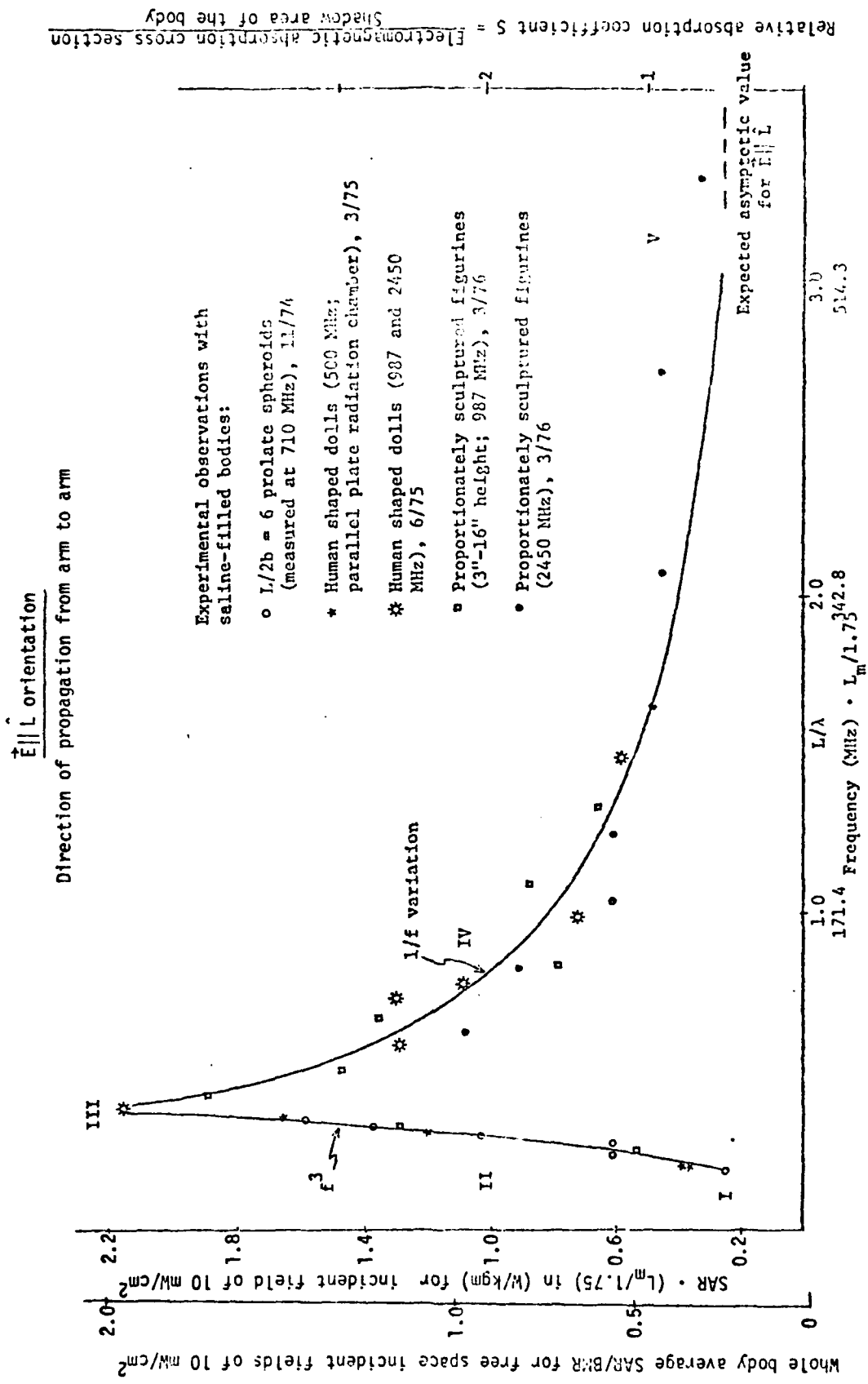


Fig. 5. Whole body absorbed power density and relative absorption coefficient S for humans for electric field polarized along the major length L of the body ($E \parallel L$ orientation).

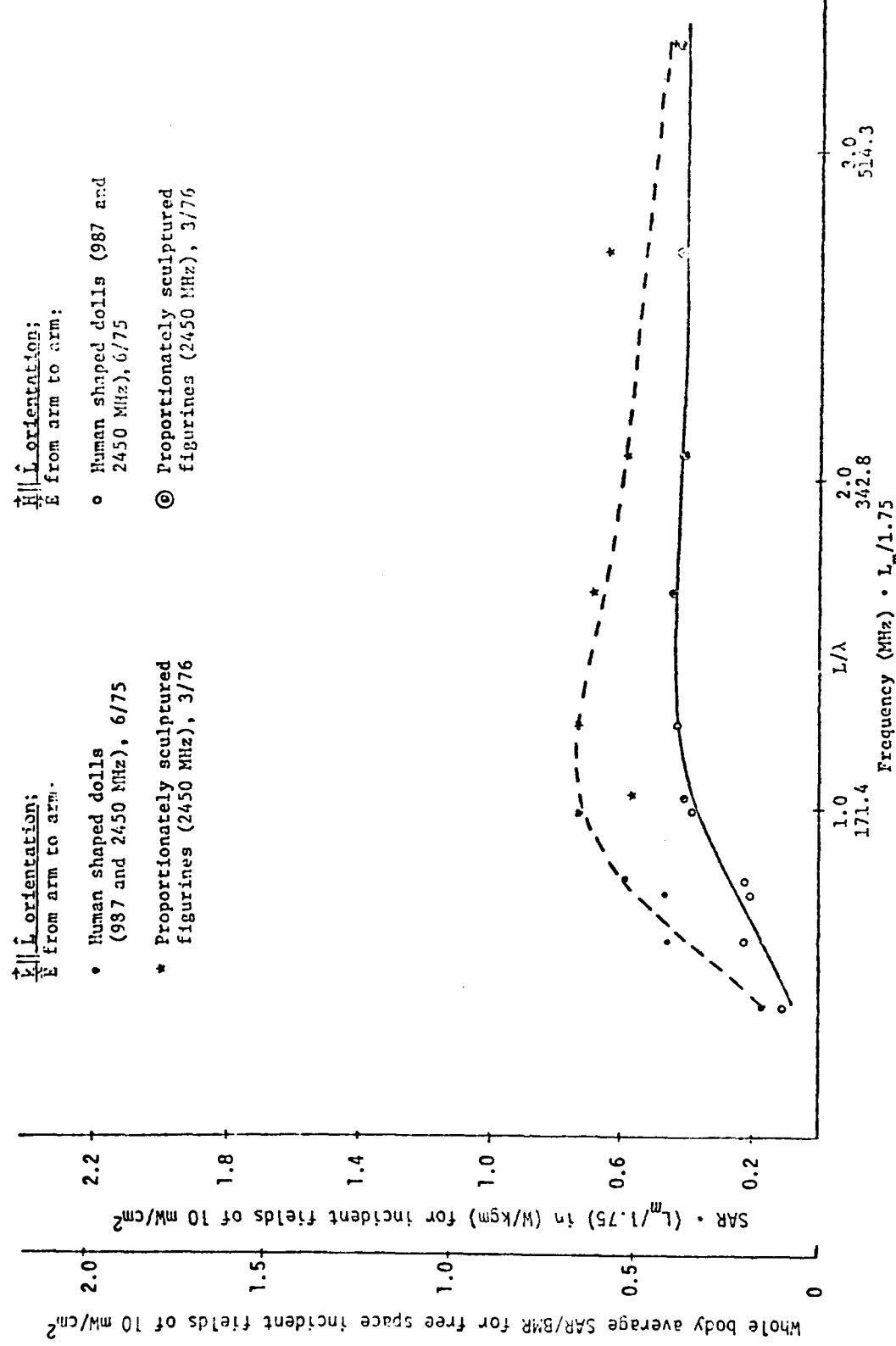


Fig. 6. Whole body absorbed power density for humans for $\vec{H} \parallel \vec{L}$ and $\vec{k} \parallel \vec{L}$ orientations. Free space radiation (no ground effects).

power absorption is used. This corresponds to propagation from arm to arm (rather than from front to back) for $\vec{E} \parallel \hat{L}$ orientation, \vec{E} parallel to arm (rather than from front to back) for $\vec{E} \parallel \hat{k}$, \hat{L} orientation, and \vec{E} from arm to arm for $\vec{H} \parallel \hat{L}$ orientation.

To date the experimental data have been obtained to 8.7 times the $\vec{E} \parallel \hat{L}$ resonance frequency of 62-68 MHz. The quantities plotted in Figs. 5 and 6 are:

- a. The relative absorption coefficient S which is a measure of the efficiency of power absorption

$$S = \frac{\text{Microwave absorption cross section}}{\text{Shadow area of the body}} = \frac{(\text{Total power absorbed in watts})}{\text{Shadow area of the body in cm}^2} \times \frac{(\text{Field intensity in watts/cm}^2)}{}$$

- b. The specific absorption rate (SAR) in watts/kgm.
- c. The SAR as units of basal metabolic rate (BMR).

For the most absorbing $\vec{E} \parallel \hat{L}$ orientation, the whole body absorption curve may be discussed in terms of five frequency regions:

Region I -- Frequencies well below resonance ($L/\lambda < 0.1-0.2$).

An f^2 type dependence derived theoretically and checked experimentally by Burney and coworkers.⁵

Region II -- Subresonance region ($0.2 < L/\lambda < 0.36$).

An $f^{2.75}$ to f^3 dependence of total power deposition has been experimentally observed for this region.

Region III -- Resonance region ($L/\lambda \approx 0.36-0.4$).

A relative absorption decreasing as $(f/f_r)^{4.2}$

4.2⁵ (Part)

resonance frequency

times the SAR

times the ENR.⁶

Region IV -- Post-resonance region to frequencies on the order of 8 to 9 times the resonance frequency f_r .

A whole body absorption reducing as $(f/f_r)^{-1}$ from the resonance value has been observed.

Region V -- $f \gg f_r$ region.

The S parameter should asymptotically approach the "optical" value which is (1 - power reflection coefficient) or about 0.5.

In comparing the graph of Fig. 5 with those of Fig. 6 (drawn to the same scale), the following points are noteworthy:

- a. For frequencies $f > (4-5)f_r$, there is little distinction between the total power absorbed for the various polarizations. For humans, this corresponds to (frequency in MHz) \times (height in meters/1.75) of about 250.
- b. The resonances for $\vec{k} \parallel \hat{L}$ and $\vec{H} \parallel \hat{L}$ orientations are not very sharp. In fact, for $\vec{H} \parallel \hat{L}$ orientation, the value gradually reaches a peak value and stays at that value for higher frequencies.

6. The frequency dependence of Fig. 5 has been used to draw the generalized curves for r_{eff} and SAR (Fig. 7) for free space irradiation for the most interesting polarization ($E \parallel L$). A resonance S value of 2.16 (q), a formula for a theory for an aspect ratio $L/2b = 3.25$ (i.e., "equivalent spheroid")^{*} is taken to draw the graphs of Fig. 7. Also shown in the same figure are the values calculated from the lethality data of Schrot and Hawkins.⁷ In calculating SAR's from their data, it is assumed that:

- a. A temperature elevation of 7.4° C results in convulsion.
- b. The temperature increase occurs in an adiabatic manner; i.e., the rate of deposition is high enough so that there is no other mechanism for gain or loss of heat from the animal body.

On account of the high field intensities of 150 mW/cm^2 used in the experiments by Schrot and Hawkins,⁷ the second assumption may be quite justified. From Fig. 7, the correlation of the empirical graphs with experimental values is good.

7. The total power absorption for a human with feet touching the ground is shown in Fig. 8. These results are projected from measurements with 4", 5", 6", and 8" tall saline-filled

* In order to determine the aspect ratio of the equivalent prolate spheroid, the bulk of the body is considered representable by a prolate spheroid of length L and diameter $2b$. The diameter $2b$ is calculated from the average circumference of the animal body.

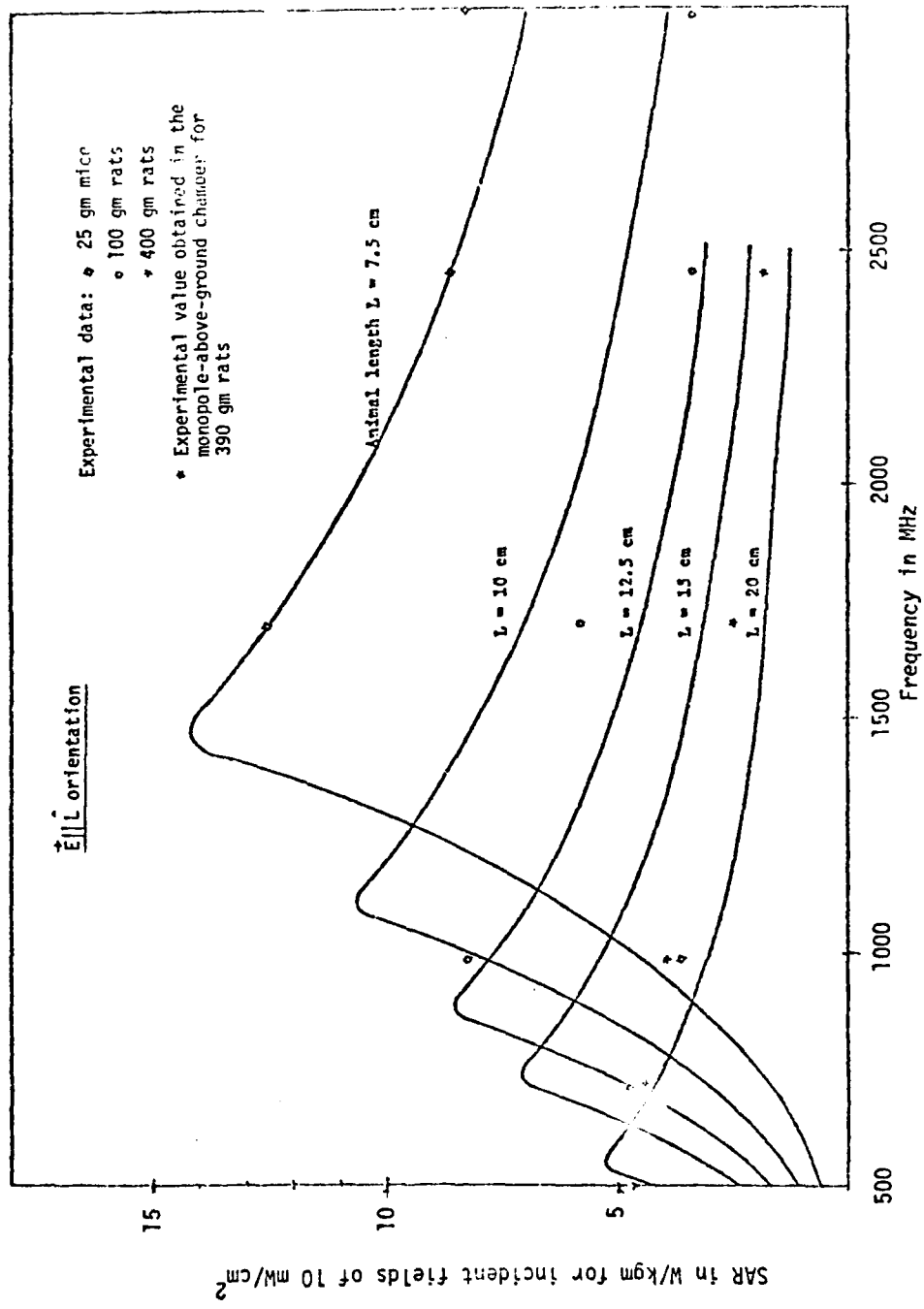


Fig. 7. Projected values of whole body absorbed power density for different size rats and mice without ground effects ($L/2b = 3.25$ where $2b$ is the "average" circumference of the animals).

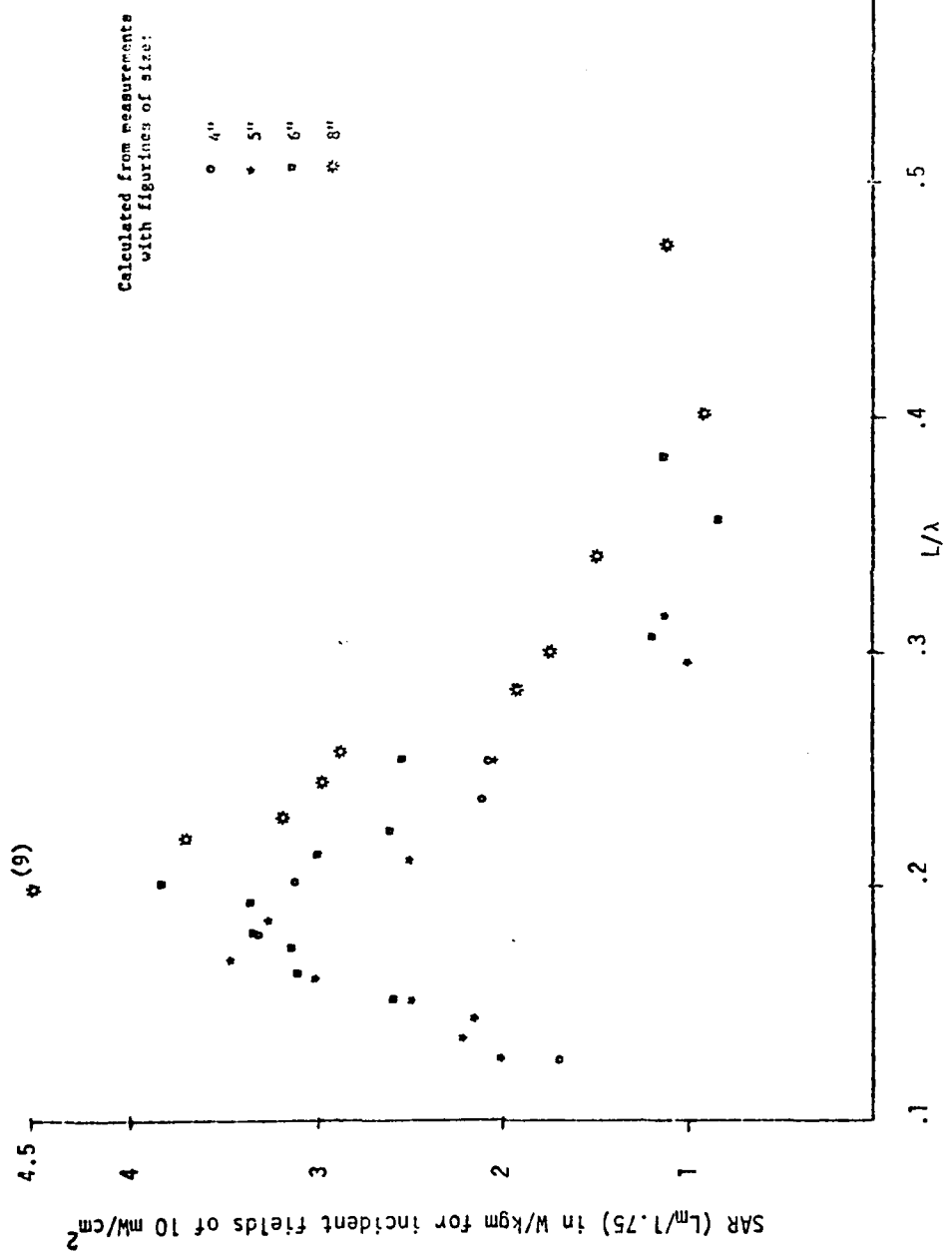


Fig. 8. Projected SAR in a human of height L_m (in meters) with feet touching ground. (For each of the points shown on the graph, three measurements were taken. The average of nine measurements gives the peak value for the 8" size at $L/\lambda = 0.2$.)

figurines exposed to E_{11} radiation at different frequencies in the monopole-above-ground radiation chamber. Comparing the results to those of free space radiation (Fig. 5), peak power absorption in this case is observed for a frequency about one-half the value for ungrounded conditions. The new resonance frequency is projected to be $(30-34) \times (1.75/L_m)$ MHz. At resonance, a value about two times the resonance value for ungrounded conditions is observed.

A point of concern is that the graph of Fig. 8 does not completely agree with the data obtained with grounded figurines in the parallel plate chamber (Fig. 16, Appendix B). While the peak absorption frequency is very similar, the maximum absorption density observed in the monopole-above-ground chamber is about half as large as that observed in the parallel plate radiation chamber. This is unlike the observations with ungrounded figurines where the parallel plate radiation chamber measurements were in excellent agreement with free space irradiation experiments. Further experiments are planned to resolve the issue of 2 versus 4 times enhancement factors observed with grounded figurines under respective resonant conditions.

8. Judging from the success of the antenna theory in explaining the resonance frequencies and absorption cross sections under grounded and ungrounded conditions, highly enhanced values of SAR are expected for resonant bodies in the presence of 180° , 90° , and other corner reflectors.² Experiments detailed in

Appendix C have indeed given SAR enhancement factors as high as 27 in proximity of reflecting surfaces under resonant conditions.

As a result of these experiments, the total power deposited in man and animals subjected to 10 mW/cm^2 incident fields has been calculated for various exposure conditions and is tabulated in Table 4. The rates of energy deposition for resonance conditions in the presence of ground effects and/or reflectors are truly staggering. Resonance SAR values as high as 56.5-103 times the BMR are predicted for adult humans. The times to convulsion of 100 gm rats (Fig. 9, Appendix C) for incident field intensities of $3-20 \text{ mW/cm}^2$ confirm some of the highest projections in the presence of reflecting surfaces.

In order to fully appreciate the reflector-caused enhancements in SAR's, it should be mentioned that, for target length L , reflectors with dimensions $2d \times 1.2 L$ (in the \vec{E} direction) are considered adequate² to simulate infinite sheets for a target to corner distance d . Furthermore the reflecting surfaces need neither be of good conducting materials nor solid in construction to cause considerable enhancements in SAR's. In fact, surfaces of insulating material with conducting rods (oriented along incident fields) that are spaced $\leq 0.1 \lambda$ act effectively as solid conducting surfaces. Experiments, nevertheless, need to be done with reduced dimensions of

Table 4. Total power deposited in man and animals at 10 mW/cm^2 .

Man (1.75 m height)

100 gm rat

400 gm rat

Prior knowledge

38 watts assuming no reflectance

19 watts assuming 50 percent reflectance

I. At resonance for free space.



151 watts

0.8 watts

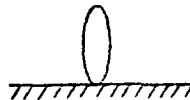
2 watts

$f \approx 62-68 \text{ MHz}$

$f \approx 987 \text{ MHz}$

$f \approx 600 \text{ MHz}$

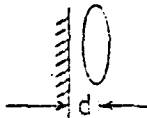
II. At resonance for conditions of electrical contact with the ground plane.



$2 \times 151 = 302 \text{ watts}$

$f \approx 31-34 \text{ MHz}$

III. At resonance for placement in front of a flat reflector.



$d \approx 0.125 \lambda$

$4.7 \times 151 = 710 \text{ watts}$

3.8 watts

9.4 watts

$f \approx 62-68 \text{ MHz}$

$f \approx 987 \text{ MHz}$

$f \approx 600 \text{ MHz}$

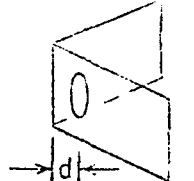
Table 4 (continued)

Man (1.75 m height)

100 gm rat

400 gm rat

IV. At resonance for placement in a 90° corner reflector.



$$d = 1.5 \lambda$$

$$27 \times 151 = 4077 \text{ watts}$$

$$21.6 \text{ watts}$$

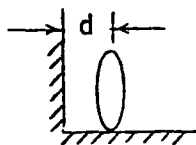
$$54 \text{ watts}$$

$$f \approx 62-68 \text{ MHz}$$

$$f \approx 987 \text{ MHz}$$

$$f \approx 600 \text{ MHz}$$

V. At resonance in electrical contact with ground plane, in front of a flat reflector.

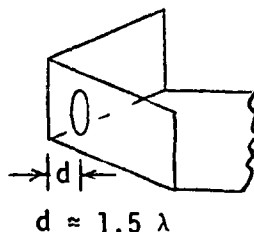


$$d \approx 0.125 \lambda$$

$$2 \times 710 = 1420 \text{ watts}$$

$$f \approx 31-34 \text{ MHz}$$

VI. At resonance in electrical contact with ground plane, in a 90° corner reflector.



$$d \approx 1.5 \lambda$$

$$2 \times 4077 = 8154 \text{ watts}$$

$$f \approx 31-34 \text{ MHz}$$

reflectors and for imperfect reflecting surfaces to determine the enhancement factors that actually result in such situations.

The corresponding data for 400 gm^{*} adult rats have been run in the monopole-above-ground chamber. The resonance frequency for these animals was pinpointed in the first instance to be 600 MHz in agreement with the graphs of Fig. 7. The mean times-to-convulsion together with the standard deviation for four animals is plotted in Fig. 9 for irradiation frequencies of 500, 550, 600, 650, and 700 MHz. Minimum time-to-convulsion is observed for irradiation frequency of 600 MHz. Below resonance, the time-to-convulsion increases more rapidly than that for frequencies above resonance. This observation is consistent with the graphs in Figs. 5 and 7, and is in agreement with the lethality data of Schrot and Hawkins.⁷

The times-to-convulsion of 400 gm rats for different locations in front of a 90° corner reflector are shown in Fig. 10. Of the three locations that were evaluated, $d^{**} = 0.4 \lambda$ is the most absorbing. For this location, the times-to-convulsion for different incident field intensities are plotted

* In actual experiments, animals within the weight range of 370-430 grams were used.

** On account of the fairly limited length (≈ 2.5 m) of the monopole-above-ground chamber, the more lethal placement $d = 1.5 \lambda$ (see Fig. 5, Appendix C) could not be tried under these exposure conditions.

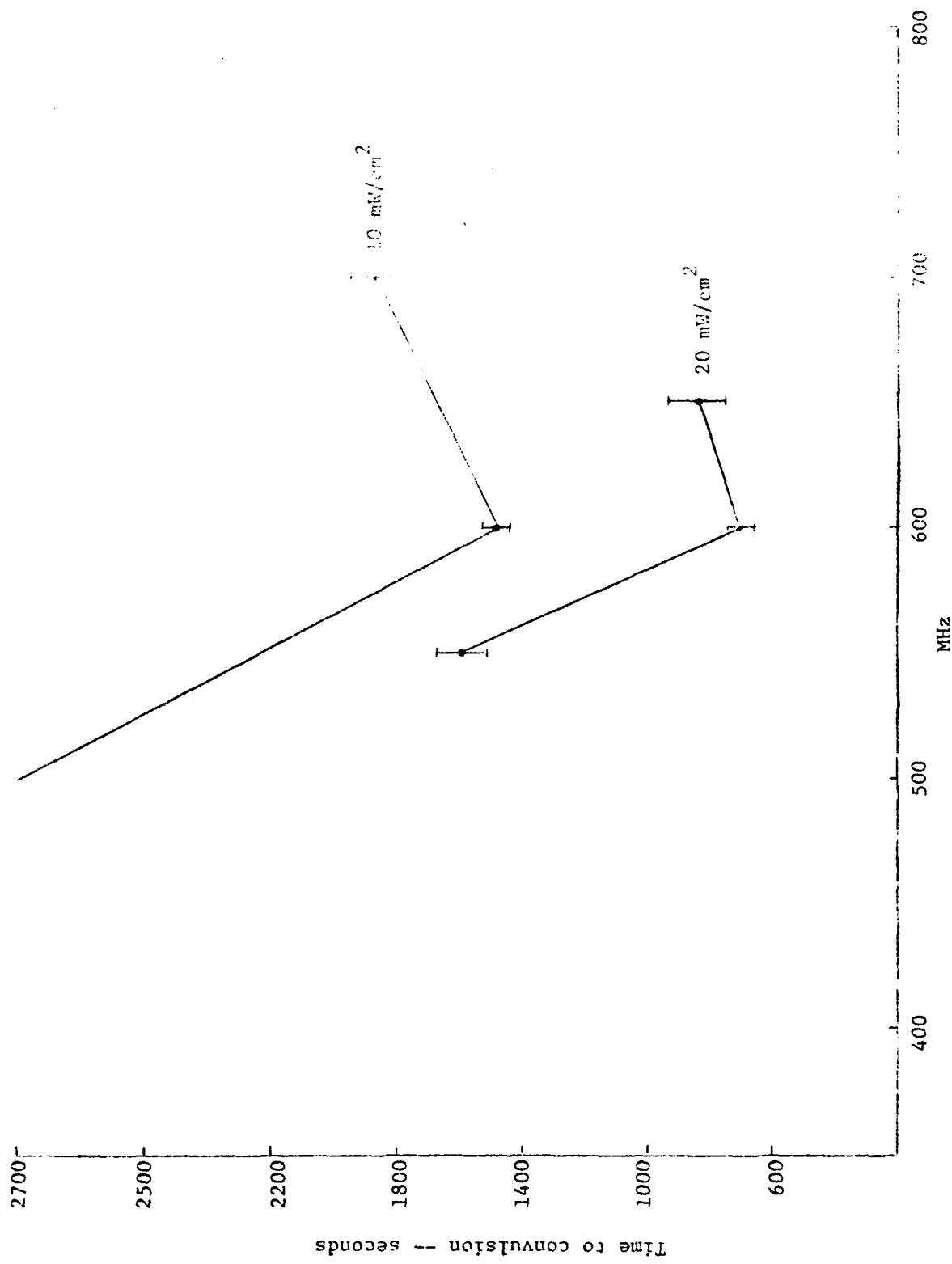
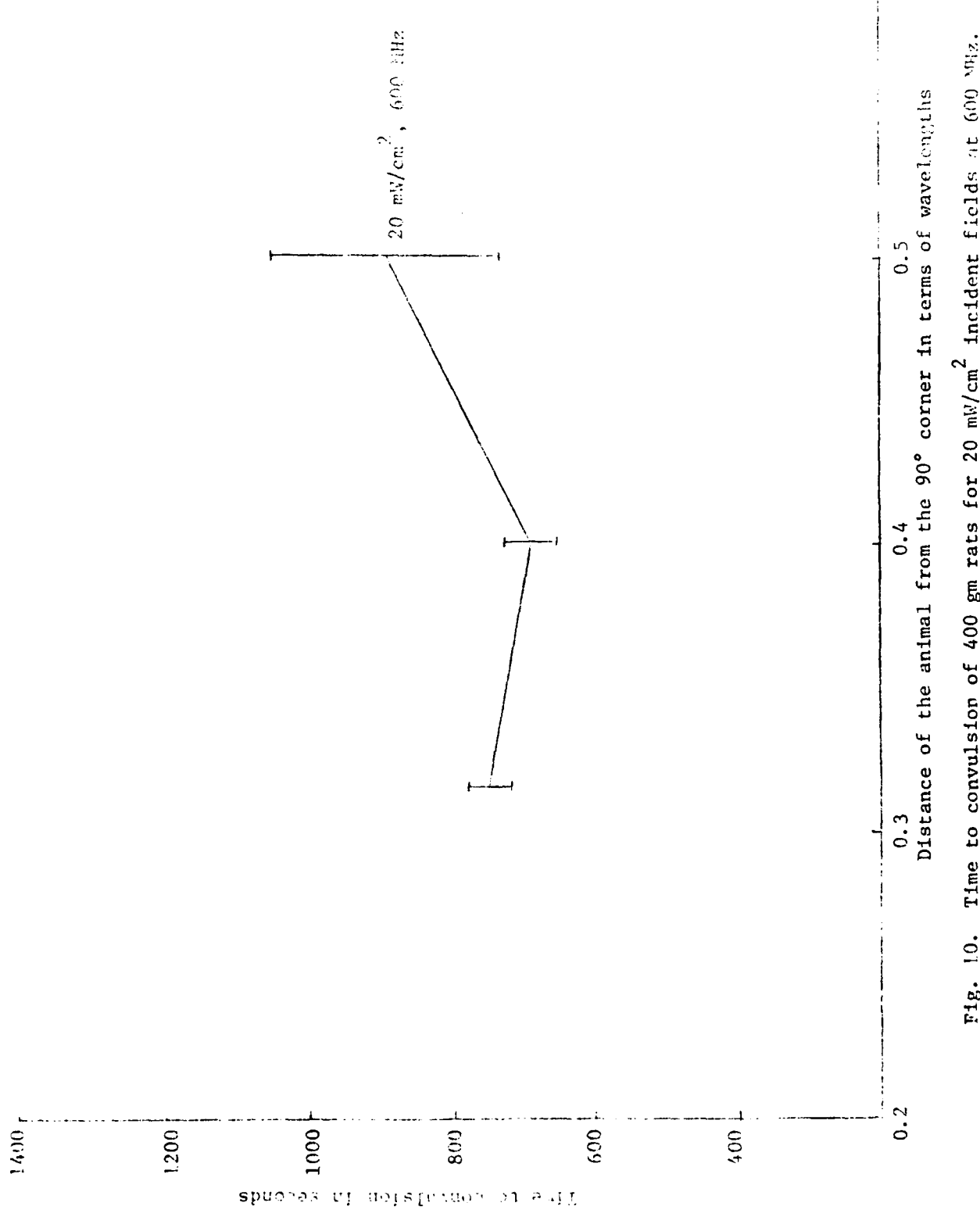


Fig. 9. Time to convulsion of 400 gm rats for 10 and 20 mW/cm^2 incident fields at different frequencies. (Animals placed $d = 0.4 \lambda$ from a 90° corner of reflecting surfaces.)



in Fig. 11.

Comparing in this situation the mean time-to-convulsion of 730 seconds for 20 mG/cm^2 incident field to the corresponding time of 455 seconds (at 710 MHz) observed by Schrot and Hawkins⁷ for free space irradiation at 150 mW/cm^2 , it is apparent that the deposition enhancement factor in the monopole-above-ground chamber on the order of 7 is not as large as 11 observed for 100 gm rats for $d \approx 0.4 \lambda$ placement. It should also be noted that Schrot and Hawkins' experiments⁷ were done at 710 MHz and they would have observed a slightly lower convulsion time than 455 seconds had they worked at the resonance frequency of 600 MHz for these animals. As discussed in the next paragraph, a lower enhancement factor has also been observed in the monopole-above-ground chamber for man models.

9. The average values of SAR for ungrounded resonant size saline-filled figurines with and without reflectors have been measured in the monopole-above-ground chamber and are tabulated in Table 5. Consistent with the 400 gm rat lethality data, somewhat smaller enhancement factors of 2.5 and 6.9, as compared to 4.7 and 11 observed under respective exposure conditions at Walter Reed Laboratories (see Appendix C, Figs. 6 and 8), are noted. Further theoretical and experimental work is needed to understand this observation. The reduced effectiveness of reflectors in the monopole-above-ground chambers is most

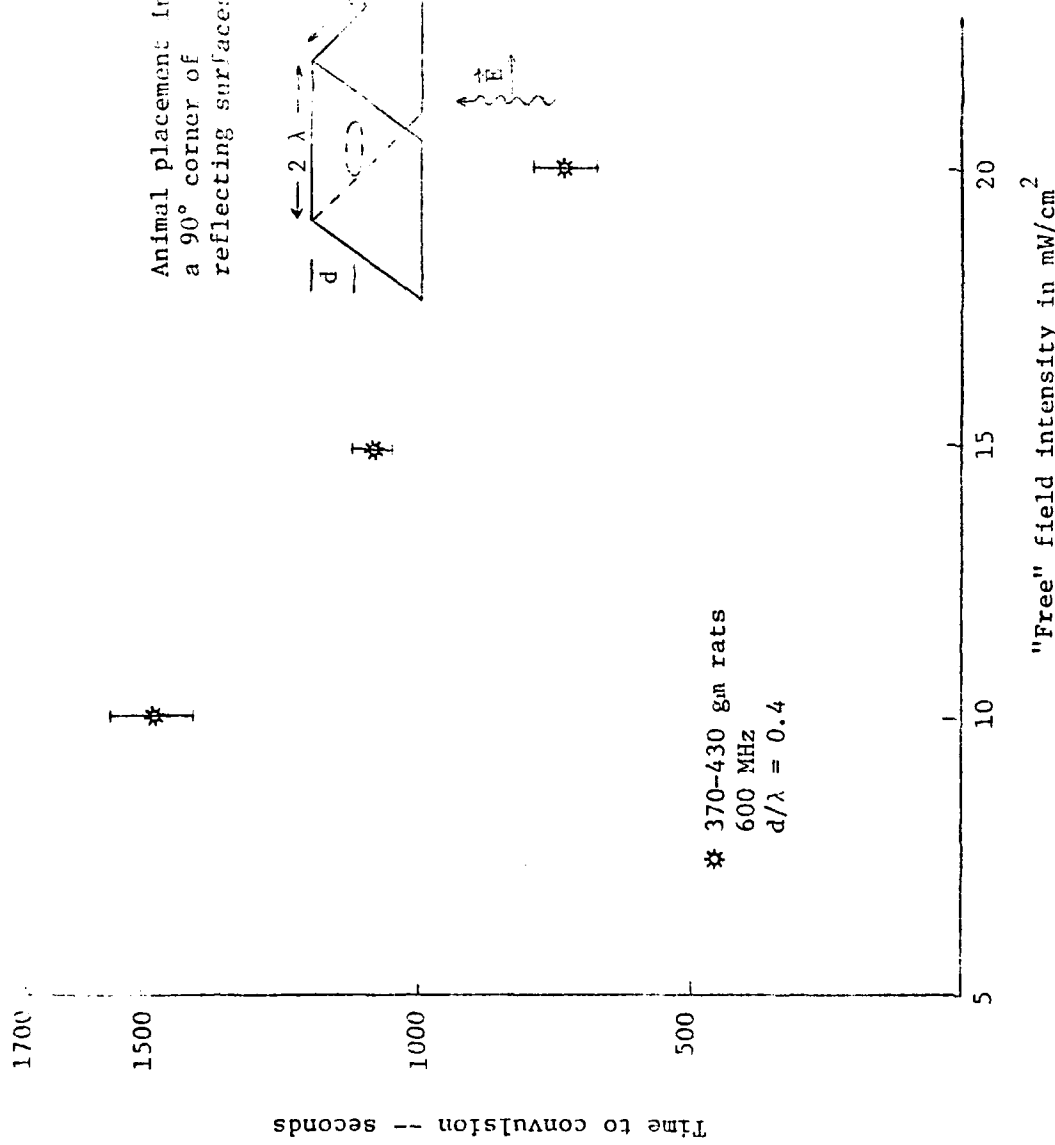


Fig. 11. Time to convulsion of 400 gm rats at their resonance frequency of 600 MHz.

Table 5. Comparison of the whole-body-average "ungrounded" SAR at resonance with and without reflectors.

Data scaled for 1.75 m.h. an from the measurements on ungrounded 8" saline-filled figurines at 600 MHz ($l/\lambda = 0.406$)

SAR in W/kgm for incident fields of 10 mW/cm^2

SAR no reflector	SAR flat reflector $d/\lambda = 0.125$	SAR 90° reflector $d/\lambda = 0.4$
2.04	5.13	14.02

probably due to the spherical nature of the wavefront as it impinges on the planar reflectors. This problem was not as severe for Walter Reed experiments on account of a larger physical separation of 14' of the transmitting antenna from the experimental area which would imply that the incident waves were closer to plane waves for those experiments.

An implication of the above measurements is that while higher enhancement factors are observed for plane waves, significantly increased SAR's are observed also for nonideal wave incidence conditions.

10. The average values of SAR for grounded resonant-size saline-filled figurines with and without reflectors have been measured in the monopole-above-ground chamber and are tabulated in Table 6. The results of these experiments were used in arriving at some of the numbers given in Table 4.
11. On account of a strong absorption in the resonance region, our

Table 6. Comparison of the whole-body-average "grounded" SAR at resonance with and without reflectors.

Data series for 1.73 m human from the "ensur" tests on grossed and 1" saline-filled figurines at 730 MHz ($d/\lambda = 0.203$)

SAR in W/kg for incident E of $10 \text{ mW}/\text{cm}^2$

SAR no reflector	SAR flat reflector $d/\lambda = 0.125$	SAR 90° reflector $d/\lambda = 0.4$
4.5	10.3	28.1

work to date has concentrated on this region. Only recently have we extended the work to about 8.7 times the resonance frequency which for man corresponds to a frequency on the order of 570 MHz. While this has allowed us to generate whole body absorption curves for man (Figs. 5 and 6) through the important resonance region, we have not addressed the question of power deposition in man at microwave frequencies. To extend the measurements on whole body absorption and to obtain distribution for man to 3300 MHz, covering thereby some fairly important microwave bands such as the L- and S-bands and the industrial heating frequency of 2450 MHz, it will be necessary to use X-band irradiation if reduced scale models are to be used for convenience of experimentation.

High power sources at X-band are not only expensive but also are not readily available for power outputs larger than 250 watts. A high gain waveguide slot array has

consequently been designed, fabricated, and tested for use at these frequencies. The radiator described in Appendix D gives an intensity that is constant to within ± 0.5 dB over a total angle of 17.6° in the H-plane and 17.5° in the E-plane. On account of a sharp reduction of fields in the H-plane beyond the work area ($\pm 7.8^\circ$), an antenna gain which is 2.45 times higher than that of a horn with a similar work area is observed. This is on account of the saving in the power that would otherwise have been radiated in undesired directions because of the smooth roll off of the horn antenna.

For a working area of $55 \times 55 \text{ cm}^2$, a distance to the radiator of 2 meters is needed. From the measured gain, a field intensity of 46.4 mW/cm^2 constant to within ± 0.5 dB is calculated for a commercially available X-band power source of 250 W. This field intensity is quite adequate for modeling experiments.

12. Numerical studies have been initiated to understand some of the salient features of our observations. Among these are the enhancements in SAR caused by ground and reflecting surfaces, the $1/f$ reduction of the absorbed power in the post-resonance region, etc.

Green's function methods such as the tensor integral equation used by Chen⁸ appear to hold the greatest promise for calculation of SAR for models of man at frequencies near whole-body resonance. Chen claims to have solved the problem and

has published results on the internal electric field and absorbed power density inside an adult torso and a child's torso induced by electric fields of frequencies ranging from 1 to 500 MHz.

In order to solve the integral equation found in Green's function methods, it is necessary to discretize by representing the fields in terms of some finite basis. For a pulse function basis, the scatterer is partitioned into a number of cells N , where N is large enough that complex permittivity and the complex time-independent electric field may be assumed constant within each subvolume. Pulse functions are commonly chosen as a basis and have been used in Chen's calculations. If linear or higher order variation of the electric field were allowed within each cell by a more accurate basis, the storage limitations of computers would require that fewer cells be used. The number of cells possible with pulse functions is adequate to represent the torso with arms, legs, etc., but such detail would not be possible with a more elaborate basis.

Strictly speaking, pulse functions are not in the domain of the operator and should not be used with the tensor integral equation or related Green's function methods. In practice usable results are obtained if enough cells are used.⁹ Since pulse functions fail to allow for any of the variation of the electric field within each cell, an upper bound on

usable cell size may be found by determining the smallest size guaranteed to have internal fields with significant variation.

Appendix E is a copy of a paper submitted for publication to the *IEEE Transactions on Microwave Theory and Techniques*. Theory is used to establish an upper bound on usable cell size for pulse function solutions. The bound has been demonstrated to be useful in our computations. Calculations made using the bound on cell size suggest that significant error is present in Chen's calculations for the adult torso beyond 100 MHz and the child torso beyond 200 MHz.

Two new discretization procedures have been developed which give improved convergence by approximating the variation of the fields within each cell but do not require increased storage or significant increase in computational effort. The procedures are described in Appendix F which is a copy of a paper submitted for publication to the *IEEE Transactions on Antennas and Propagation*. The new methods have been used successfully in the two-dimensional problem of TM excitation of an infinite cylinder of arbitrary cross section shape. The extension to the three-dimensional problem with and without ground and reflector effects is planned.

13. To verify important observations by animal experiments, attention was devoted to proper design of the rat chambers. To improve microwave transparency, the animal holders were

fabricated with bottom and top made of rods perpendicular to the electric field to reduce possible reflections. The front and back plates in the plane of the electric field were made of styrofoam to minimize reflections. The design of the chamber was reported in Quarterly Report No. 5 of this contract, and photographs of the same are reproduced in Fig. 12 for ready reference. We have found the holder with styrofoam sides (holder B) to be adequate in containing 400 gram Long Evans rats for short time periods. We have attempted to use this holder design for the behavioral experiments. We find, however, that the styrofoam sides do not provide adequate structural support for mounting a plastic response lever and glass food pellet tube. To alleviate this difficulty we have replaced the styrofoam sides of this holder design with 1/16-inch Plexiglas panels. We have contained 400 gram Long Evans rats in this holder (Fig. 13) for up to eight-hour periods in 5 mW/cm^2 , 600 MHz, CW radiation fields. The addition of the plastic response lever and glass food pellet tube (Fig. 14) was easily accomplished on this holder. We have used this chamber daily in training stable VI-30" baseline responding in Long Evans rats and find this a superior holder.

14. The first series of dosimetric measurements on the Long Evans rat have been completed in the monopole-above-ground radiation chamber. Sixteen Long Evans male rats (380-400 grams) were



Holder A



Holder B

Fig. 12. Photographs of two rat holders that should be "relatively transparent" to microwaves of $E \parallel L$ polarization.

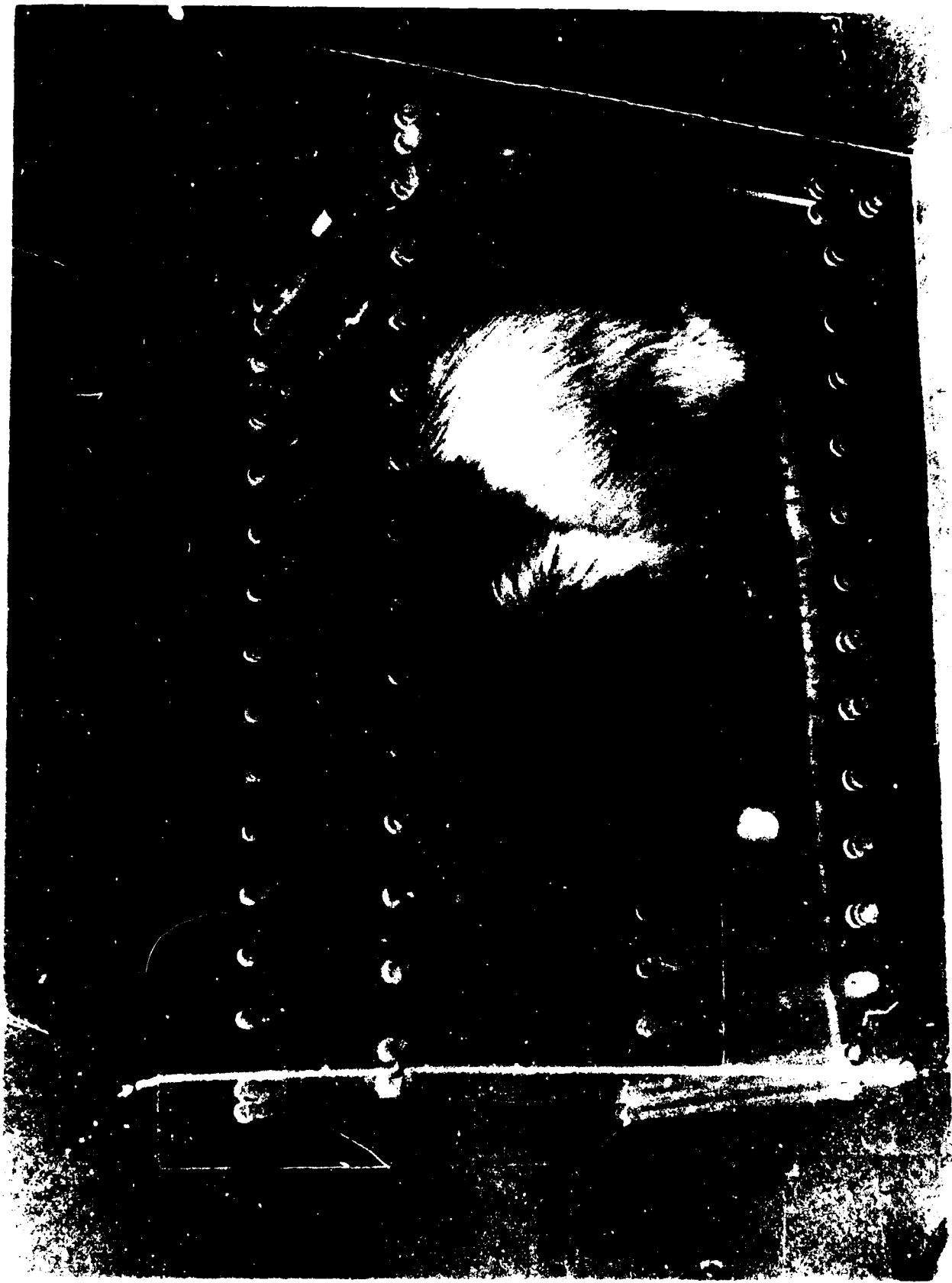


Fig. 13. Plexiglas rat holder.

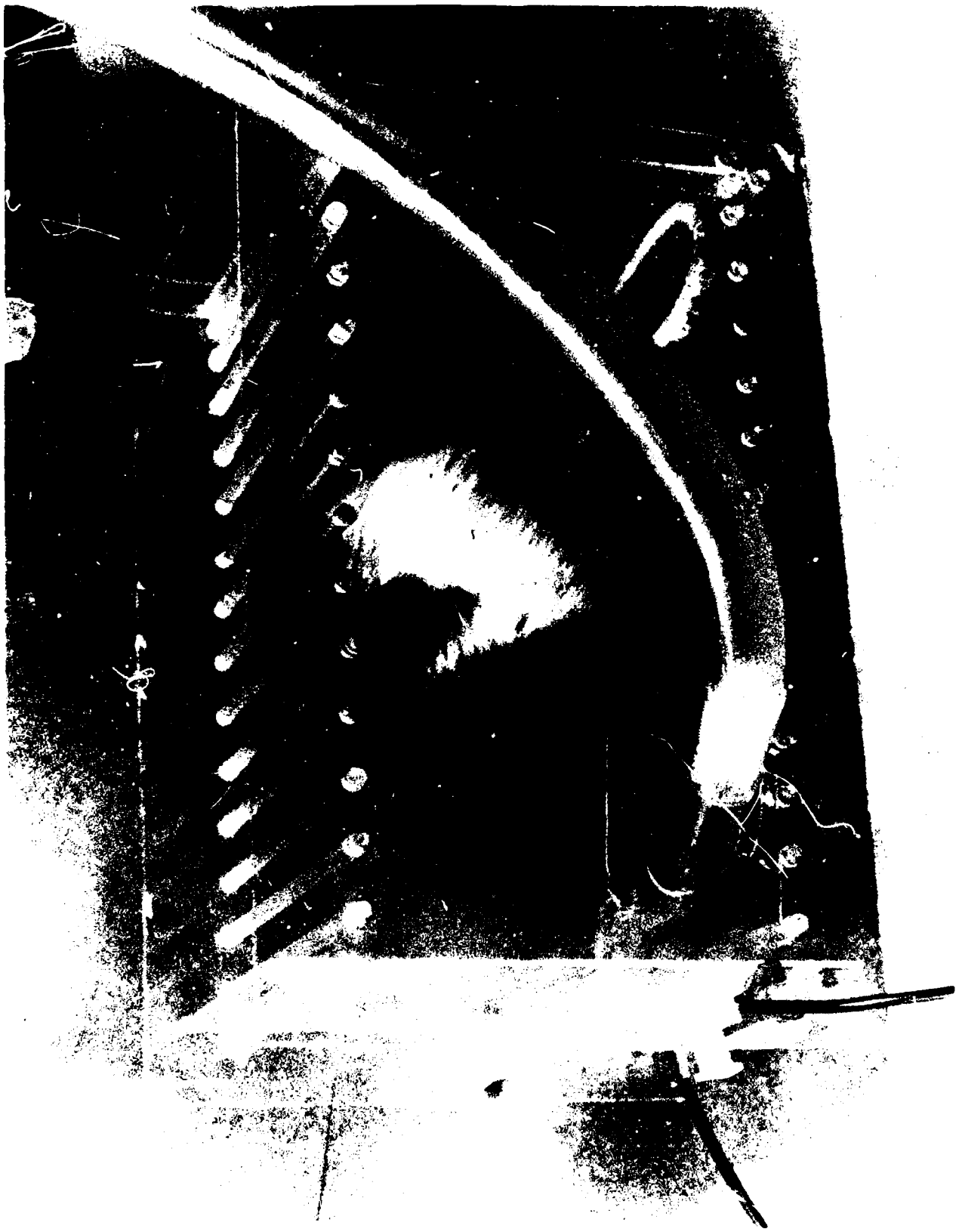


Fig. 14. Plexiglas rat holder with response lever and pellet tube.

anesthetized with Nembutal (45 mg/kg). The LCOF temperature probe¹⁰ was placed 7 cm in the colon of each rat. The rats were individually irradiated once to 400, 500, 600, or 700 MHz, 10 mW/cm^2 E₁₁ field intensities, for ten minutes. Temperature rise of the colonic area was recorded using the LCOF temperature probe and a Hewlett-Packard stripchart recorder. The results of this experiment are presented in Table 7. The average α values indicate an enhanced absorption of energy at 600 MHz $[0.67 \text{ (mW/gm)}/(\text{mW/cm}^2)]$ compared with 400 $[0.39 \text{ (mW/gm)}/(\text{mW/cm}^2)]$, 500 $[0.46 \text{ (mW/gm)}/(\text{mW/cm}^2)]$, and 700 MHz $[0.50 \text{ (mW/gm)}/(\text{mW/cm}^2)]$. These values of absorbed energy compare quite favorably with calculated power absorption for a 400 gm rat at 650 MHz $[0.60 \text{ (mW/gm)}/(\text{mW/cm}^2)]$.¹¹ Colonic temperature rise for individual rats is shown in Fig. 15. A stripchart recording of colonic temperature rise is presented for each of the frequencies studied to date (400, 500, 600, 700 MHz). Visual inspection of each recording shows that the temperature rise during irradiation seems a linear function. Use of 10 mW/cm^2 field intensities is adequate to demonstrate the resonance phenomenon in Long Evans rats. We will, however, continue the dosimetric measurements using higher field intensities and whole body calorimetry.

15. Three experiments have been completed to investigate thyroid (T_4) response to resonant electromagnetic power absorption in rats.

Table 7. Energy absorption in 400-gram Long Evans rats.

Field intensity: 10 mW/cm^2 ; anesthetized
rats 45 mg/kg. Nembutal (1)

MHz	Animal Weight (gm)	$\Delta T^\circ\text{C}$	Temperature rise		α
			Time (min.)	ml/gm	
400	1. 412	0.40°	10	2.737	0.2737
	2. 395	0.55°	10	3.83	0.3830
	3. 385	0.73°	10	5.09	0.5090
	4. 392	0.59°	10	4.11	0.4110
	\bar{X} 396	0.57°		3.94	0.3939
	SD 11.5	0.14°		0.97	0.0967
500	1. 418	0.77°	10	5.360	0.5360
	2. 414	0.45°	10	3.140	0.3140
	3. 398	0.75°	10	5.230	0.5230
	4. 408	0.71°	10	4.950	0.4950
	\bar{X} 409.5	0.67°		4.67	0.4670
	SD 8.7	0.15°		1.03	0.1034
600	1. 380	1.23°	10	8.569	0.8569
	2. 370	0.76°	10	5.295	0.5295
	3. 428	0.90°	10	6.271	0.6271
	4. 412	0.98°	10	6.830	0.6830
	\bar{X} 397.5	0.97°		6.740	0.6740
	SD 27.1	0.20°		1.370	0.1370
700	1. 409	0.83°	10	5.78	0.5780
	2. 420	0.45°	7	4.48	0.4480
	3. 404	0.57°	10	3.97	0.3970
	4. 380	0.85°	10	5.92	0.5920
	\bar{X} 403.3	0.68°		5.04	0.5038
	SD 16.9	0.20°		0.96	0.0963

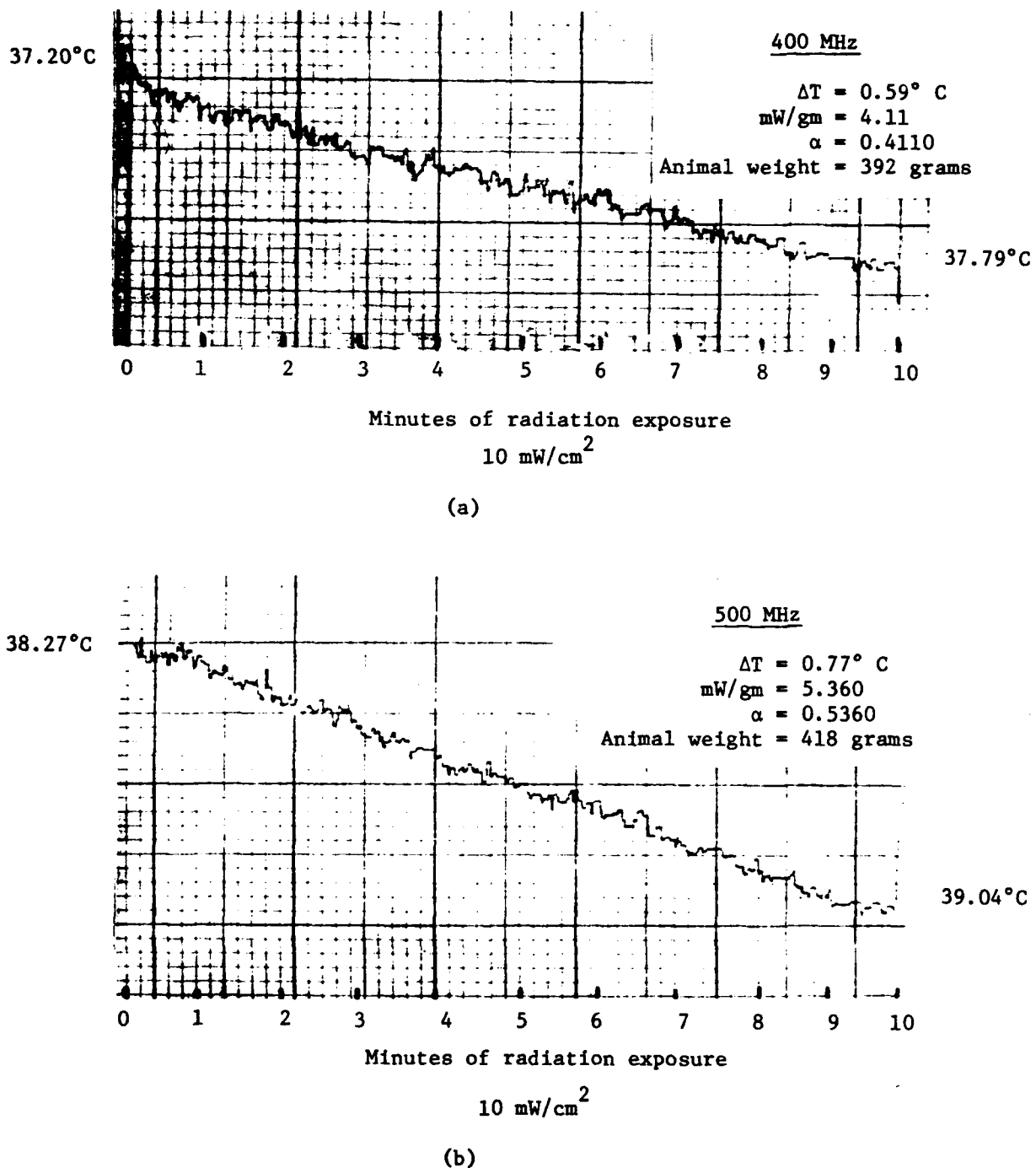


Fig. 15. Rat colonic temperature rise during irradiation at 400, 500, 600, and 700 MHz (10 mW/cm^2).

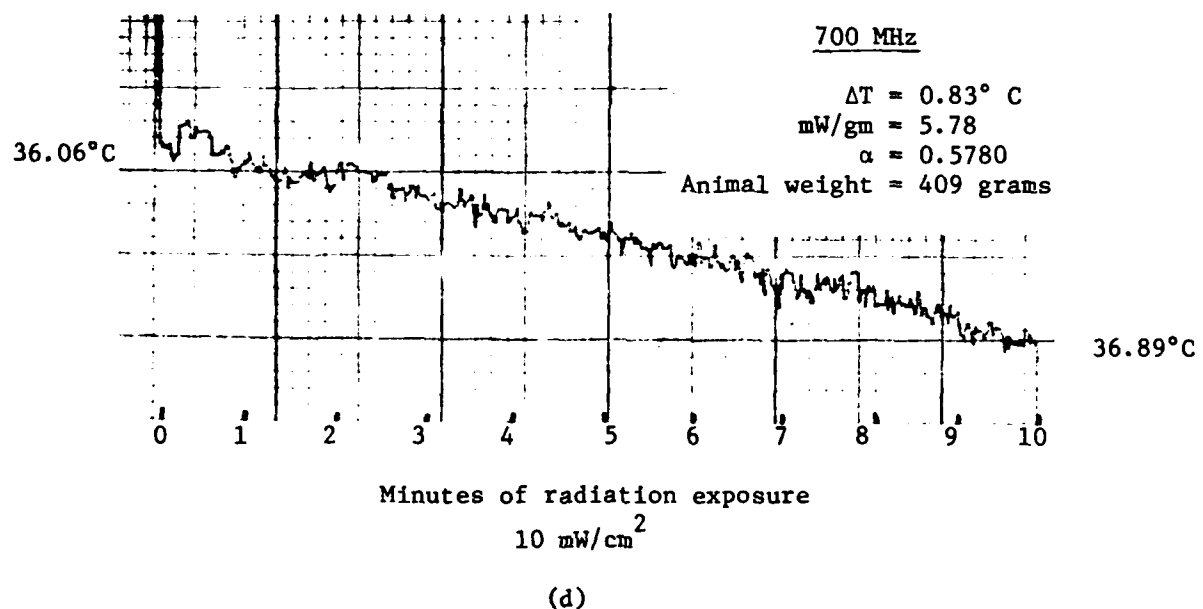
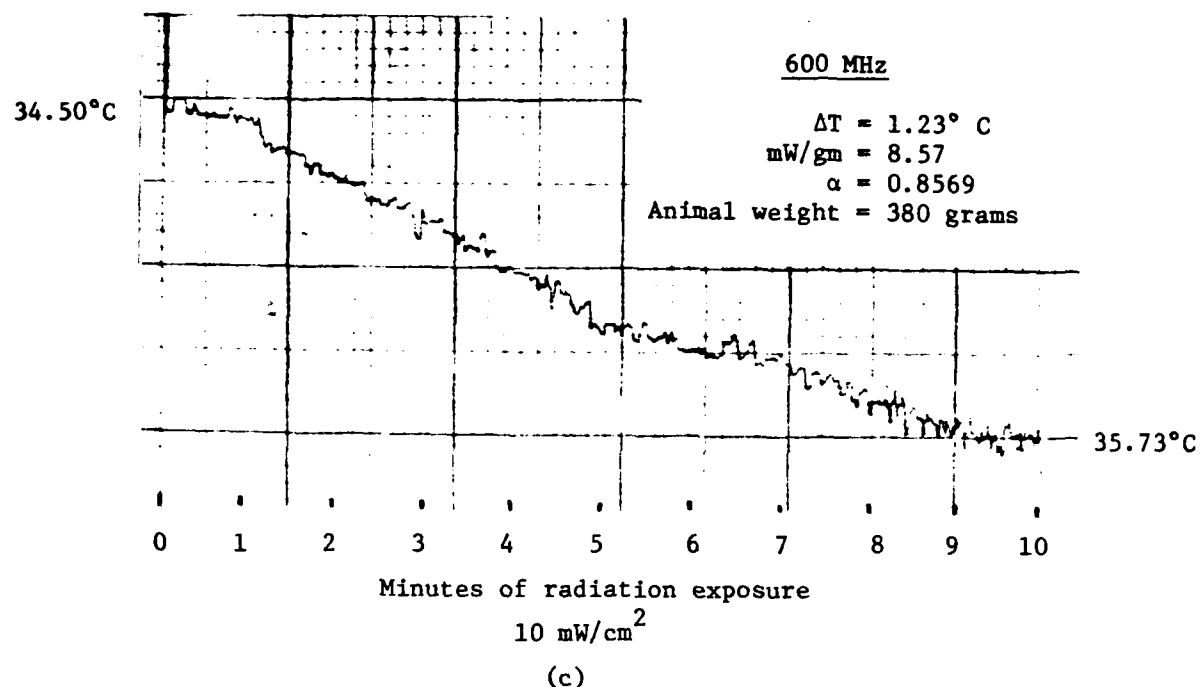


Fig. 15 (continued).

The first experiment was designed to investigate the effect of short duration chronic exposure of rats to low level radiation at the resonance frequency. Four Long Evans rats (30-40gms body weight) were exposed to 500 MHz at 23.85 mW/cm² radiation at E_{||}L orientation in the parallel plate radiation chamber. Exposures were 15 minutes duration, daily, five days per week for three weeks. Colonic temperature measurements were made with a BAT-8 digital electronic temperature probe before and after each radiation exposure. Average colonic temperature rise data during irradiation and sham irradiation are presented in Table 8.

Table 8. Average weekly temperature rise during irradiation and sham irradiation.

	Week 1		Week 2		Week 3	
	Radiated Animals	Sham Animals	Radiated Animals	Sham Animals	Radiated Animals	Sham Animals
ΔT Mean °C	2.03	1.07	2.21	0.99	1.26	0.99
Standard Deviation °C	0.51	0.46	0.65	0.46	0.47	0.46

Four rats in the same weight range underwent identical handling procedures and 15-minute confinement in the radiation chamber. All animals were housed within the radiation chamber in the styrofoam holder B shown in Fig. 12. Blood samples were drawn from all animals under ether anesthesia by tail snip at the

start of the study (baseline) and at the end of each week. All samples were drawn at approximately the same time of day. T_4 levels were analyzed by Beckman radiimmuno assay. The mean and standard deviations of $\mu\text{g} T_4 \text{ per ml}$ are presented in Fig. 1a. The results shown suggest no alteration in T_4 levels due to repeated short-term radiation exposure. The data were analyzed by repeated measures analysis of variance.¹² The results of this test indicate no significant difference between the control and irradiated animals ($P > .10$). There was a difference across weeks ($P < .01$) which was significant. This difference was most likely due to the low measured values of T_4 on week 2. Since the values for control animals were also low, it seems evident that this change is due not to microwave exposure but perhaps to some other factor such as stress during the time the exposures were carried out.

In the above study, blood samples were drawn 2 to 4 hours after radiation exposure and under ether anesthesia. Two additional studies were conducted to:

- a. Withdraw blood both as soon as possible and at extended times after a single radiation exposure.
- b. Collect blood samples by a method least stressful to the animal.

Toward this goal twenty-six Long Evans rats (380-430 gms body weight) had, under Nembutal anesthesia, in-dwelling catheters

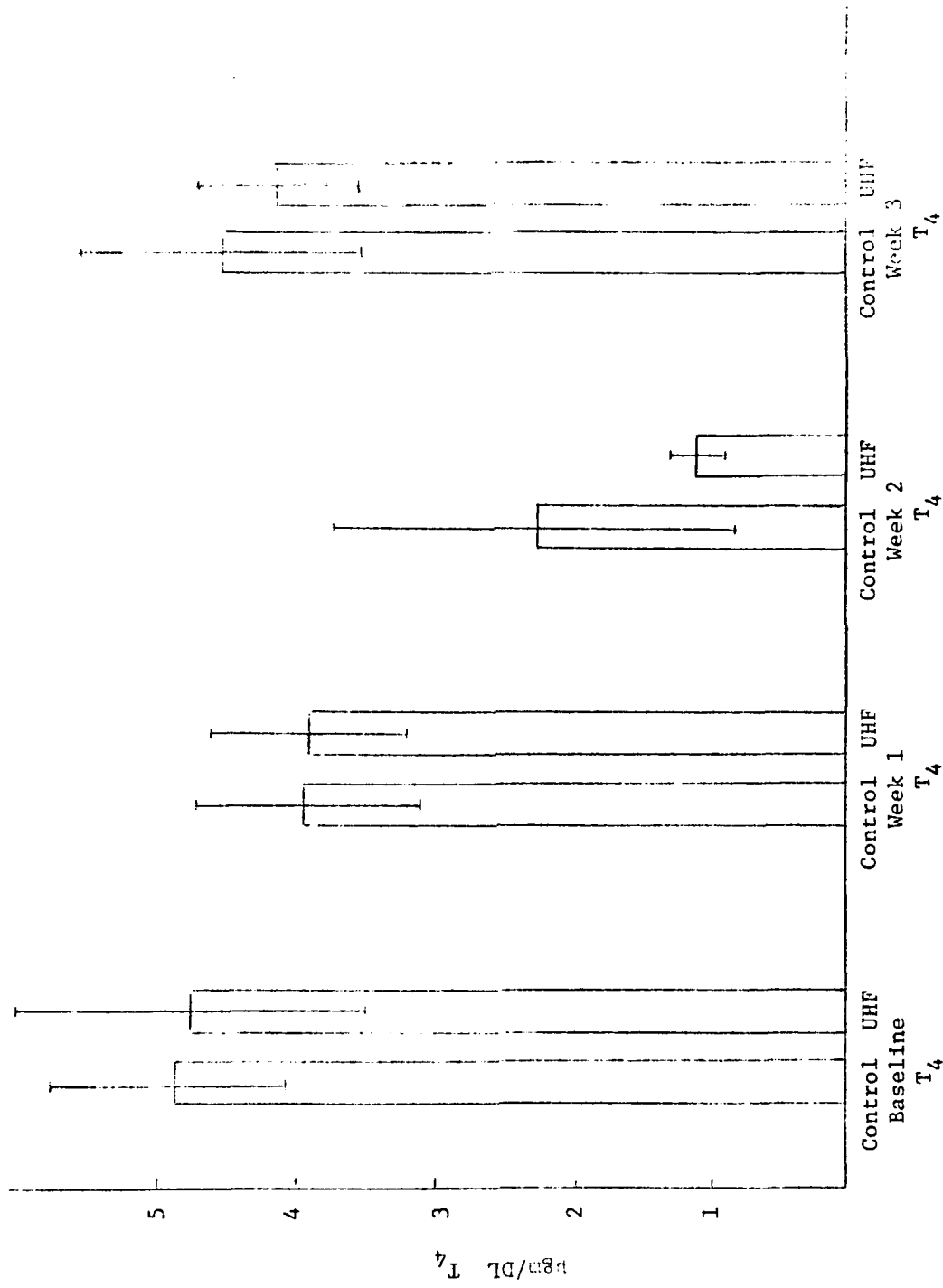


Fig. 16. T_4 levels of control and UHF radiated rats.

placed in the femoral artery of the right leg. The catheters were drawn subcutaneously up to the dorsal surface of the neck and sutured in place. All animals utilized skin catheters (22 gauge) (Becton Dickinson, Inc., Franklin Lakes, NJ, U.S.A.). Each experiment began 3 to 5 days after surgery.

To determine the effect of resonance frequency radiation on thyroid function (T_4 release), seventeen animals were divided into five groups. A blood sample (.4 ml) was withdrawn from each of the seventeen animals and was considered a baseline value. Each group of animals was then exposed once to 600 MHz radiation in $\vec{E} \parallel \vec{L}$ orientation at 100 (N = 3), 75 (N = 4), 50 (N = 4), and 25 (N = 2) mW/cm^2 , respectively, for five minutes. The fifth group underwent sham irradiation procedures. All radiation exposures were done in the monopole-above-ground radiation chamber immediately after the withdrawal of blood for a baseline value. During irradiation and sham irradiation within the monopole-above-ground chamber, rats were housed in the Plexiglas holder (Fig. 13) described in this report. Additional samples were drawn from the animals at 15 and 90 minutes after the initial baseline sample was drawn. Average body temperature rise during radiation and sham irradiation is presented in Table 9. All blood samples were analyzed for T_4 by Pantex radioimmuno assay of thyroxine. The results of this analysis are presented in Fig. 17. Examination of these data

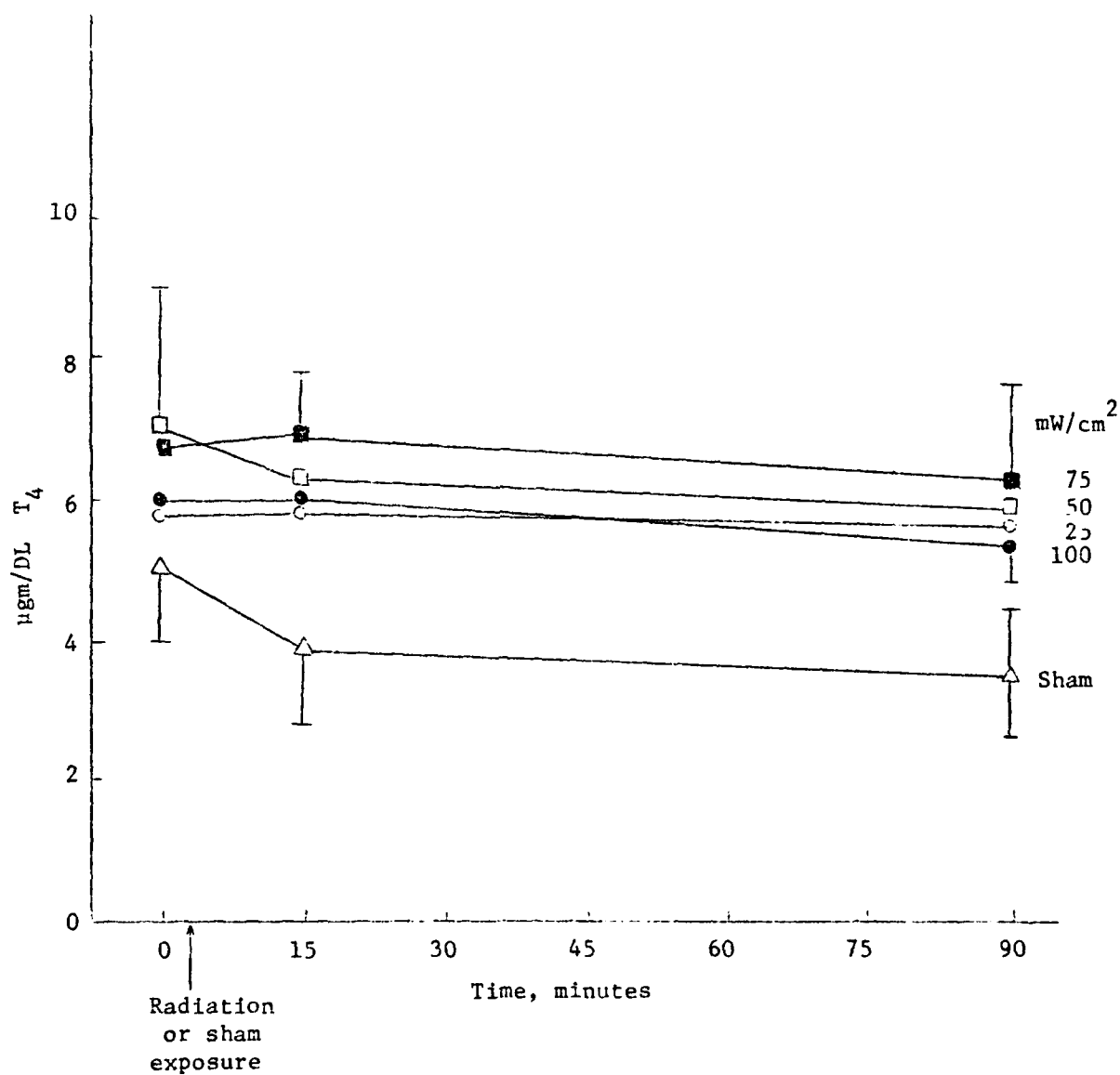


Fig. 17. Thyroxine (T_4) response to 600 MHz radiation. (Standard deviations are not shown overlapping.)

Table 9. Average colonic temperature rise during radiation and sham irradiation.

	Group I 100 mW/cm ² (N = 5)	Group II 75 mW/cm ² (N = 4)	Group III 50 mW/cm ² (N = 4)	Group IV 25 mW/cm ² (N = 2)	Group V Sham Radiation (N = 4)
ΔT Mean °C	3.10	1.90	1.20	0.57	0.29
Standard Deviation °C	0.51	0.41	0.14	0.10	0.28

again reveals little effect of low or high intensity resonant radiation exposure on thyroxine (T_4) levels.

To determine any long term effects of short duration irradiation, the remaining nine animals were divided into two groups. Five animals were exposed to 600 MHz radiation for five minutes at 100 mW/cm² and four animals underwent sham irradiation procedures as in the above study. Average body temperature rise during radiation and sham irradiation is presented in Table 10.

Table 10. Average colonic temperature rise during radiation and sham irradiation.

	Group I 100 mW/cm ²	Group II Sham Irradiation
ΔT Mean °C	2.92	0.23
Standard Deviation	0.66	0.13

Baseline blood samples were drawn as in the above study. Irradiation samples were drawn from the nine rats at 6, 14, 48, and 168 hours after the baseline sample. All samples were again analyzed for T_4 by Parke radioassay as % of thyroxine. The results of this analysis, Fig. 18, again reveal little effect of resonant radiation exposure on T_4 response in the rat as compared to sham irradiated animals.

In the three studies described above, there is a gradual decrease in T_4 with time. This effect, however, appears for both irradiated and sham irradiated animals. Animals of the first experiment subjected to repeated exposure of low level radiation (23.85 mW/cm^2) did appear very docile and lethargic upon handling compared to the sham irradiated controls. This may have been due to the daily thermal load to which the animals were subjected. This effect was not observed for animals of the second and third experiments. Nevertheless, the gradual decrease in T_4 appears to be due not to microwave exposure but rather to some other factor. Although the evidence is by no means conclusive, it seems apparent, under the experimental conditions used, that no direct effects of resonance frequency irradiation on thyroid function were observed in the adult rat.

16. Experiments have recently been completed to determine the effect of resonant and nonresonant electromagnetic power absorption on rats performing a lever-pressing task on a variable

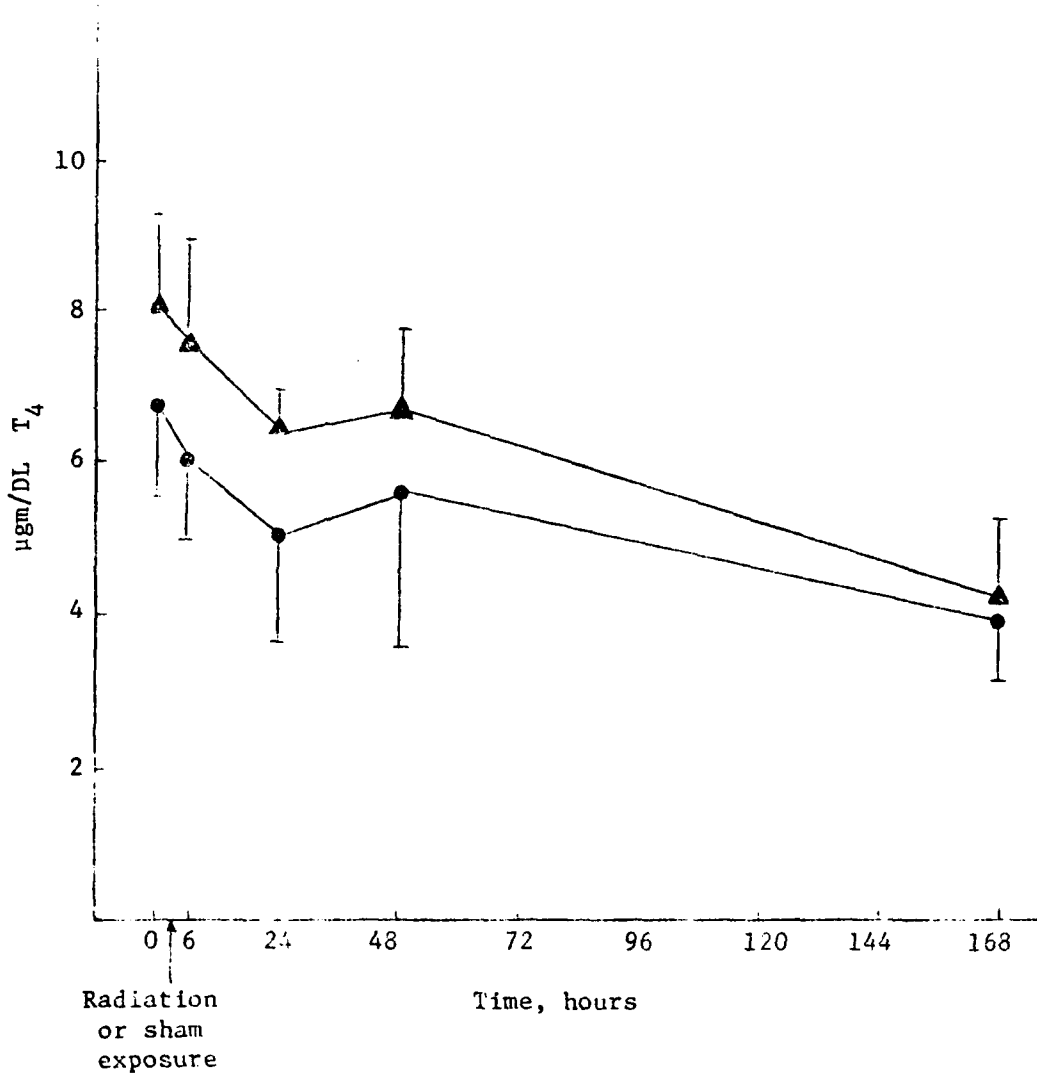


Fig. 18. Thyroxine (T₄) response to 600 MHz radiation. (Standard deviations are not shown overlapping.)

interval (30-second) reinforcement schedule. Eleven male adult (120-450 grams in body weight) were trained to perform a lever-pressing task in an "8-arm" response chamber in the manner described in radiation chamber. Five rats were individually and randomly exposed to 400, 500, 600, and 700 MHz CW radiation at 20 mW/cm^2 field intensity with the length of the animal parallel to the electric fields. All radiation exposures produced behavioral deficits. The suppression of behavior was greatest for exposures to 600 MHz radiation. The six remaining rats were exposed to 600 MHz CW radiation at field intensities of 5, 7.5, 10, and 20 mW/cm^2 while performing the behavioral task. The exposures at 20 and 10 mW/cm^2 produced suppression of behavior, while exposures at 5 and 7.5 mW/cm^2 showed no measurable effect on performance. In addition some rats were exposed to pulsed 600 mHz radiation (1000 pps at 3 and 30 microsecond pulse durations). Pulsed radiation conditions showed no measurable effect on rat performance. The data show that the resonant frequency of power absorption for the adult Long Evans rat is 600 MHz, while suppression of VI-30 second responding, due to short-term radiation exposure, requires a field intensity of 10 mW/cm^2 or greater. A copy of this paper (submitted to *Radio Science* for editorial review) is attached as Appendix G.

Papers Published or Presented, Meetings Attended

1. O. P. Gandhi, "Frequency and Orientation Effects on Unstressed Animals to Electromagnetic Waves", *IEEE Transactions on Biomedical Engineering*, Vol. BME-22, November 1975, pp. 536-542.
2. O. P. Gandhi, "Conditions of Strongest Electromagnetic Power Deposition in Man and Animals", *IEEE Transactions on Microwave Theory and Techniques*, Vol. MIT-23, December 1975, pp. 1021-1029.
3. J. A. D'Andrea, O. P. Gandhi, and R. Kesner, "Behavioral Effects of Resonant Electromagnetic Power Absorption in Rats", *1975 USNC/URSI Meeting Digest of Technical Papers*. Complete paper to be published in the proceedings of the series on Microwave Biological Effects.
4. O. P. Gandhi, K. Sedigh, G. S. Beck, and E. L. Hunt, "Distribution of Electromagnetic Energy Deposition in Models of Man with Frequencies Near Resonance", *1975 USNC/URSI Meeting Digest of Technical Papers*, p. 201; complete paper to be published in the proceedings of the series on Microwave Biological Effects.
5. O. P. Gandhi, E. L. Hunt, and J. A. D'Andrea, "Electromagnetic Power Deposition in Man and Animals with and without Ground and Reflector Effects", *1976 USNC/URSI Meeting Digest of Technical Papers*, p. 42; complete paper to be published in the proceedings of the series on Microwave Biological Effects.
6. J. A. D'Andrea, O. P. Gandhi, and J. L. Lords, "Behavioral Effects of Resonant Electromagnetic Energy Absorption in Rats", *1976 USNC/URSI Meeting Digest of Technical Papers*, p. 93; complete

paper to be published in the proceedings of the series on Microwave Biological Effects.

7. M. J. Hagmann and O. P. Gandhi, "Parameters for Numerical Biological Effects using a 2-D Uniform SISO Array with Constant Incident Intensity", *1976 USNC/URSI Meeting Digest of Technical Papers*, p. 66; complete paper to be published in the proceedings of the series on Microwave Biological Effects.
8. O. P. Gandhi and K. Sedigh, "Biological Phantom Materials for Simulating Man at Different Frequencies", *1976 USNC/URSI Meeting Digest of Technical Papers*, p. 40.
9. M. J. Hagmann, O. P. Gandhi, and C. H. Durney, "Upper Bound on Cell Size for Moment-Method Solutions with Hard Scatterers", submitted for publication to *IEEE Transactions on Microwave Theory and Techniques*.
10. M. J. Hagmann, O. P. Gandhi, and C. H. Durney, "Procedures for Improving Convergence of Moment-Method Solutions in Electromagnetics", submitted for publication to *IEEE Transactions on Antennas and Propagation*.

Papers in Preparation

1. O. P. Gandhi and E. L. Hunt, "Electromagnetic Absorption in Man and Animals with and without Ground Effects", to be submitted for publication to *IEEE Transactions on Microwave Theory and Techniques*.
2. O. P. Gandhi and E. L. Hunt, "Enhancement in Electromagnetic Power

Deposition for Man and Animals in the Presence of Reflecting Surfaces", to be submitted for publication to *IEEE Transactions on Nuclear Science and Radiation Physics*.

3. J. A. D'Andrea, O. P. Gandhi, M. J. Heggemann, and K. L. Hunt, "Pruska Response Cage for Rats Used in Biobehavioral Microwave Radiation Research", to be submitted for publication to *Journal of Microwave Power*.

REFERENCES

1. E. C. Jordan and K. C. Balmain, *Electromagnetic Waves and Radiating Systems*, Prentice-Hall, Inc., Englewood Cliffs, New Jersey, 1973, pp. 335-338.
2. H. Jasik, *Antenna Design Handbook*, McGraw-Hill Book Company, New York, 1961, p. 11-3.
3. H. Dreyfuss, *The Measure of Man, Human Factors in Design*, Whitney Library of Design, New York, 1967.
4. O. P. Gandhi, K. Sedigh, G. S. Beck, and E. L. Hunt, "Distribution of Electromagnetic Energy Deposition in Models of Man with Frequencies Near Resonance", *1975 USNC/URSI Meeting Digest of Technical Papers*, p. 201. Complete paper to be published in the proceedings of the series on Microwave Biological Effects.
5. H. Massoudi, C. H. Durney, and C. C. Johnson, "Theoretical Calculations of Power Absorbed by Monkey and Human Spheroidal and Ellipsoidal Phantoms in an Irradiation Chamber", *1975 USNC/URSI Meeting Digest of Technical Papers*, p. 199. Complete paper to be published in the proceedings of the series on Microwave Biological Effects.
6. A. C. Guyton, *Textbook of Medical Physiology*, W. B. Saunders Company, Philadelphia, 1968.
7. John Schrot and T. D. Hawkins, "Microwave Frequency and E-Field Orientation Interact with Animal Size", *1975 USNC/URSI Meeting Digest of Technical Papers*, p. 233; complete paper to be published in the proceedings of the series on Microwave Biological Effects.

8. K. M. Chen and B. S. Guru, "Induced EM Field and Absorbed Power Density Inside Human Tissues by 1 to 500 MHz EM Waves", Technical Report No. 1, SF Center EM 74-10 (April) 1976.
9. S. F. H. Hwang, "Electromagnetic Radiation and Human Health", New York, 1968.
10. C. C. Johnson, G. H. Durney, J. L. Lords, and G. K. Livingston, "Fiberoptic Liquid Crystal Probe for Absorbed Radio Frequency Power Temperature Measurement in Tissue During Irradiation". In Paul Tyler (Editor), "Biologic Effects of Nonionizing Radiation", *Annals of New York Academy of Sciences*, 1975, Vol. 247, pp. 527-532.
11. P. W. Barber, "Electromagnetic Power Deposition in Prolate Spheroid Models of Man and Animals at Resonance", submitted for publication to *IEEE Transactions on Biomedical Engineering*.
12. B. J. Winer, *Statistical Principles in Experimental Design*, McGraw-Hill Book Company, New York, 1971, pp. 514-599.

APPENDIX A

BIOLOGICAL PHANTOM MATERIALS FOR SIMULATING MAN AT DIFFERENT FREQUENCIES

Om P. Gandhi and Kazem Sedigh
Departments of Electrical Engineering and Bioengineering
University of Utah, Salt Lake City, Utah

Abstract

The paper gives compositions of biological phantom materials for simulating man over the frequency range 13-230 MHz (including the important resonance regions of 31 and 65 MHz). These materials have been developed to fill eight proportionately scaled man-shaped cavities of height 7.6-40.6 cm for dosimetric measurements at 300, 400, 600, 915, and 985 MHz. Complex permittivity (ϵ_c) measurements at the irradiation frequencies were made using a modified version of the coaxial line method used previously by Guy. Models reduced by β in all dimensions allow simulation of man at frequencies given by $(\text{experimentation frequency})/\beta$, provided materials with ϵ_c at the (lower) simulated frequencies are used. Whole-body "average" values of ϵ_c at simulated frequencies were first calculated on the basis of 65 percent muscle and tissues of high water content and 35 percent fat, bone, and tissues of low water content from extrapolated values for these tissues from Johnson and Guy's article. Several compositions of salt, polyethylene powder, Superstuff, and water were first measured for ϵ_c 's at the six experimental frequencies. Interpolated compositions were then measured and modified, if necessary, for desired permittivities.

Paper presented at the 1976 URSI meeting, Series on Biological Effects of Electromagnetic Waves, October 10-15, University of Massachusetts, Amherst.

BIOLOGICAL PHANTOM MATERIALS FOR SIMULATING
MAN AT DIFFERENT FREQUENCIES

Om P. Gandhi and Kazem Sedigh
Departments of Electrical Engineering and Bioengineering
University of Utah, Salt Lake City, Utah

Introduction

An important aspect of electromagnetic wave biological-effects research is the quantification of absorbed dose and its distribution in biological systems. For humans the experimentation may be done by using either the full scale or reduced scale models that use materials having the same complex permittivity $\epsilon_c = (\epsilon_r - j\sigma/\omega\epsilon_0)$ as that of the system that is to be simulated.

For whole body exposure situations, reduced scale models are preferred for convenience of handling. From electromagnetic field theory, a body reduced by a factor of β in all dimensions may be used to obtain absorption characteristics of the full body, provided an irradiation frequency scaled up by a factor of β is used. For distribution of power deposition, high field intensities on the order of $50-150 \text{ mW/cm}^2$ are generally needed to prevent the pattern from being smeared by heat diffusion. A limitation often encountered is that the high power sources needed for experimentation are not very widely alterable in their operation frequencies. Use of carefully proportioned different size models at a given experimental frequency may

Paper presented at 1976 USNC/URSI meeting, Amherst, Massachusetts,
October 11-15, 1976.

therefore be used to simulate man at frequencies given by (experimental frequency)/ β . It is necessary, however, that for such experiments the complex permittivity for the mixtures used in the various models be different and have the values corresponding to the values for man at the reduced frequency that is being simulated. With these scaling precautions, the distribution of power deposition in the reduced-scale model is identical (though the magnitudes are higher by a factor of β) to that of the full-scale body.

To simulate lower frequencies where wavelengths are considerably larger than the dimensions of individual parts of the body, whole body "average" values may be used for the ϵ_c 's of the homogeneous filler media. This is a valid procedure to frequencies on the order of 200-300 MHz. At higher frequencies a more detailed representation of the body is, however, needed. Different compositions of biological-phantom materials should then be used to simulate the "average" electrical properties of individual parts of the body. It is fortuitous that at such frequencies the depth of penetration in the torso^{*} is on the order of a few centimeters,¹ and only the compositions of the top layers may therefore be considered to calculate the "average" ϵ_c . For legs, arms, head, etc., a more careful determination of ϵ_c may be in order, based in the first instance on the distribution of power deposition as though these parts were isolated from the rest of the

* While detailed power distributions in the torso are not known and this assumption may indeed need to be justified, the previous experiments with spherical targets¹ also showed that the penetration of waves at larger frequencies [$\lambda \leq$ diameter d] was superficial in nature.

body.

For near-field or part-body exposure situations, full scale models ($\beta = 1$) are quite convenient and may therefore be preferred. Experiments of this type are often needed in arriving at the optimum design for applicators.

Materials and Methods of Procedure

As described above it is necessary to develop biological-phantom mixtures for complex permittivities at the experimental frequencies that simulate man at lower frequencies. For available experimental frequencies of 300, 400, 600, 915, and 985 MHz, the ϵ_c 's needed for eight proportionately scaled man-models have been calculated and are given in Table 1 for an illustrative case of 600 MHz. Corresponding numbers have been calculated for the remaining four frequencies and require ϵ_r 's varying between 35 and 105 and σ varying between 2.3 and 14 mho/m.

Using the homogeneous compositions developed here, it should be possible to obtain dosimetric measurements for man over the frequency region 13-230 MHz, which includes the important resonance regions^{2,3} of 33 and 65 MHz.

Nine mixtures of compositions given in Table 2 were measured at the five experimental frequencies, using the arrangement⁴ of Fig. 1. A slotted coaxial line (General Radio type 874 LB) was filled with the respective mixtures and used to measure the attenuation constants α and propagation constants β through the media with the help of the

Table I. Calculation of the electrical properties
needed of the biological phantom material.

Experimental frequency = 600 MHz

Model size inches	Scaling factor for 1.75 m man	Simulated frequency MHz	Muscle, skin, and tissues with high water content	Fat, bone, and tissues with low water content	Whole body "average"	Conductivity σ for reduced scale model mho/m
			ϵ_r	σ mho/m	ϵ_r	σ mho/m
3	23.0	26.1	115.8	0.61	20.0	0.03
4	17.2	34.8	104.1	0.66	16.9	0.03
5	13.8	43.5	96.1	0.70	14.3	0.03
6	11.5	52.3	92.3	0.73	13.2	0.03
8	8.6	69.7	84.8	0.79	11.1	0.05
10	6.9	87.1	77.3	0.85	9.0	0.05
13	5.7	113.2	69.7	0.94	7.25	0.05
15	4.9	139.3	65.7	1.04	6.86	0.06

* Whole body "average" computed on the basis of 65 percent muscle, skin, and tissues with high water content and 35 percent fat, bone, and tissues with low water content.

Table 2. The compositions of the nine mixtures used for measurements of dielectric properties.

Mixture	Percent by Weight			
	H ₂ O	NaCl	SS*	PEP**
I	75	13.0	12.0	0
II	75	11.1	7.9	6.0
III	75	9.8	8.2	7.0
IV	75	9.0	8.0	8.0
V	75	5.45	10.55	9.0
VI	75	4.45	10.55	10.0
VII	75	4.0	10.5	10.5
VIII	75	3.9	10.1	11.0
IX	75	2.0	10.0	13.0

* Superstuff -- A gelling agent, obtained from Whamo Manufacturing Company, San Gabriel, California.

** Polyethylene powder -- obtained from Wedco, Inc., California.

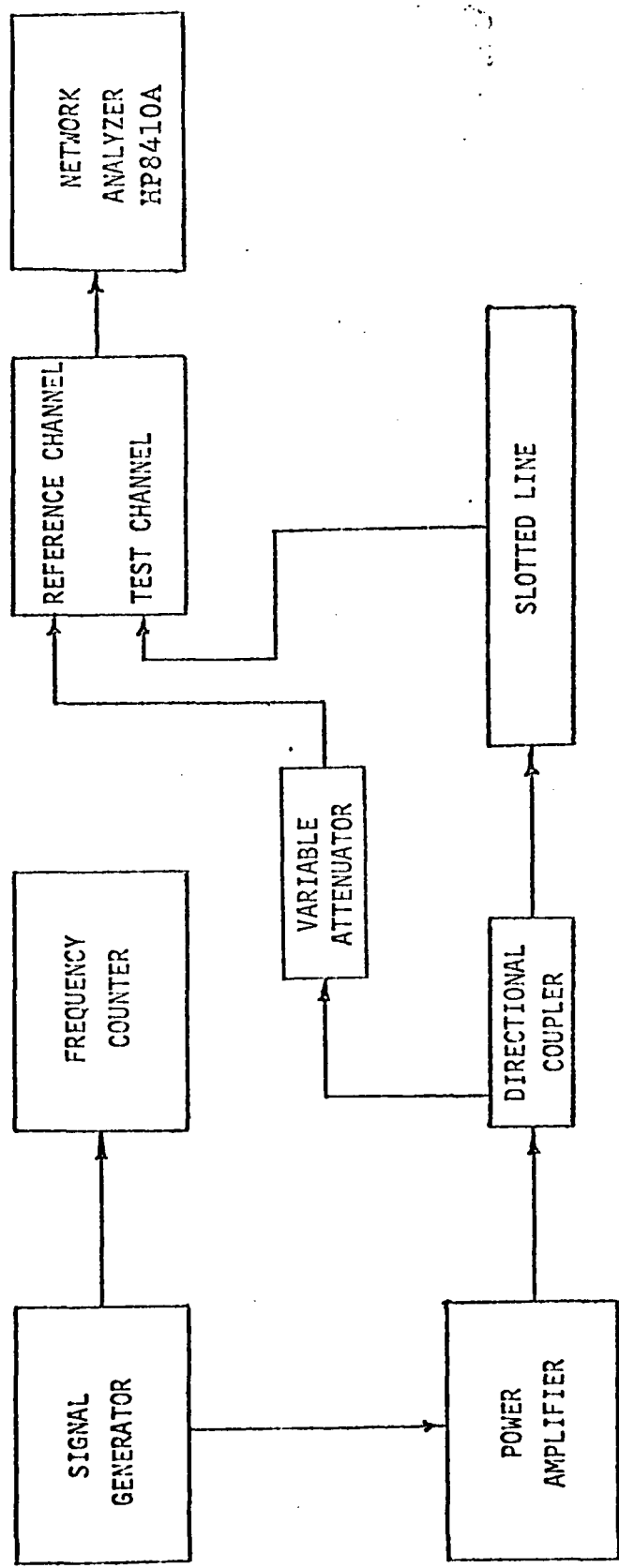


Fig. 1. Block diagram of the setup for coaxial slotted line measurement of complex permittivity.

Hewlett-Packard network analyzer model 8410A. Due to the high loss of the materials, measurements were taken at 0.2 cm intervals and 4 to 6 readings were used for the calculations of α and β . In order to find ϵ_r and σ of the materials, the following equations⁵ were used:

$$\beta = \frac{\omega}{c} \sqrt{\frac{\epsilon_r}{2} (G + 1)} \quad (1)$$

$$\alpha = \frac{\omega}{c} \sqrt{\frac{\epsilon_r}{2} (G - 1)} \quad (2)$$

where c is the velocity of light (3×10^8 meter/second) and

$$G = \frac{1 + (\alpha/\beta)^2}{1 - (\alpha/\beta)^2} = \sqrt{1 + \left(\frac{\sigma}{\omega \epsilon_0 \epsilon_r}\right)^2} \quad (3)$$

Upon rearranging the terms,

$$\epsilon_r = \frac{2(\alpha/(\omega/c))^2}{G - 1} \quad (4)$$

and

$$\sigma = (G^2 - 1)^{1/2} \omega \epsilon_0 \epsilon_r = 2\alpha^2/(\omega/c)^2 \omega \epsilon_0 \sqrt{\frac{G - 1}{G + 1}} \quad (5)$$

The values of ϵ_r and σ , for the nine mixtures, measured at the five experimental frequencies are given* in Tables 3 and 4. The values of

* For these mixtures with high $\sigma/\omega \epsilon_0 \epsilon_r$, G is very much higher than unity which results in α and β being comparable in magnitude to one another. Small errors in determination of either α or β results in a much larger error in G and consequently ϵ_r . This method, though reasonably accurate for determination of σ , does not appear to be very good for ϵ_r for high loss ($\sigma/\omega \epsilon_0 \epsilon_r \gg 1$) materials.

Table 3. Values of the dielectric constant and conductivity of the various mixtures measured at frequencies 300, 400 and 600 MHz.

Mixture	300 MHz		400 MHz		600 MHz	
	ϵ_1	σ	ϵ_1	σ	ϵ_1	σ
I	63.52	14.09	71.6	12.73	51.80	15.70
II	34.25	12.05	48.72	11.74	54.65	12.90
III	21.35	11.73	67.89	9.28	53.50	12.61
IV	46.47	8.89	71.52	8.45	46.77	9.98
V	39.45	5.03	45.36	5.94	51.90	6.26
VI	64.37	5.06	58.79	4.20	55.99	5.44
VII	41.62	5.1	33.74	5.62	59.91	4.84
VIII	39.09	4.02	18.82	4.68	55.87	4.04
IX	57.82	2.59	62.11	2.25	38.64	3.29

Table 4. Values of the dielectric constant and conductivity of the various mixtures measured at frequencies 915 and 985 MHz.

Mixture	f = 915 MHz			f = 985 MHz		
	ϵ_1	σ	$\epsilon_2 = \sigma/\omega\epsilon_0$	ϵ_1	σ	$\epsilon_2 = \sigma/\omega\epsilon_0$
I	33.88	12.78	251.18	44.38	13.62	248.66
II	52.56	12.98	255.11	57.06	12.16	222.01
III	49.52	9.74	191.43	51.57	9.95	181.66
IV	43.12	9.22	181.21	47.25	9.06	165.41
V	48.36	6.01	118.12	48.56	6.82	124.52
VI	51.91	5.27	103.58	50.73	5.32	97.13
VII	62.4	4.91	96.50	63.53	5.13	93.66
VIII	52.08	4.28	84.12	48.44	4.13	75.40
IX	52.89	2.68	52.67	27.05	1.49	27.20

conductivity at different RF frequencies are plotted in Fig. 2 for different salt contents and compared with the dc⁶ and low frequency⁴ ($f = 0.1$ MHz) values. The conductivity increases linearly with the percentage of salt and is relatively independent of the frequency. For any required conductivity, therefore, a percentage of salt needed for the mixture can therefore be estimated from Fig. 2. To date we have not developed any simple relationship for ϵ_r' 's needed for the simulating media.

For simulation at lower frequencies (including the important resonance regions), $\sigma/\omega\epsilon_0$ is 2 to 4 times ϵ_r' (see e.g. Table 4) and therefore dominates the complex permittivity of the medium. Matching $\sigma/\omega\epsilon_0$ accurately with the required values while allowing a slight mismatch in ϵ_r' therefore does not cause great errors in dosimetric measurements for simulated frequencies less than about 200 MHz. This point has been confirmed by measuring distribution of absorbed energy using the liquid crystal fiber optic temperature probe⁷ for near-resonant condition ($L/\lambda = 0.417$) for free-space irradiation. The model was filled with a biological phantom material* simulant of man at 71.6 MHz. The distribution pattern scaled to values for the full scale body is

* For $L/\lambda = 0.417$ or a 5" model at 985 MHz to simulate 1.75 meter man (at 71.6 MHz), it is necessary that the complex permittivity $\epsilon_r' - j\sigma/\omega\epsilon_0$ of the filler medium be $58.4 - j130.6$, computed on the basis of 65 percent muscle, skin, and tissues with high water content and 35 percent fat, bone, and tissues with low water content. The composition used for free-space irradiation experiments (5.75 percent NaCl, 10.25 percent Superstuff, 9 percent polyethylene powder, and 75 percent water) has a measured permittivity of $49.5 - j131.7$.

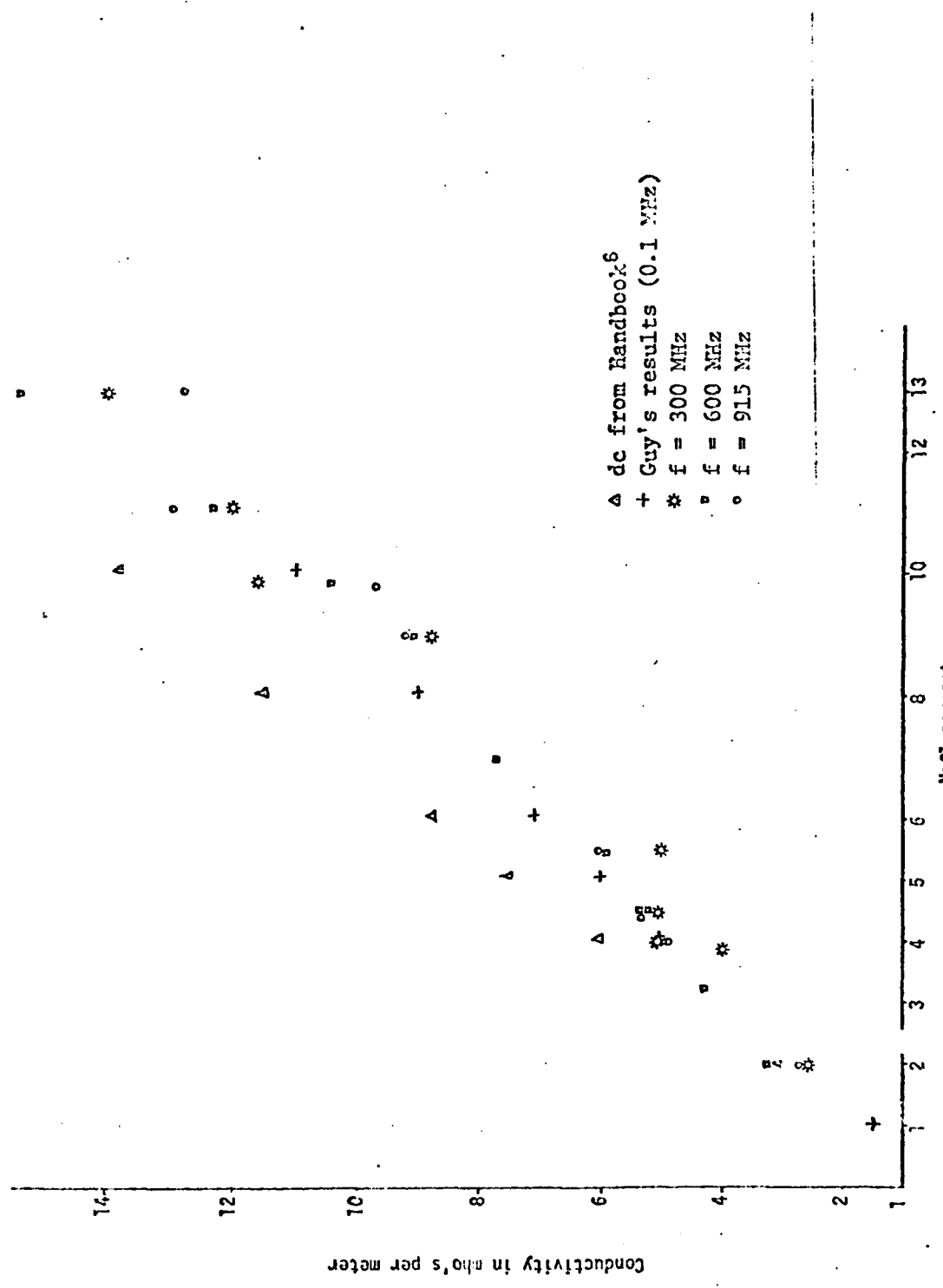


Fig. 2. Electrical conductivity of phantom materials and saline versus percentage of salt for different frequencies.

shown in Fig. 3. For free-space irradiation specific absorption rates (SAR) considerably higher than the whole-body average are observed for the neck, the legs, and the elbows, with the lower torso receiving SAR's comparable to the average value and the upper torso receiving SAR's lower than the average value. Noting that the values indicated in Fig. 3 are relative to whole-body saline-filled average, it is remarkable that the weighted average of the numbers obtained with the biological phantom mixture is not far off from one, or the value obtained with the saline-filled figurine.

Conclusions

In the foregoing we have given the measured properties of some biological-phantom mixtures for experimental frequencies to 985 MHz. From these results it is possible to obtain the salt content for a conductivity required of the biological-phantom material. Work is continuing with mixtures of different water and Superstuff contents to develop a ternary diagram that may be of help in obtaining required ϵ_r 's.

Acknowledgment

This work was supported by U. S. Army Medical Research and Development Command, Washington, D. C., under contract DAMD 17-74-C-4092.

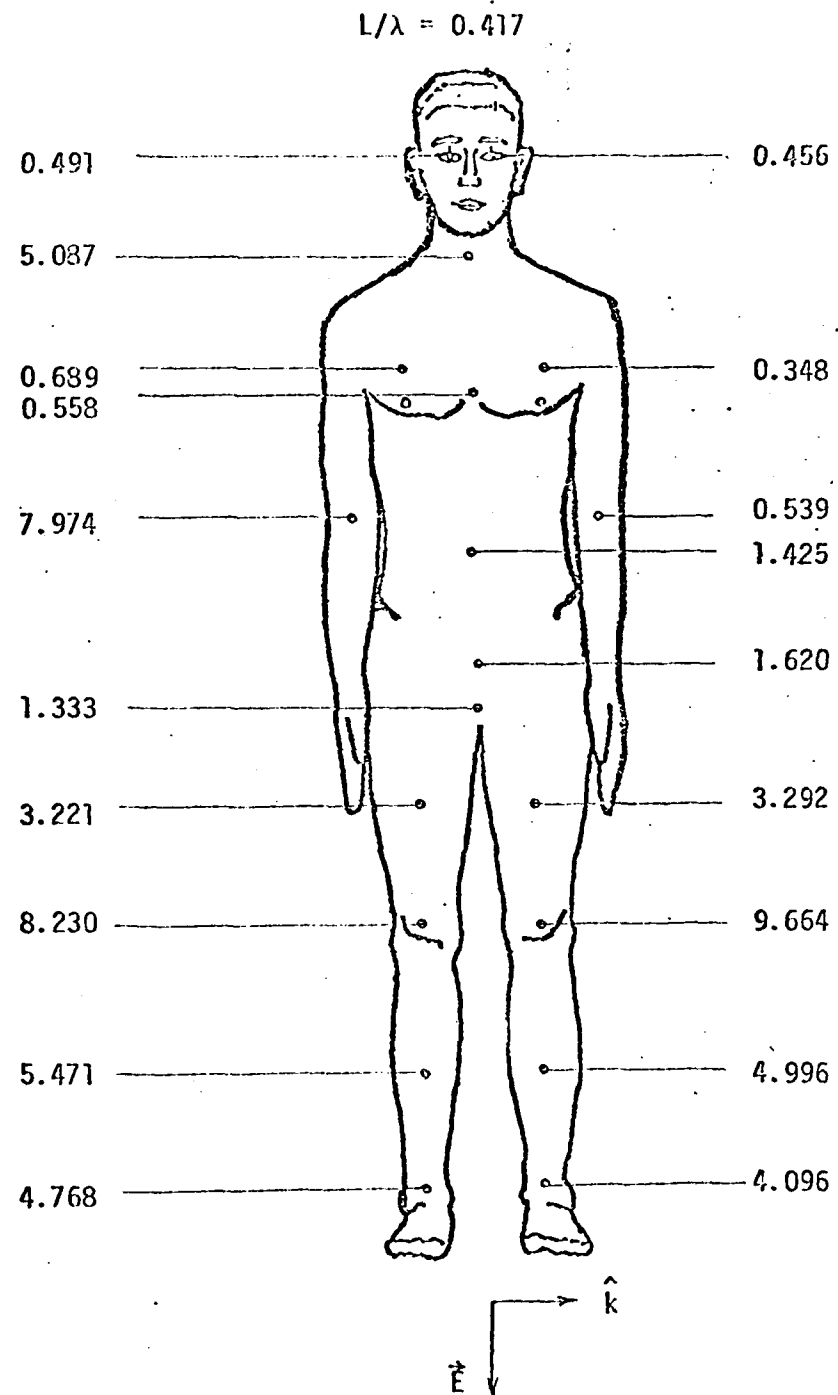


Fig. 3. Distribution of power deposition for a human in free space. The numbers indicated are relative to whole body average SAR of $(1.75/I_m) \cdot 1.88 \text{ W/kgm}$ for 10 mW/cm^2 incident fields.

REFERENCES

1. C. C. Johnson and A. W. Guy, "Nonionizing Electromagnetic Wave Effects in Biological Materials and Systems", *Proceedings of the IEEE*, Vol. 60, 1972, pp. 692-718.
2. O. P. Gandhi, "Conditions of Strongest Electromagnetic Power Deposition in Man and Animals", *IEEE Transactions on Microwave Theory and Techniques*, Vol. MTT-23, December 1975, pp. 1021-1029.
3. O. P. Gandhi, K. Sedigh, G. S. Beck, and E. L. Hunt, "Distribution of Electromagnetic Energy Deposition in Models of Man with Frequencies Near Resonance", *1975 USNC/URSI Meeting Summary of Papers*, p. 201. Complete paper to be published in the proceedings of the series on microwave biological effects.
4. A. W. Guy, C. C. Johnson, J. C. Lin, A. F. Emery, and K. K. Kraning, "Electromagnetic Power Deposition in Man Exposed to HF Fields and the Associated Thermal and Physiologic Consequences", Report SAM-TR-73-13 prepared for U. S. A. F. School of Aerospace Medicine, Brooks Air Force Base, Texas, December 1973.
5. C. H. Durney and C. C. Johnson, *Introduction to Modern Electromagnetics*, McGraw-Hill, Inc., 1969.
6. *Handbook of Chemistry and Physics*, Chemical Rubber Publishing Company.
7. T. C. Rozzell, C. C. Johnson, C. H. Durney, J. L. Lords, and R. G. Olsen, "A Nonperturbing Temperature Sensor for Measurements in Electromagnetic Fields", *Journal of Microwave Power*, Vol. 9, 1974, pp. 241-249.

APPENDIX B

DISTRIBUTION OF ELECTROMAGNETIC ENERGY DEPOSITION IN MODELS OF MAN WITH FREQUENCIES NEAR RESONANCE

* Om P. Gandhi, Kazem Sedigh, and Cary S. Beck
Departments of Electrical Engineering and Bioengineering
University of Utah
Salt Lake City, Utah 84112

Edward L. Hunt
Department of Microwave Research
Walter Reed Army Institute of Research
Washington, D. C. 20012

ABSTRACT

Experimental results are described for whole-body absorption (for orientations $\vec{E} \parallel \vec{L}$, $\vec{E} \perp \vec{L}$, and $\vec{E} \perp \vec{L}$) of a series of saline-filled and biological-phantom figurines of major lengths (L) that varied from 0.4 to 1.5 λ . Measurements are also reported for several exposure conditions on the density of energy deposition for different regions of the body. *In the absence of ground effects*, a whole-body absorption cross section as high as 4.2 times the shadow cross section has been measured for $\vec{E} \parallel \vec{L}$ at the resonance frequency (in MHz) of $68 \times (1.75/\text{height } L_m \text{ of the human in meters})$. Under these frequency and polarization conditions, a whole-body-average energy deposition rate of $(2.15) \times (1.75/L_m)$ watts/kgm is projected for incident plane waves of 10 mW/cm^2 . The highest rate of energy deposition is observed for the neck region of the body where a value as high as 28.7 times the whole body average has been measured under conditions of $\vec{E} \parallel \vec{L}$ resonance. Maximum whole-body absorption under *grounded conditions* is observed at a frequency about one half that of the ungrounded body. For grounded resonance condition an absorption cross section as high as 14 times the shadow area has been measured. Here, while the neck is still one of the hot spots, the zone of maximum power deposition is the ankle region.

1. INTRODUCTION

We have previously [1, 2] reported on the observation of strong resonance of whole-body absorption of electromagnetic waves in biological bodies. In the absence of ground effects, highest rate of energy deposition occurs for fields polarized along the longest dimension of the body for frequencies such that the major length is on the order of 0.4 times free space wavelength (λ) of radiation. At resonance an effective absorption area of about 3-4 times the shadow cross section has been measured using saline-filled prolate spheroidal "equivalents" of man. In these prolate spheroids, a major to minor axes ratio of 6 was used. On the basis of some preliminary experiments, peak absorption, in the presence of ground effects, has been observed for frequencies one half

* Also consultant to the Division of Neuropsychiatry, Walter Reed Army Institute of Research, Washington, D. C. 20012.

as much as for bodies isolated in free space.

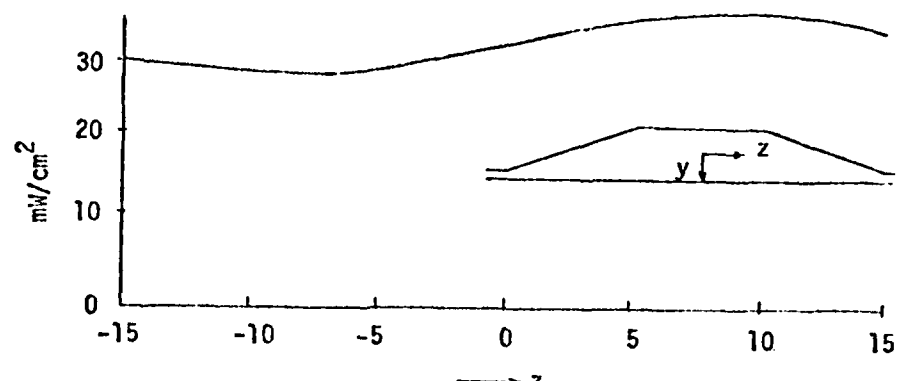
In this paper we report further results on this important phenomenon. In particular, data are presented on whole-body absorption of saline-filled figurines of major lengths L varying from 0.3 to 1.5 λ . Measurements are also reported on the distribution of power deposition in biological-phantom figurines exposed to free-space irradiation at both 985 and 2450 MHz and to fields in the TEM parallel plate [2] chamber. The results obtained under the latter irradiation conditions are shown to be remarkably similar to those with free-space radiation. The highest intensity of energy deposition in both chambers is observed for the neck region of the body. The α parameter (defined as the ratio of watts/kg of absorbed energy to mW/cm^2 of incident field intensity) for the neck region is approximately 30 times that observed for the whole-body average. Initial results are given on figurines with feet touching the ground plane of the parallel-plate chamber.

2. MATERIALS AND METHODS

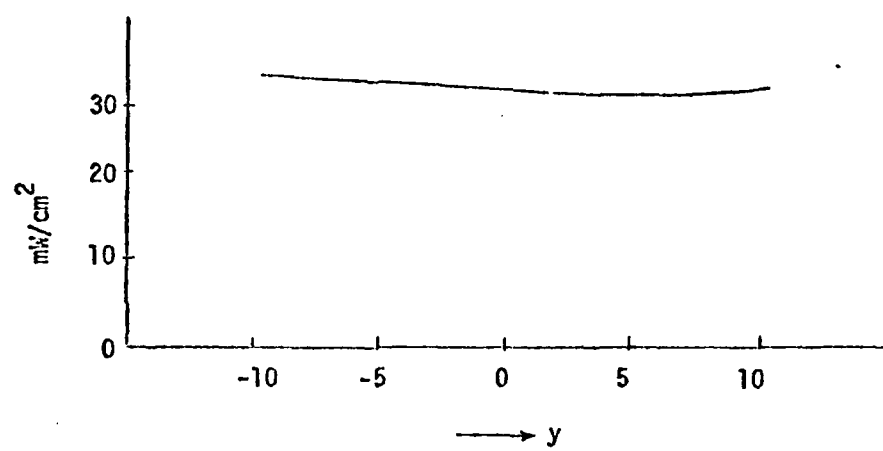
Cavities corresponding to human shapes were formed in styrofoam by using 12.1, 18.4, 22.3, and 23.5 cm tall dolls as molds. After styrofoam had been formed, the dolls were cut in half around the sagittal plane for easy removal of the molds. Three cavities, one resealed for filling with 0.9 percent saline and two for stuffing with biological-phantom materials, were formed for each of the four sizes.

Different compositions of the biological-phantom material were used to fill the figurines for parallel-plate and free-space irradiation experiments. From our previous results [1], the frequency of maximum absorption for a 1.75 meter tall human is on the order of 63-70 MHz ($L/\lambda \approx 0.37-0.4$). In order to model human for this frequency band, an "average" electrical relative permittivity ϵ_r was first calculated on the basis of 65 percent muscle, skin, and tissues with high water content and 35 percent fat, bone, and tissues with low water content. The value of ϵ_r needed for modeling for the 63-70 MHz band was calculated [3] to be $60.5 - j143$. The use of whole-body "average" ϵ_r is justified because the dimensions of individual constituents are so much smaller than the wavelength of radiation for this band. For use at 500 MHz in the parallel plate chamber, the composition of the biological-phantom material was 3.26 percent NaCl, 8.74 percent Superstuff (obtained from Whamo Manufacturing Company, San Gabriel, California), and 87.0 percent water. This has a measured [4] dielectric constant of 66 and a conductivity σ of 4.39 mho/meter . At the experimental frequency of 500 MHz, the complex relative permittivity of the material is therefore $\epsilon_r = 66 - j \sigma/\omega\epsilon_0 = 66 - j157.9$. A different composition of 8.03 percent NaCl, 13.23 percent Superstuff, and 78.74 percent water was used for free-space irradiation experiments at 985 MHz. For use at this frequency $\epsilon_r = 66 - j164.3$, once again close to the needed value of $60.5 - j143$.

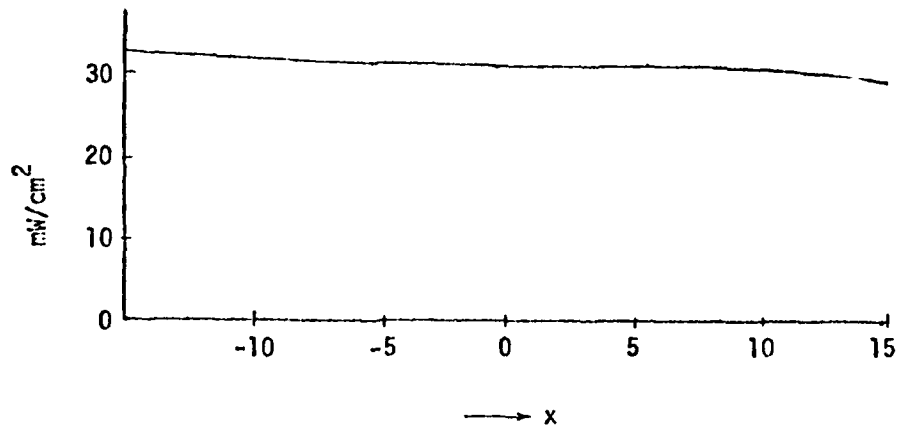
The irradiation facilities used were the parallel plate TEM chamber at 500 MHz and free-space anechoic chambers at 985 and 2450 MHz. For the parallel plate chamber [2], the working area consists of a copper plate of width 63.5 cm separated by a 25.4 cm clearance from the ground plane of 116.8 cm width. The overall transmission length of 198.2 cm is occupied by two symmetrical tapered sections of 61 cm axial length, the central working area of 61 cm length, and two 1.6 cm end sections connected to UG58/U input and output coaxial connectors. A 100 W, 200 to 500 MHz Epsco signal source was used to feed power to this chamber. The fields in the central (working) region of the chamber were mapped with a General Microwave Corporation Raham model 1 (300-18,000 MHz) field mapping probe. The variation of the field intensity in the working region is shown in Figs. 1(a), (b), and (c). The 985 and 2450 MHz free space fields were provided by Scientific Atlanta pyramidal horns radiating into the



(a)



(b)



(c)

Fig. 1. Field intensity in the parallel plate chamber at various locations of the working region (measurement frequency of 300 MHz; power input = 100 W).

respective anechoic chambers at the Department of Microwave Research, Walter Reed Army Institute of Research, Washington, D. C.

The whole body power absorption was obtained from the temperature rise of saline-filled figurines. The temperature before and after irradiation was measured with a digital thermometer after shaking the styrofoam cavity figurines in order to equalize the temperature over the volume of the saline. To determine the distribution of power deposition, biological-phantom figurines were exposed to the highest available radiation intensities to speed up the heating process and thus reduce the heat diffusion to cooler areas of the body. Temperature under irradiation was recorded using the liquid crystal temperature probe [5].

The incident field intensities used in the experiments were considerably higher for free-space exposures on account of a 2000 W power source available at Walter Reed Laboratories. The field intensities used for free-space and parallel-plate irradiations were 100 and 26.5 mW/cm², respectively.

From the measured increase in temperature ΔT , the density of power absorption in W/kgm is calculated from the expression $(4180 \Delta T \times \text{specific heat of the medium in calories/gm}^{\circ}\text{C})/\text{irradiation time in seconds}$. This divided by the field intensity in mW/cm² gives the α parameter either for the whole body (for saline-filled figurines) or for different parts of the body (for biological-phantom figurines). The values of the α parameter so calculated are then reduced by the model scaling factor (height of the human/length of the figurine) to obtain the corresponding values for humans.

3. RESULTS

Free-Space Irradiation Experiments

The whole body average value of α defined in W/kgm of absorbed power density divided by incident field intensity in mW/cm² is calculated (by scaling) from the measured results at 985 and at 2450 MHz and is plotted in Fig. 2. For each of the orientations $\vec{E} \parallel \vec{L}$, $\vec{k} \parallel \vec{L}$, and $\vec{H} \parallel \vec{L}$, two distinct exposure configurations are possible. (The vectors \vec{E} , \vec{H} , and \vec{k} are along the electric and magnetic fields and along the direction of propagation, respectively; \vec{L} is along the major length L of the body.) For electric field along the major length, for example, these are:

1. Power propagating from front to back.
2. Power propagating from arm to arm.

A 5 to 10 percent larger whole-body absorption is found for case 2 for electric polarization. The results for this most absorbing configuration are also plotted in Fig. 2. Table 1 summarizes the projected α for the six distinct orientations under respective conditions of maximum absorption. The most difference in absorption is found for k -polarization ($k \parallel L$) where a 50 percent increase in overall absorption is measured for electric field from arm to arm as compared to the case where the electric field is from front to back of the body. The results observed with saline-filled figurines are qualitatively similar to those observed with rectangular parallelopipeds [6] of biological-phantom material. At $(68 \times 1.75/L_m)$ MHz which is the frequency of maximum whole body power deposition (see Fig. 2), the $\alpha \times (L_m/1.75)$ values for $k \parallel L$ and $E \parallel L$ orientations are 0.017 and 0.011, respectively, and both of these values are more than an order of magnitude smaller than the value for electric polarization of 0.216 (W/kgm)/(mW/cm²). From α parameter the relative absorption coefficient S (defined as the electromagnetic absorption cross section divided

Relative absorption coefficient $S = \frac{\text{microwave absorption cross section}}{\text{shadow area of the body}}$

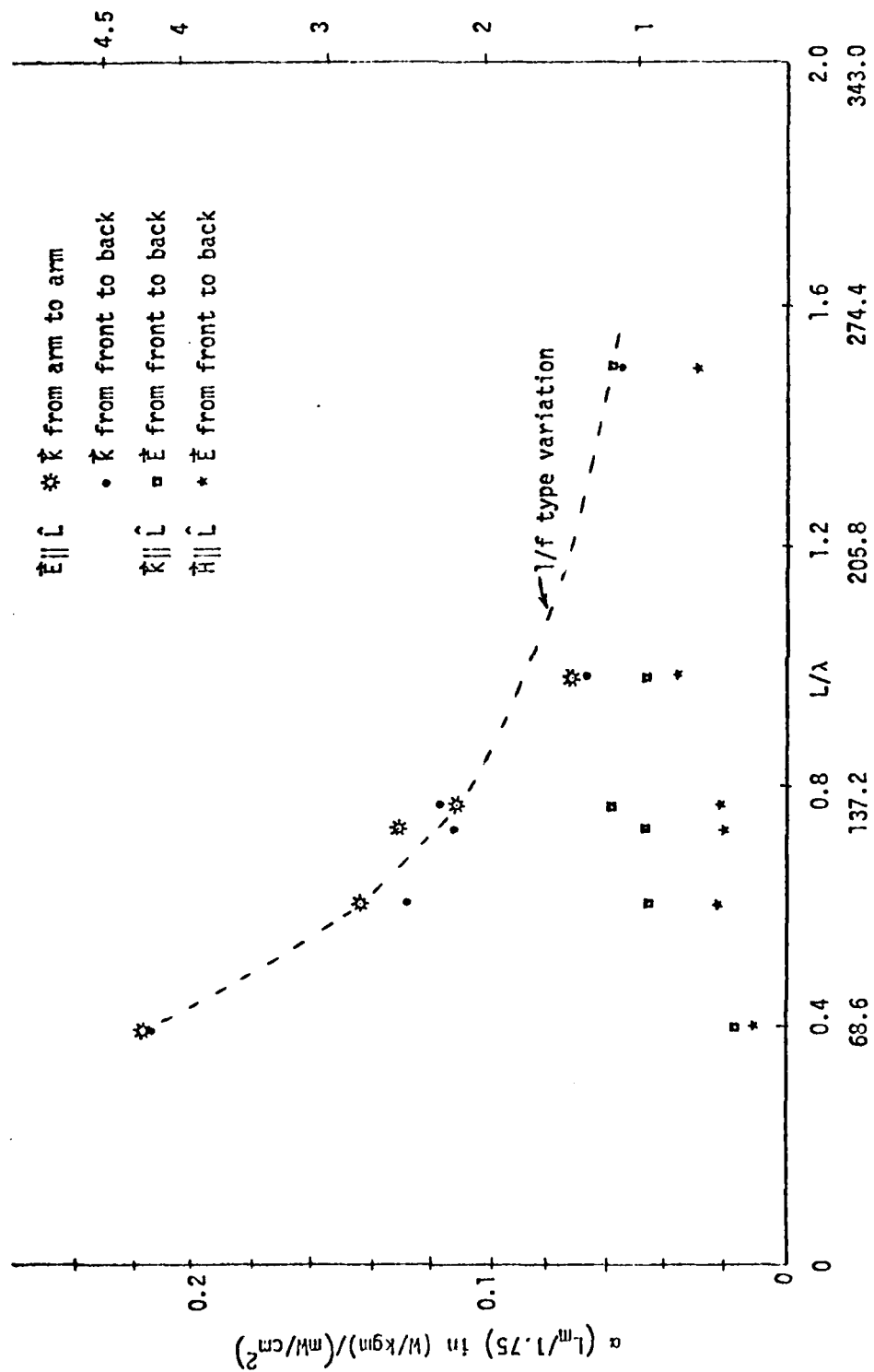


Fig. 2. Projected rate of energy deposition in a human of height L_m meters (scaled from measurements performed on saline-filled dolls under free-space irradiation conditions at 985 and 2400 MHz). The standard deviation of three measurements for each of the data points is less than 3 percent.

Table 1. Projections for whole body electromagnetic absorption in a human of height L_m meters.

	$\vec{E} \parallel \vec{L}$ Electric Field Along the Major Length		$\vec{E} \parallel \vec{L}$ Power Propagating from Head to Toe		$\vec{E} \parallel \vec{L}$ Magnetic Field Along the Major Length	
	Power Propagating from Arm to Arm	Power Propagating from Front to Back	\vec{E} from Arm to Arm	\vec{E} from Front to Back	\vec{E} from Arm to Arm	\vec{E} from Front to Back
Average absorbed power density at respective resonance frequencies for 10 mW/cm ² incident fields (W/kgm)	$2.18 \left(\frac{1.75}{L_m} \right)$	$2.15 \left(\frac{1.75}{L_m} \right)$	$0.71 \left(\frac{1.75}{L_m} \right)$	$0.47 \left(\frac{1.75}{L_m} \right)$	$0.43 \left(\frac{1.75}{L_m} \right)$	$0.37 \left(\frac{1.75}{L_m} \right)$
Frequency of maximum absorption (MHz)	$= 67.9 \left(\frac{1.75}{L_m} \right)$	$= 67.9 \left(\frac{1.75}{L_m} \right)$	$143-171 \left(\frac{1.75}{L_m} \right)$	$143-171 \left(\frac{1.75}{L_m} \right)$	$143-171 \left(\frac{1.75}{L_m} \right)$	$143-171 \left(\frac{1.75}{L_m} \right)$
Whole body average α in (W/kgm) / mW/cm ²	$0.218 \left(\frac{1.75}{L_m} \right)$	$0.215 \left(\frac{1.75}{L_m} \right)$	$0.071 \left(\frac{1.75}{L_m} \right)$	$0.047 \left(\frac{1.75}{L_m} \right)$	$0.043 \left(\frac{1.75}{L_m} \right)$	$0.037 \left(\frac{1.75}{L_m} \right)$
Condition for maximum absorption	$L \approx 0.4 \lambda$	$L \approx 0.4 \lambda$	$L \approx 1.0-1.1 \lambda^*$	$L \approx 1.0-1.1 \lambda^*$	$L \approx 1.0-1.1 \lambda^*$	$L \approx 1.0-1.1 \lambda^*$

*This agrees with our previously reported condition of $kL = 2\pi L/\lambda \approx a/b$. For man $a/b = 6-6.5$, giving therefore an $L/\lambda = 1.0-1.1$.

by the shadow area of the body) is calculated from the expression:

$$S = \alpha \times \frac{\text{weight of the body}}{\text{shadow area of the body}}$$

The value of the S coefficient thus calculated for $\vec{E} \parallel \vec{L}$ and $\vec{H} \parallel \vec{L}$ orientations is also shown in Fig. 2. At resonance an effective absorption area of 4.2 times the shadow cross section is measured. For the post-resonance region to frequencies on the order of 3 to 4 times the resonance frequency f_r , a whole-body absorption reducing as $(f/f_r)^{-1}$ from the resonance value may be seen from Fig. 2.

The measured rates of temperature increase are used to calculate α 's for various parts of the body in a human for different exposure parameters. The values of α multiplied by the field intensity in mW/cm^2 give the rates of deposition in W/kgm . Figures 3-5 give the rates of energy deposition for 10 mW/cm^2 incident fields for prescribed exposure conditions. While Figs. 3-5 give an idea of the rates of energy deposition, the temperature rise for the various parts in an actual human would, of course, depend upon several complex factors such as blood circulation, convective cooling, etc.

Experiments in the Parallel-Plate Radiation Chamber

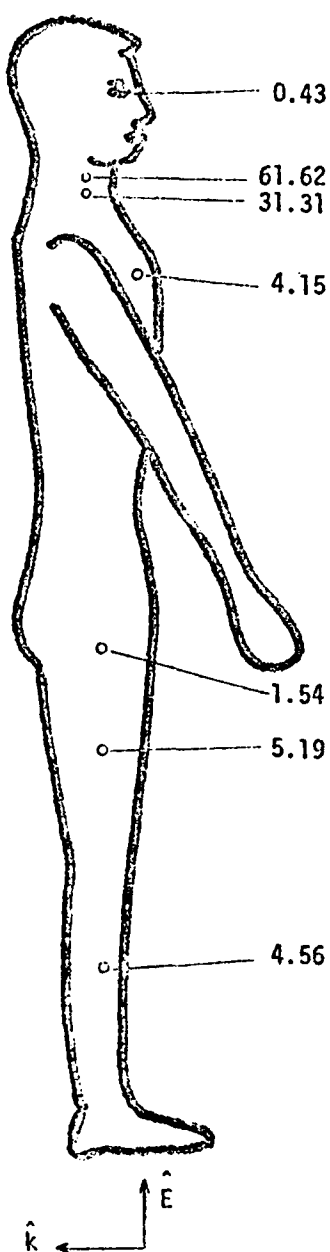
The TEM radiation chamber was used to measure the whole body α parameter of the four sizes of the saline-filled figurines at the highest power source frequency of 500 MHz. The α parameters so obtained were scaled to the values for humans and these are plotted in Fig. 6 as a function of L/λ . For $\vec{E} \parallel \vec{L}$ orientation the results are noteworthy in two respects:

1. Maximum power absorption is observed for $L/\lambda = 0.37$. This is in agreement with the condition for maximum absorption observed with free-space experiments (Fig. 2). This result is surprising in that the parallel plate chamber seems to simulate the free-space plane waves rather than the ground plane effects. As will be pointed out later, physical contact with the ground plate does indeed allow this chamber to simulate ground effects.
2. The value of α at resonance observed with the parallel plate chamber is about 80 percent of the value obtained from free-space irradiation experiments. In view of the fact that different frequencies, figurine sizes, and calibrating field probes were used for the two radiation conditions, the two results should be considered in remarkably good correlation.

While we have always been convinced of the validity of using a parallel plate transmission line to provide a medium of plane waves, and the above results are a further confirmation of our feelings, doubts have, however, been expressed by some researchers in the field regarding this transmission line. Also a handicap of the parallel plate line is the rather limited space available between the two plates, and this hinders its application to frequencies where the target size may be comparable to or larger than one half the free-space wavelength. On account of these reasons, we have designed [2] and installed a monopole-above-ground radiation chamber. The anechoic chamber is formed by lining a $10' \times 10' \times 7.5'$ Faraday screen room with sheets of microwave absorbing material of pyramidal (Eccosorb VHP-18) and planar (Eccosorb AN-79) varieties. The radiator consists of a quarter-wave monopole above ground mounted in a 45° corner reflector. Due to the high gain of the antenna, field intensities on the order of 13 mW/cm^2 have been measured at 2.4 meters from the radiator for 100 watts input to the antenna. An MCL model 11145

$$P_{av} = 2.15 \cdot (1.75/L_m)$$

(saline-filled)



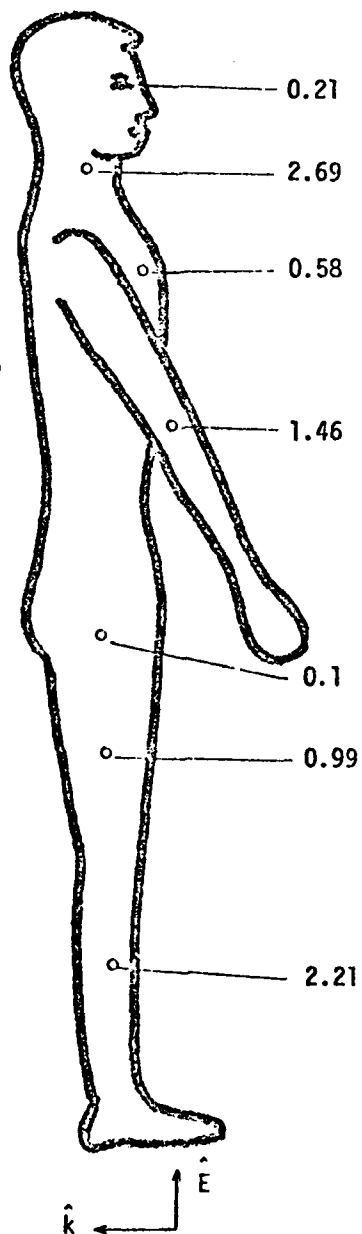
FREE-SPACE IRRADIATION

Fig. 3. Power deposition in W/kgm for 1.75 m human under $\vec{E} \parallel \hat{L}$ resonance condition ($L/\lambda = 0.4$, $67.9 \cdot (1.75/L_m)$ MHz). Incident fields: 10 mW/cm^2 .

For a human of height L_m meters, the numbers marked alongside the figure should be multiplied by $(1.75/L_m)$.

$$P_{av} = 0.67 \cdot (1.75/L_m)$$

(saline-filled)



FREE-SPACE IRRADIATION

Fig. 4. Power deposition in W/kgm for 1.75 m human ($L/\lambda = 0.985$, $169 \cdot (1.75/L_m)$ MHz). Incident fields: 10 mW/cm^2 .

For a human of height L_m meters, the numbers marked alongside the figure should be multiplied by $(1.75/L_m)$.

$$P_{av} = 0.71 \cdot (1.75/L_m)$$

(saline-filled)

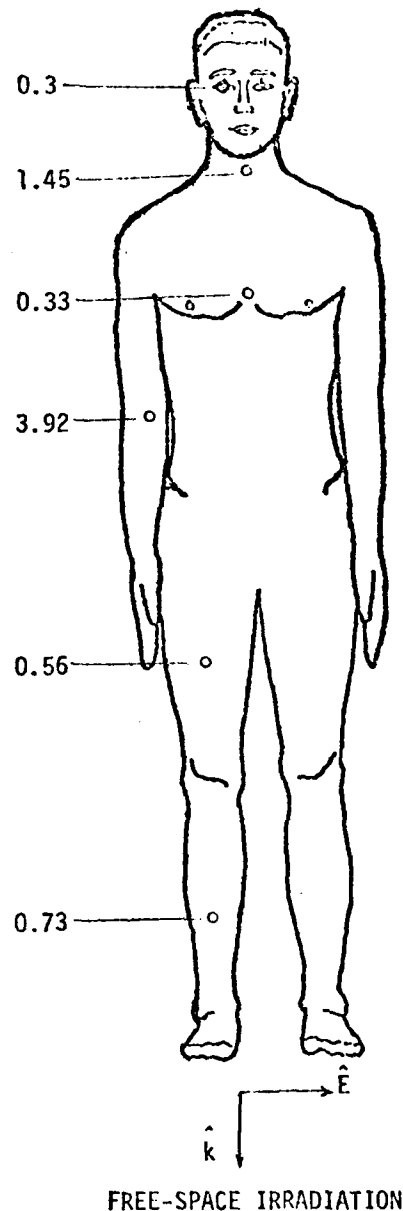


Fig. 5. Power deposition in W/kgm for 1.75 m man for $\vec{k} \parallel \hat{L}$ resonance condition ($L/\lambda \approx 1, 169 \cdot (1.75/L_m)$ MHz). Incident fields: $10 \text{ mW}/\text{cm}^2$.

For a human of height L_m meters, the numbers marked alongside the figure should be multiplied by $(1.75/L_m)$.

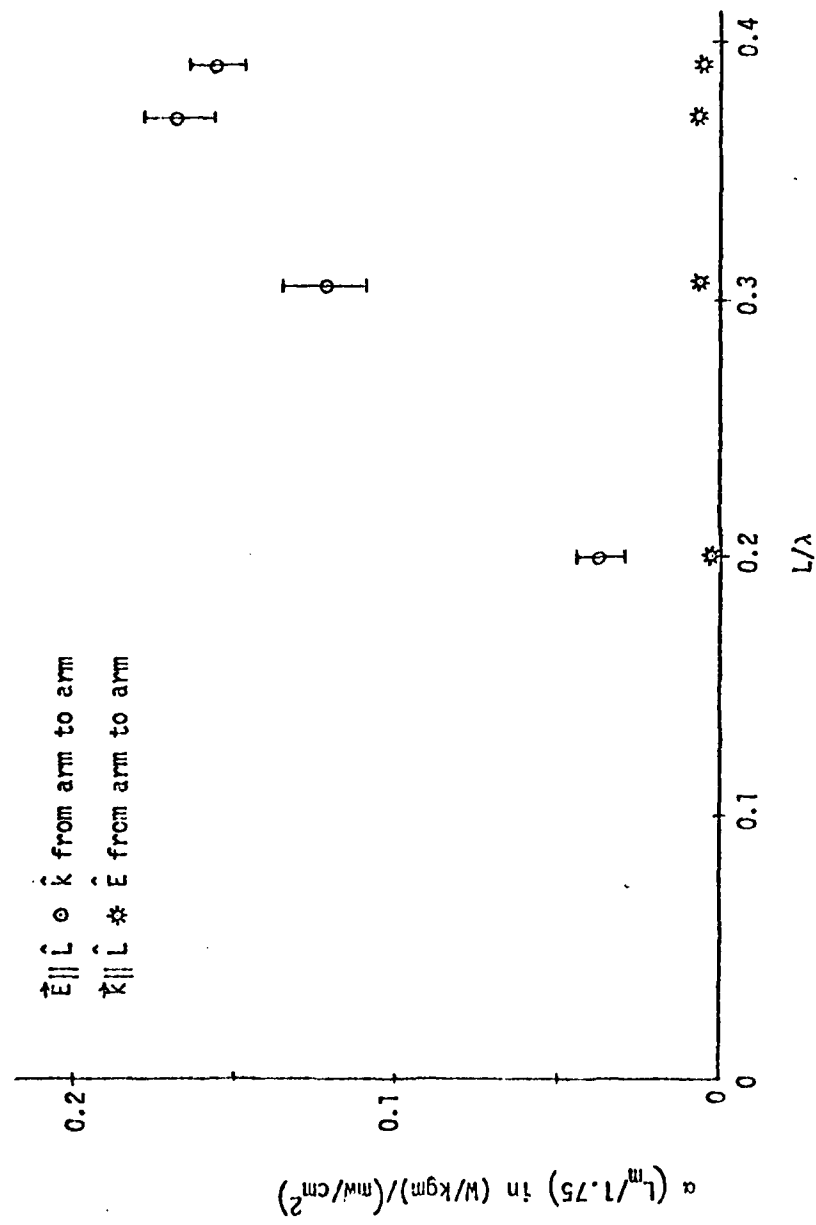


Fig. 6. Projected rate of energy deposition in a human of height L_m meters (scaled from measurements performed on saline-filled dolls in the parallel-plate chamber at 500 MHz. The standard deviation of three measurements for each of the data points is shown.

1000 W output 400-800 MHz RF amplifier is presently on order, and this would be used in the continuing dosimetry experiments. While detailed data from this chamber are not available at this time, preliminary experiments have given a values fairly comparable to those of Fig. 6.

Figures 7-11 give the rates of energy deposition in various parts of the body determined from the parallel plate chamber for prescribed exposure conditions. At least three measurements were taken to obtain the values indicated on these diagrams. A standard deviation of less than 5 percent for hotter regions of the body and a value of less than 10 percent for the cooler regions were calculated from the experimental data. From Figs. 7-11 the important features to note are:

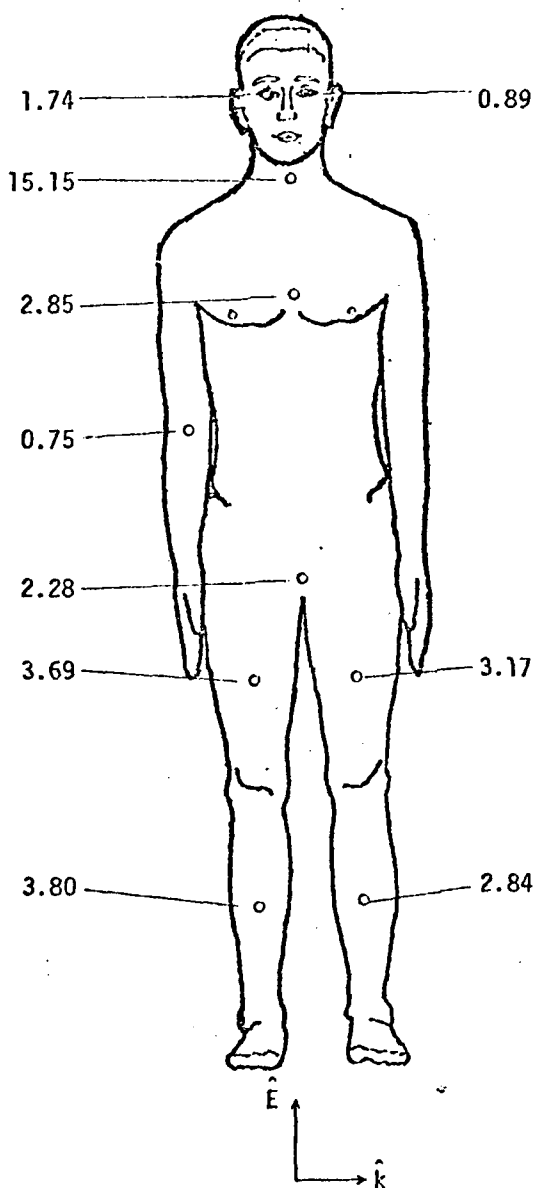
1. Maximum rate of energy deposition once again is observed for the neck for $\vec{E} \parallel \hat{L}$ resonance and near-resonance conditions. For this region an energy deposition of nearly 10 times the whole body average is observed. This ratio is considerably lower than 28.7 observed with free-space irradiation (Fig. 3) on account of low field intensities used to date with parallel plate chamber experiments. This would cause a lower power deposition rate resulting in heat being carried away from the "hot" neck region to the cooler torso and head regions of the body. With the future availability of higher field intensities ($\sim 150 \text{ mW/cm}^2$), it is felt that energy deposition rates comparable to those observed under free-space irradiation conditions may indeed be obtained with parallel plate TEM chambers.
2. For $\vec{E} \parallel \hat{L}$ orientation, a more detailed examination of the heating of leg shows a higher rate of energy deposition in the knee and ankle regions (Figs. 8 and 9). These also are the zones of smaller cross-sectional areas than the rest of the leg. The plot of α as a function of the cross-sectional area over the entire length of the leg is shown in Fig. 12. A rate of energy deposition varying inversely as the cross-sectional area is observed. If a constant current were flowing through the entire leg, a $(\text{cross-sectional area})^{-2}$ type dependence of α would be expected. However, even from antenna theory, a diminishing value of current is anticipated as one approaches the ankle region. This may well be the reason for the experimentally observed $(\text{cross-sectional area})^{-1}$ dependence of α .
3. A detailed examination of the heating pattern of the arm (Figs. 8 and 9) shows the maximum rate of deposition in the elbow region. It should be mentioned that the arms are in the plane of the body in our figurines. In Figs. 3, 4, and 9, the arms are shown protruding only for clarity of marking the measured values.
4. For $\vec{k} \parallel \hat{L}$ orientation (Figs. 4 and 11), maximum rates of energy deposition are observed for the elbow followed by the neck region.

Power Deposition in the Presence of Ground Effects

Experiments were performed with the 18.4 cm saline-filled figurine grounded to the bottom plate of the parallel plate chamber by means of a thin wire probe forming the electrical connection through a rubber cork at the base of the figurine. On account of an increased rate of energy deposition under these conditions, only two minutes of irradiation time (as against five minutes in experiments with ungrounded figurines) was found to be adequate for these exposures. The values of α calculated from the measurements over the frequency band 220-500 MHz are plotted in Fig. 13. Also shown in the same figure are the values projected for humans of different heights and the relative absorption coefficient S . Peak power absorption is observed for a frequency slightly

$$P_{av} = 1.68 \cdot (1.75/L_m)$$

(saline-filled)



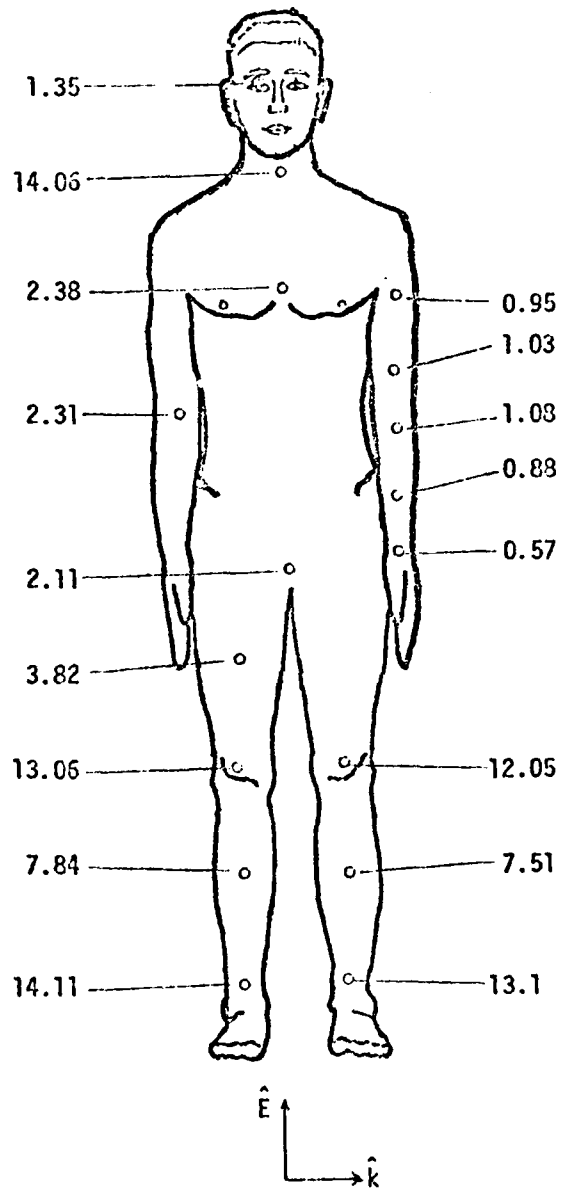
PARALLEL-PLATE RADIATION CHAMBER

Fig. 7. Power deposition in W/kg_m for 1.75 m human ($L/\lambda = 0.37$, $63.5 \cdot (1.75/L_m)$ MHz). Incident fields: 10 mW/cm^2 .

For a human of height L_m meters, the numbers marked alongside the figure should be multiplied by $(1.75/L_m)$.

$$P_{av} = 1.23 \cdot (1.75/L_m)$$

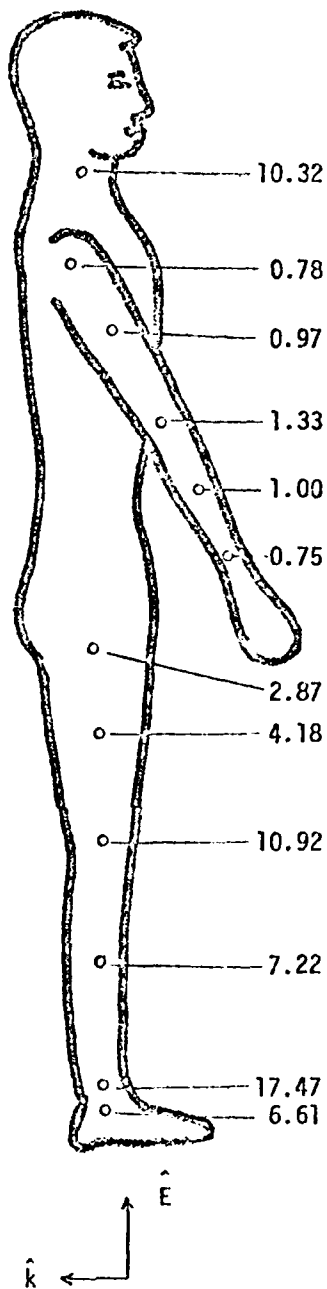
(saline-filled)



PARALLEL-PLATE RADIATION CHAMBER

Fig. 8. Power deposition in W/kgm for 1.75 meter human ($L/\lambda = 0.31, 52.6 \cdot (1.75/L_m)$ MHz). Incident fields: 10 mW/cm^2 .

For a human of height L_m meters, the numbers marked alongside the figure should be multiplied by $(1.75/L_m)$.



PARALLEL-PLATE RADIATION CHAMBER

Fig. 9. Power deposition in W/kgm for 1.75 m human ($L/\lambda = 0.31$, $52.6 \cdot (1.75/L_m)$ MHz). Incident fields: $10 \text{ mW}/\text{cm}^2$.

For a human of height L_m meters, the numbers marked alongside the figure should be multiplied by $(1.75/L_m)$.

AD-A100 028

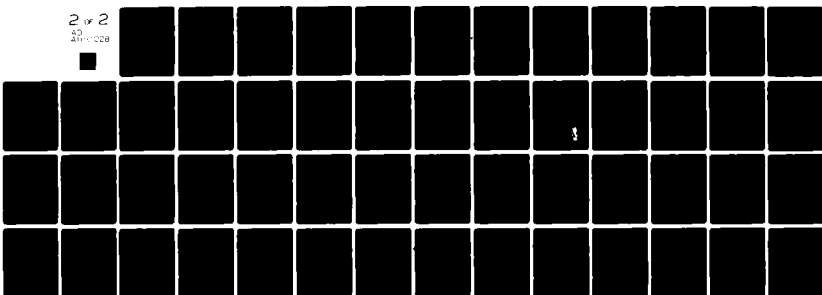
UTAH UNIV SALT LAKE CITY
BEHAVIORAL AND BIOLOGICAL EFFECTS OF RESONANT ELECTROMAGNETIC A--ETC(U)
NOV 76 O P GANDHI, J A D'ANDREA, M J HAGMANN DAMD17-74-C-5092

F/G 6/18

NL

UNCLASSIFIED

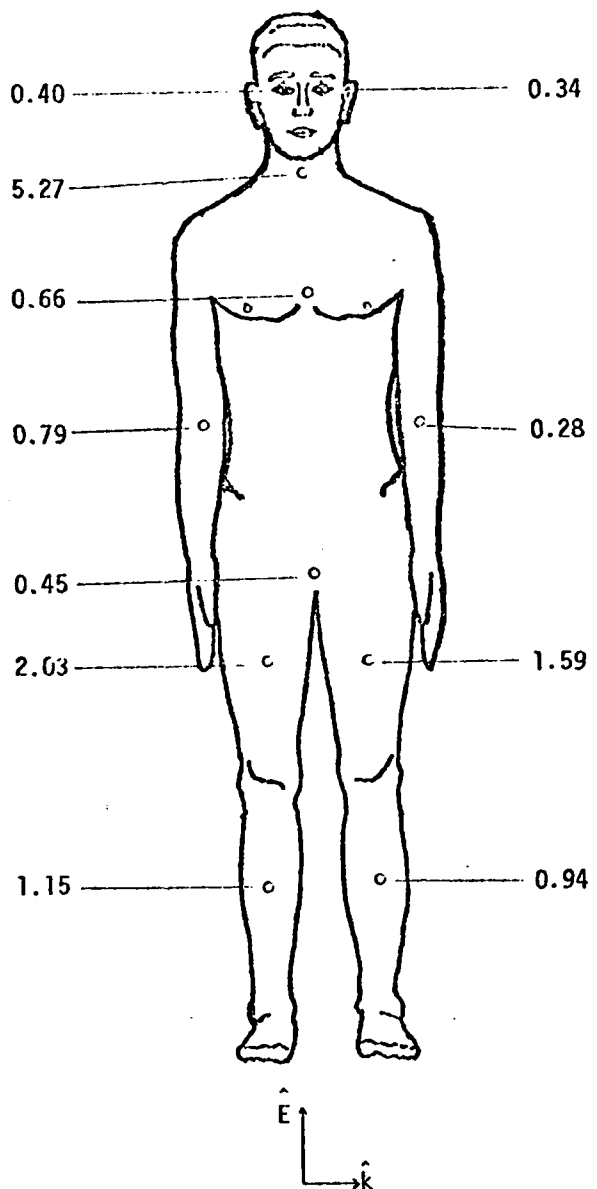
2 or 2
40
40-10008



END
DATE
FILMED
7-81
DTIC

$$P_{av} = 0.38 \cdot (1.75/L_m)$$

(saline-filled)



PARALLEL-PLATE RADIATION CHAMBER

Fig. 10. Power deposition in W/kg_m for 1.75 m human ($L/\lambda = 0.2$, $34.6 \cdot (1.75/L_m)$ MHz). Incident fields: 10 mW/cm^2 .

For a human of height L_m meters, the numbers marked alongside the figure should be multiplied by $(1.75/L_m)$.

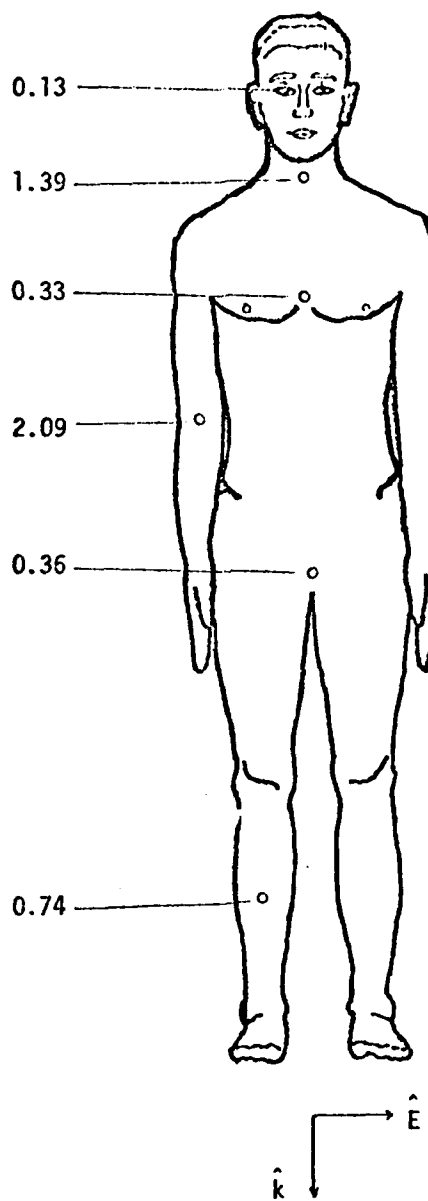


Fig. 11. Power deposition in W/kgm for 1.75 m man ($L/\lambda = 0.39$, $67.1 \cdot (1.75/L_m)$ MHz). Incident fields: $10 \text{ mW}/\text{cm}^2$.

For a human of height L_m meters, the numbers marked alongside the figure should be multiplied by $(1.75/L_m)$.

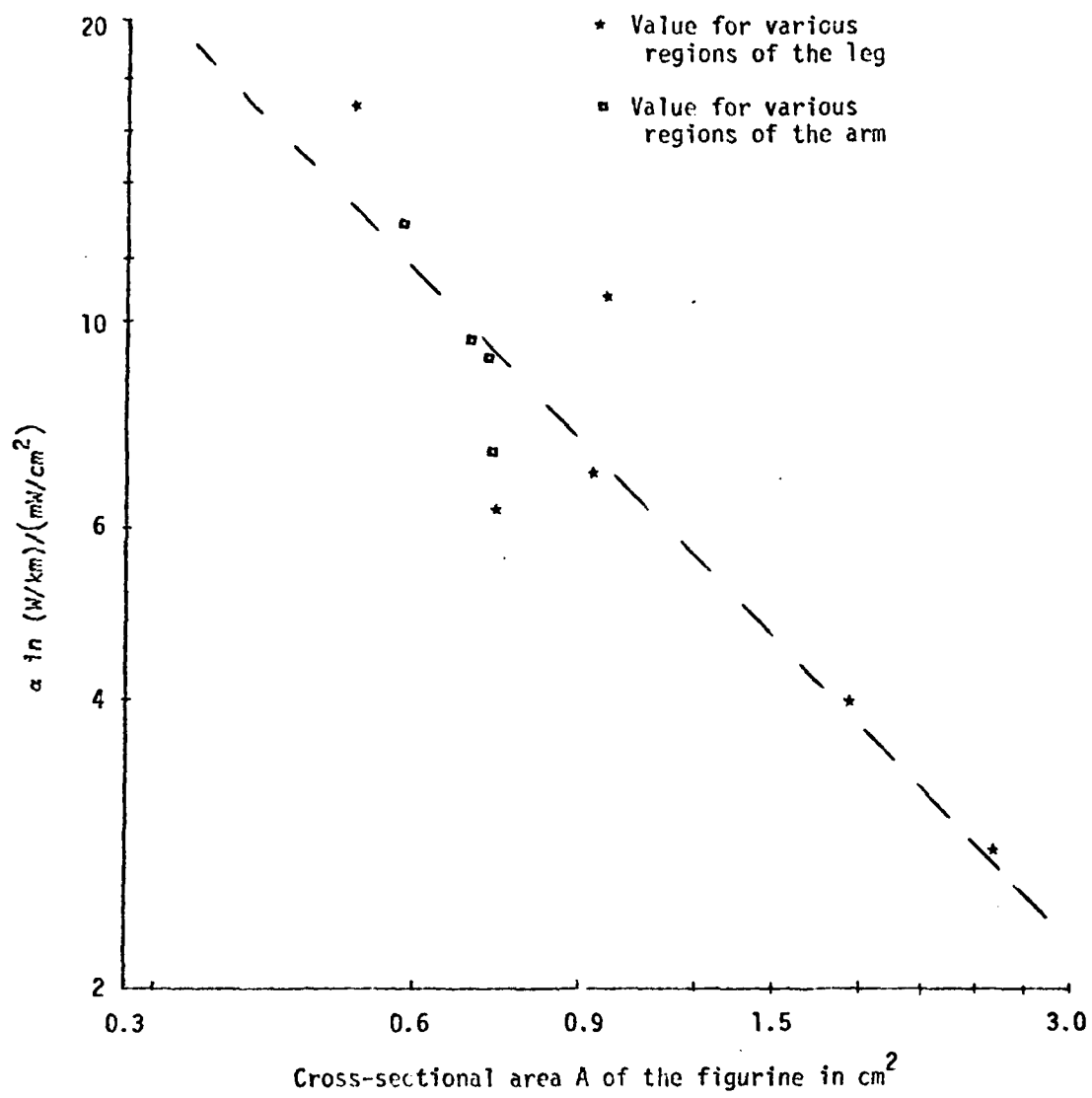


Fig. 12. Plot of α as a function of the cross-sectional area for arms and legs (18.4 cm figurine; 500 MHz, $L/\lambda = 0.31$).

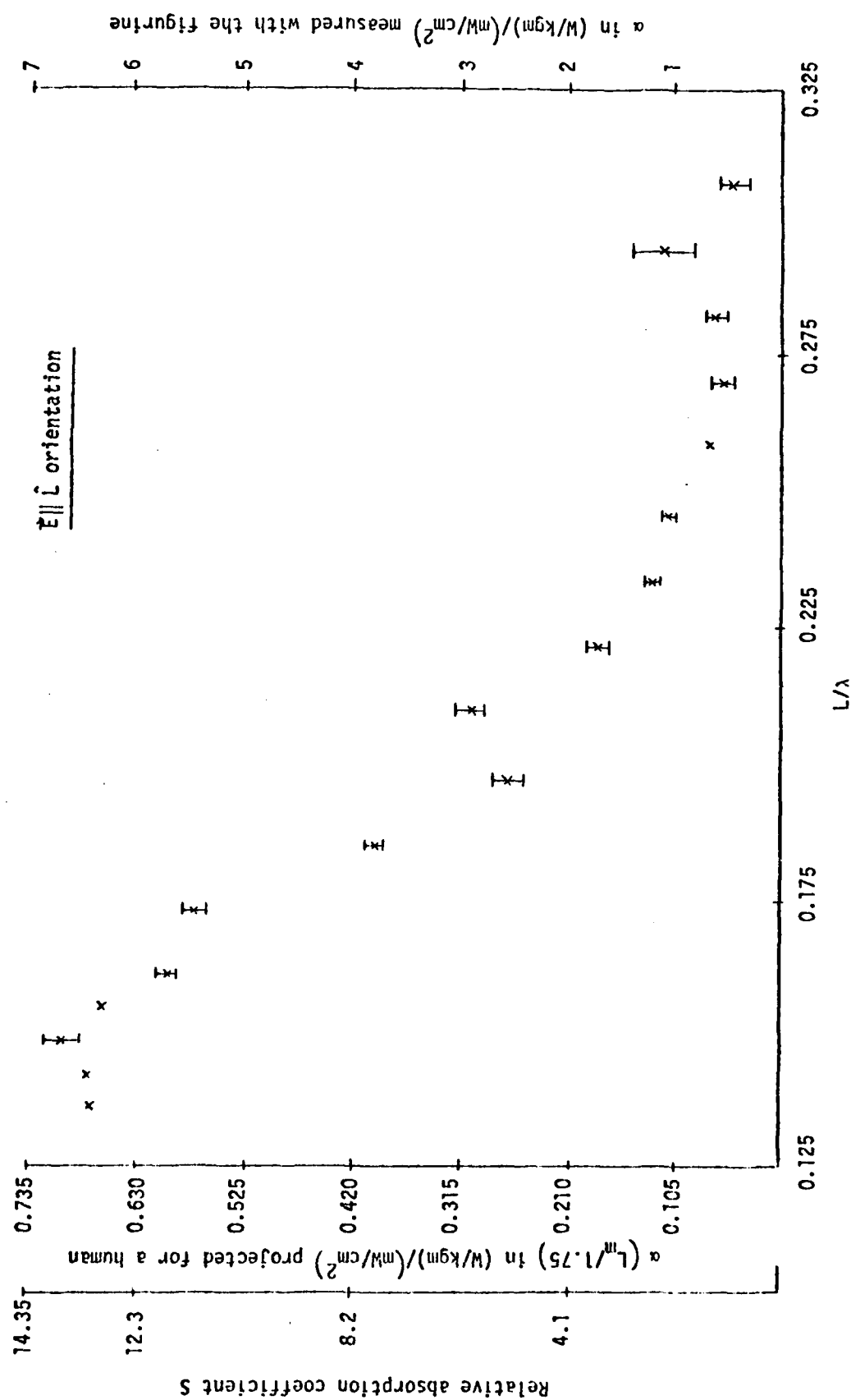


Fig. 13. Projected rate of energy deposition in a human of height L_m meters with feet touching ground. The standard deviation of three measurements for each of the data points is shown.

lower than one half the value for ungrounded conditions. At resonance an effective absorption area of nearly 14 times the shadow cross section is measured which is about 4 times the value measured at resonance under ungrounded conditions in the parallel plate chamber. Both these results are predicted approximately by antenna theory. The derivations giving an S of 4.2 for free-space irradiation and a four-times enhancement in the absorption cross section of an isolated versus a grounded body are illustrated in Figs. 14 and 15.

Judging from the success of the antenna theory in explaining most of the whole body absorption observations under grounded and ungrounded conditions, highly enhanced values of S may result for bodies in the presence of 180° , 90° , and other corner reflectors. Preliminary experiments in the monopole-above-ground chamber have shown this to be true indeed. S parameters on the order of 20 and higher have been observed to date. Further experiments are in progress to completely understand these effects.

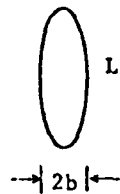
The distribution of power deposition under grounded resonance conditions has been determined using the biological-phantom figurine with feet touching the ground plate of the parallel plate chamber. The rates of energy deposition projected for a human exposed to 10 mW/cm^2 fields are shown in Fig. 16. The points to note are:

1. The whole body average value is fairly close to that obtained with saline-filled figurine grounded by means of a wire probe, lending some credence to this method of grounding for saline-filled figurines.
2. While the neck is still one of the hot spots, the region of maximum power deposition shifts to the lower half of the leg under grounded conditions.
3. Consistent with the previous observations (Figs. 8 and 9) on the detailed distribution in the leg region, the zones of maximum power deposition are the ankle and the knee, which also correspond to the areas of minimum cross section in the leg.

4. CONCLUSIONS

In the absence of ground effects, a whole body absorption cross section as high as 4.2 times the shadow cross section has been measured for electric polarization at the resonance frequency (in MHz) of $(68) \times (1.75/\text{height } L_m \text{ of the human in meters})$. Under these frequency and polarization conditions, a whole-body-average energy deposition rate of $(2.15) \times (1.75/L_m)$ watts/kgm is projected for incident plane wave fields of 10 mW/cm^2 . At higher frequencies (to $f = 3-4 f_r$), the whole body absorption reduces as $(f/f_r)^{-1}$ from the resonance value. The distribution of power deposition is given for the various regions of the body for several exposure conditions. For $\vec{E} \parallel \vec{f}$, resonance conditions, the highest rate of energy deposition is observed for the neck region of the body, and a value as high as 28.7 times the whole body average is measured.

Maximum whole body absorption under grounded conditions is observed at a frequency about one half that of the ungrounded body. For grounded resonance condition an absorption cross section as high as 14 times the shadow area has been measured. Antenna theory has been used to explain this highly enhanced absorption cross section. The distribution of power deposition is determined for grounded resonance condition. While the neck is still one of the hot spots, the zone of maximum power deposition is the ankle region. Judging from the success of antenna theory in explaining most of the whole body absorption observations under grounded and ungrounded condition, highly enhanced deposition rates are anticipated for bodies in the presence of 180° , 90° , and other



A biological body isolated in free space

For resonance, $L \approx 0.5 \lambda$

Power absorbed = (incident field intensity P_{inc}) • (effective area of the antenna)

$$= P_{inc} \frac{\lambda^2 G}{4\pi}$$

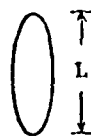
where G , the gain of the antenna, is 1.64

$$\text{Electromagnetic absorption cross section} = \frac{\text{power absorbed}}{P_{inc}} = \frac{1.64\lambda^2}{4\pi}$$

For humans $a/b \approx 6.34$ which gives an S of 4.21 in close agreement with experimentally observed values for human-shaped figurines under free-space irradiation.

Fig. 14. Derivation of the S parameter of a biological body isolated in free space.

I

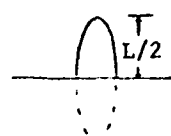


Body of shadow area A in free space.

Resonance condition $L \approx 0.5 \lambda$

EM absorption cross section = $4.2 A$

II



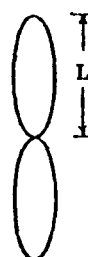
One half body placed above ground.

Resonance condition $L \approx 0.5 \lambda$

EM absorption cross section = $8.4 A$

(From antenna theory, the gain of a monopole above ground is twice as much as that of a twice-length dipole.)

III

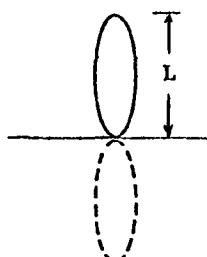


Two bodies, each of shadow area A, placed end to end.

Resonance condition $L \approx 0.25 \lambda$

EM absorption cross section = $4.2 \times 2A$

IV



A body of shadow area A above ground.

Resonance condition $L \approx 0.25 \lambda$

EM absorption cross section = $8.4 \times 2A$

A four-times enhancement at resonance for conditions I and IV may be seen while the resonance frequency is reduced to one half the value.

Fig. 15. Comparison of the S parameter for a body in free space with the value for the same body in the presence of a ground plane.

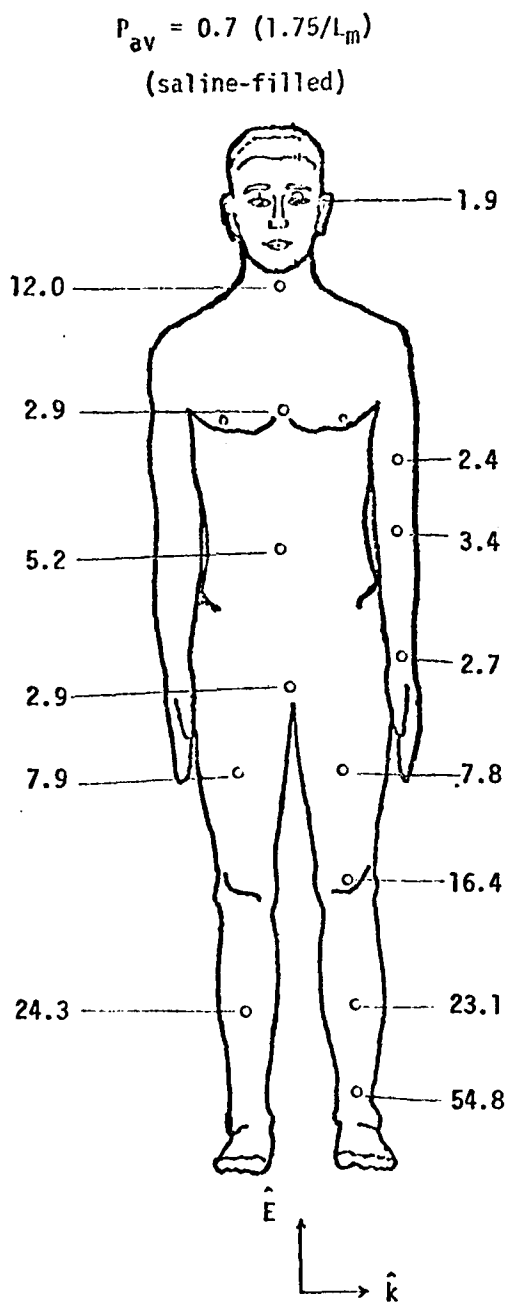


Fig. 16. Energy deposition in mW/gm for 1.75 m tall human under resonance condition ($l/\lambda = 0.15$, 25.2 MHz) for feet touching ground; incident power: 10 mW/cm^2 .

For a human of height L_m meters, the numbers marked alongside the figure should be multiplied by $(1.75/L_m)$.

corner reflectors.

5. REFERENCES

1. Gandhi, O. P. Polarization and frequency effects on whole animal absorption of RF energy. Proc. IEEE, 62, 1171-1175, 1974.
2. Gandhi, O. P. Conditions of strongest electromagnetic power deposition in man and animals. IEEE Trans. MTT-23, 1021-1029, 1975.
3. Johnson, C. C., and A. W. Guy. Nonionizing electromagnetic wave effects in biological materials and systems. Proc. IEEE, 60, 246-253, 1972.
4. Guy, A. W., C. C. Johnson, J. C. Lin, A. F. Emery, and K. K. Kraning. Electromagnetic power deposition in man exposed to HF fields and the associated thermal and physiologic consequences. USAF School of Aerospace Medicine, Brooks Air Force Base, Texas, Report SAM-TR-73-13, December 1973.
5. Rozzell, T. C., C. C. Johnson, C. H. Durney, J. L. Lords, and R. C. Olsen. A nonperturbing temperature sensor for measurements in electromagnetic fields. J. Microwave Power, 9, 241-249, 1974.
6. Gandhi, O. P. Orientational and frequency effects on whole animal absorption of RF energy. J. Indian Inst. of Sci., 56, 315-364, 1974.

ACKNOWLEDGMENT

The technical support of J. H. Jacobi and P. B. Brown, Department of Microwave Research, Walter Reed Army Institute of Research, is gratefully acknowledged. This work was supported by the U. S. Army Medical Research and Development Command under Contract DAMD 17-74-C-4092.

APPENDIX C

Deposition of electromagnetic energy in animals and in models of man with and without grounding and reflector effects

Om P. Gandhi

Departments of Electrical Engineering and Bioengineering, University of Utah, Salt Lake City, Utah 84112

Edward L. Hunt

Department of Microwave Research, Walter Reed Army Institute of Research, Washington, D. C. 20012

John A. D'Andrea

Departments of Electrical Engineering and Bioengineering, University of Utah, Salt Lake City, Utah 84112

Generalized curves are given for rates of whole-body absorption of electromagnetic energy by models of human beings as a function of frequency. Exposures were made in free space, or when the model made electrical contact with the ground. The effects of the presence of reflecting surfaces also were analyzed. Peaks of absorption with and without a ground, are projected, respectively, to be (31 to 34 MHz) and (62 to 68 MHz) \times (1.75/height of model in meters). Rates of energy deposition are given for models of man and for animals subjected to radiation at a power density of 10 mW/cm^2 for the various conditions of exposure. At resonance, values of whole-body absorption as high as 4,077 to 8,154 watts for the adult human being are predicted. The times-to-convulsion of ~ 100 -g rats at power densities of 3 to 20 mW/cm^2 confirmed predictions of extremely high rates of absorption in the presence of reflecting surfaces.

1. INTRODUCTION

We have previously reported on the observation of a strong resonance in the whole-body absorption of electromagnetic waves by biological bodies [Gandhi, 1974, 1975]. For plane-wave irradiation in free space, the highest rate of energy deposition occurs in fields that are polarized along the longest dimension of the body ($E \parallel L$) and for frequencies such that the major length (L) is approximately 0.36 to 0.40 times the free-space wavelength (λ) of radiation. Peaks of whole-body absorption for two other configurations (major length oriented along the direction of wave propagation or along the vector of the magnetic field) were also reported [Gandhi, 1974, 1975] for L/λ on the order of $L/4\pi b$ where $2\pi b$ is the weighted averaged circumference of the animals.

A handicap of past measurements has been that commercially available dolls that have been used as molds for models are not properly proportioned. Using carefully sculptured, accurately scaled figurines [Dreyfuss, 1967], measurements have now been extended to cover the region $0.2 < L/\lambda < 3.3$. Specific absorption rates (SARs) are given in this paper under three configurations in free space for the frequency range 0.5 to 8.7 times the $E \parallel L$ resonance frequency f_r , which, for man, is $65 \times (1.75/\text{length in meters}) \text{ MHz}$. From these results, antenna theory is used to develop an empirical equation for the SAR, for the $E \parallel L$ orientation of models, at resonant and supraresonant frequencies. A comparison with the lethality data of Schrot and

Hawkins [1975] confirms the validity of the equation for rats and mice of differing sizes.

Results are also presented for a simulated human being with its feet in electrical contact with the ground. In such an exposure, a resonant frequency one-half as high with a peak absorption twice that of free-space irradiation is observed.

Energy deposition rates are given for models of man and for animals that were exposed to radiation at power densities of 10 mW/cm^2 under various conditions of exposure.

2. ELECTROMAGNETIC ENERGY ABSORPTION IN MAN IN FREE SPACE

The procedure for obtaining the mass-normalized rate of electromagnetic energy deposition (SAR) through the use of reduced-scale models has been detailed in earlier publications [Gandhi, 1975; Gandhi *et al.*, 1975]. The SAR in W/kg is calculated from the temperature rise, ΔT , of 7.6, 10.2, 12.7, 15.2, 20.3, 25.4, 33.0, and 40.6 cm high, saline-filled (0.9% NaCl) figurines from the expression $(4,180 \Delta T) \times$ specific heat of the medium in $\text{calories/g}^\circ\text{C}$ /irradiation time in seconds. The SARs so calculated are divided by the model's scaling factor (height of the human/length of the figurine) to obtain the value for a human being. At least three measurements were taken to calculate the averaged SARs that are given in this paper. Unless otherwise stated, the standard deviation of the measurements is less than

± 3%. The values obtained with saline-filled figurines were found to agree with the average of the values for individual parts of the body for tissue-simulating figurines, which lends some credence to this method of arriving at the whole-body absorption curves for man. A more accurate procedure that is yet to be carried out is calorimetric measurement of whole-body energy deposition in figures that are filled with materials that duplicate the differing conductive and dielectric properties of various tissues.

Curves for whole-body absorption by models of man exposed to radiation in free space are given in Figures 1 and 2. For each of the indicated polarizations, the orientation resulting in a maximum rate of energy deposition was used [Gandhi *et al.*, 1975]. These orientations correspond to propagation normal to the sagittal plane -- from arm to arm (rather than from front to back) -- for $E \parallel \hat{L}$ orientation; E normal to the sagittal plane (rather than from front to back) for $k \parallel \hat{L}$ orientation; and E normal to the sagittal plane for $H \parallel \hat{L}$ orientation.

To date, the experimental data have been obtained to 8.7 times the $E \parallel \hat{L}$ resonant frequency which lies between 62 to 68 MHz. The quantities plotted in Figures 1 and 2 are:

1. The relative absorption coefficient S , which is a measure of the efficiency of energy absorption:

$$S = \frac{\text{Microwave absorption cross section}}{\text{Physical cross section of the body}} = \frac{(\text{Whole-body rate of energy absorption in watts}) / (\text{Field intensity in watts/cm}^2)}{\text{Physical cross section of the body in cm}^2}$$

2. The specific absorption rate (SAR) in W/kg .

3. The SAR as compared to basal metabolic rate (BMR).

In calculating the SAR-to-BMR ratios for Figures 1 and 2, a basal metabolic rate [Guyton, 1968] of 100 kilocalories/hr is assumed which corresponds to 1.66 W/kg for a 70-kg man. A higher metabolic rate (MR) of 1.66 to 1.96 W/kg is assumed to occur during normal activity such as standing while relaxed, dressing and undressing, etc.; use of any number in this range would not appreciably alter the SAR/MR ratios shown in Figures 1 and 2.

For the most highly absorbing $E \parallel \hat{L}$ orientation, the whole body absorption curve may be discussed in terms of five regions of frequency:

Region 1 -- Frequencies well below resonance ($L/\lambda < 0.1-0.2$). An f^2 -type dependence derived theoretically and checked experimentally by Durney and coworkers [Massoudi *et al.*, 1975].

Region 2 -- Subresonant region ($0.2 < L/\lambda < 0.36$). An $f^{2.75}$ to f^3 dependence of rate of energy deposition has been experimentally observed for this region.

Region 3 -- Resonant region ($L/\lambda \approx 0.36-0.4$). A relative absorption cross section S_{res} on the order of

0.665 $L/2b$ (derivable also from antenna theory [Gandhi *et al.*, 1975]) has been measured for this region, where L is the major length of the body and $2\pi b$ is its weighted averaged circumference. For an adult human being, $L/2b \approx 6.34$, $S_{\text{res}} \approx 4.21$. This corresponds to SAR ($L_m/1.75$) ≈ 2.15 for an incident power density of 10 mW/cm^2 . For a man of height 1.75 meters, the resonant frequency is on the order of 62 to 68 MHz and at resonance, the SAR is 1.3 times the BMR.

Region 4 -- Supraresonant region, i.e., to frequencies on the order of 1.8 S_{res} times the resonant frequency f_r (for human beings this covers the region $f_r < f < 8 f_r$). A whole-body absorption rate reducing as $(f/f_r)^{-1}$ from the resonant value has been observed.

Region 5 -- $f \gg f_r$ region. The S parameter should asymptotically approach the "optical" value, which is (1 - power reflection coefficient) or about 0.5.

In comparing the graph of Figure 1 with those of Figure 2 (drawn to the same scale), the following points are noteworthy:

1. For frequencies (4-5) $f_r < f < (8-9) f_r$, there is little distinction between averaged rates of energy absorption for the various polarizations. For humans, this corresponds to (frequency in MHz) \times (height in meters/1.75), to a range of frequencies between 250 and 550 MHz.

2. The resonances for $k \parallel \hat{L}$ and $H \parallel \hat{L}$ orientations are not very sharp. Indeed, for the $H \parallel \hat{L}$ orientation, the SAR gradually reaches a peak value and stays at that value at higher frequencies.

3. ENERGY DEPOSITION IN RATS AND MICE FOR FREE-SPACE IRRADIATION

Antenna theory and the observed frequency dependence that is shown in Figure 1 have been used to develop the following empirical equations for rats and mice and for other animals that may be represented by an equivalent prolate spheroid of dimensions L and $2b$ along the major and minor axes, respectively.

$$\text{Resonant frequency } f_r = 11.4/L_{\text{cm}} \quad (1)$$

$$S_{\text{res}} = 0.665 L/2b \quad (2)$$

where

$$L/2b = 0.724 \frac{L_{\text{cm}}^3}{\text{mass of the animal in g}}^{1/2} \quad (3)$$

For the supraresonant frequency region $f_r < f < (1.8 S_{\text{res}}) f_r$, and at an incident power density of 10 mW/cm^2 ,

$$\text{SAR in } \text{W/kg} = \frac{59.54}{f_{\text{GHz}}} \frac{L_{\text{cm}}}{\text{Mass in g}} \quad (4)$$

The equations have been used to generate the generalized curves for rats and mice (Figure 3) under free-space irradiation for the polarization ($E \parallel \hat{L}$) that produces

DEPOSITION OF EM ENERGY

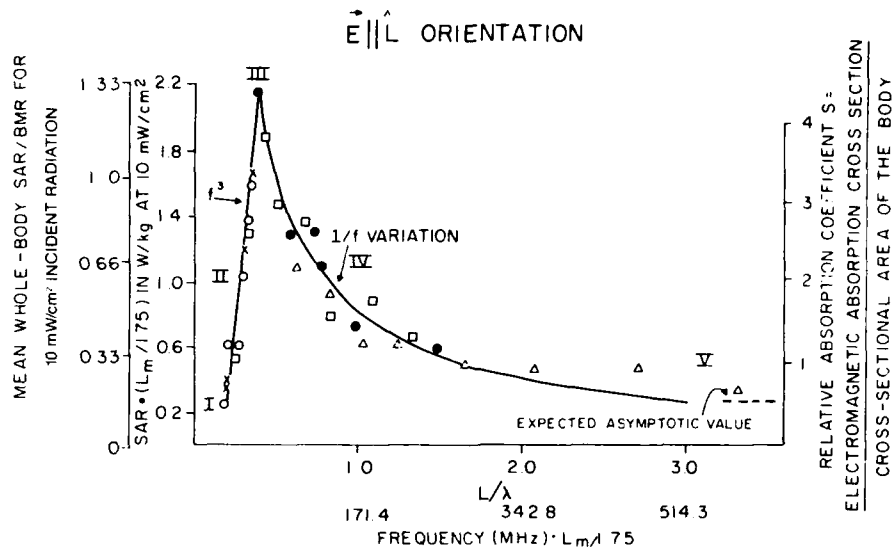


Fig. 1. Whole-body averaged SARs and the relative absorption coefficient, S , of saline-filled models of human beings during microwave irradiation in the free field. The E -field vector is parallel with the long axis of the model. Direction of propagation is normal to sagittal plane. Legend: \circ = prolate spheroids of $(L/2b) = 6$, at 710 MHz; x = human-shaped dolls at 500 MHz (parallel-plate transmission line); \bullet = human-shaped dolls at 987 and 2450 MHz; \square = accurately proportioned figurines, 7 to 41 cm in length, at 987 MHz; \blacktriangle = the proportioned figurines at 2450 MHz.

the highest SAR. A cross-sectional enhancement factor S_{res} of 2.16 (given from equation (2) [also, Gandhi et

al., 1975] for an aspect ratio $L/2b = 3.25$ equivalent prolate spheroid) is assumed in the graphics of Figure 3. Also shown in the figure are the values calculated from the lethality data of Schrot and Hawkins [1975]. In calculating the SAR from their data, it is assumed that: (a) an elevation of temperature of 7.4°C results in a convulsion, and (b) The ΔT occurs in an adiabatic manner; i.e., the rate of energy deposition is high enough so that there is no other mechanism for gain or loss of heat from the animal's body.

Because of the high power density (150 mW/cm^2) used in the experiments by Schrot and Hawkins, the second assumption may be quite justified. From inspection of Figure 3, it can be seen that there is a good correlation between empirical and experimental values.

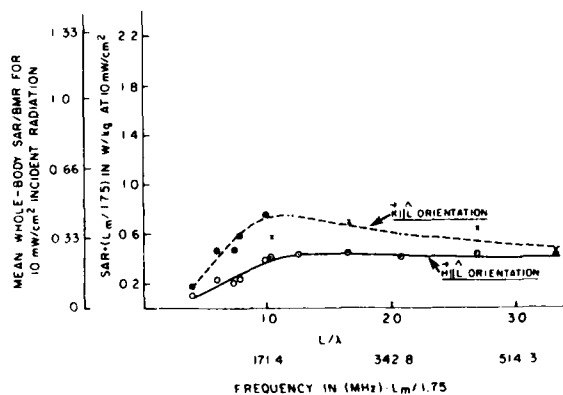


Fig. 2. Whole-body averaged SARs of saline-filled models of human beings during microwave irradiation in the free field. Dashed line: best fit with data-points where propagation vector, A , is parallel with long axis of the model (from head to toe) and E -field vector is normal to sagittal plane. Continuous line: best fit with data points where H -field vector is parallel with long axis of model and E -field vector is normal to sagittal plane. Legend: \bullet = human-shaped dolls at 987 and 2450 MHz; x = proportioned figurines at 2450 MHz; \circ = human-shaped dolls at 987 and 2450 MHz; \oplus = proportioned figurines at 2450 MHz.

4. WHOLE-BODY ABSORPTION BY MAN IN ELECTRICAL CONTACT WITH THE GROUND

Whole-body absorption by a model of a human being with feet in electrical contact with the ground is shown in Figure 4. The results are projected from measurements with 10.2, 12.7, 15.2, and 20.3 cm (height) saline-filled figurines that were exposed to $E \parallel L$ radiation at different frequencies in the monopole-above-ground radiation chamber [Gandhi, 1975]. This chamber, which uses a radiator that is a quarter-wave above ground, provides in conjunction with figurines a proper simulation of grounding effects on energy absorption. Comparing the

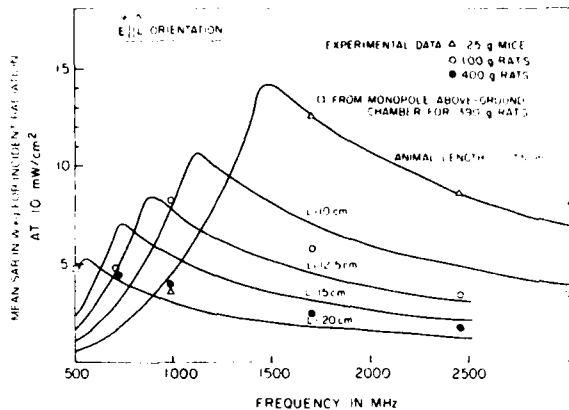


Fig. 3. Theoretical projections (continuous lines) of whole-body SARs of mice and rats of varying mass and axial length for microwave irradiation in the free field. Data points are based on experiments in the free field, or on irradiation in the monopole-above-ground chamber.

results to those of free-space radiation, peak absorption occurs at a frequency about one-half the value for the ungrounded condition. The new resonant frequency is projected to be $(31-34) \times 1.75/L_m$ MHz. At resonance, the SAR is about twice that of irradiation in free space.

5. ENERGY DEPOSITION IN THE PRESENCE OF FLAT REFLECTORS

Judging from the success of antenna theory in predicting resonant frequencies and absorption cross sections of different bodies under grounded and ungrounded

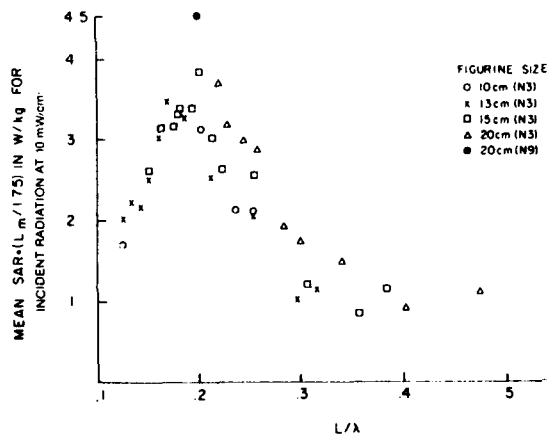


Fig. 4. Projected SARs for a human being of height L (in meters) as a function of L/λ . Feet are in conductive contact with ground. Sample size (N) is shown in parentheses in body of figure.

conditions, highly enhanced SARs are expected for resonant bodies near flat (180°) reflectors and near 90° and other corner reflectors [Jasik, 1961]. Gains or enhancements of absorption that are associated with half-wavelength dipoles in the presence of a typically encountered corner reflector are given in Figure 5. To test the validity of antenna theory in predicting enhancements of rates of energy absorption, experiments were performed with a near-resonant ($L/\lambda = 0.417$) figurine placed at different distances in front of a flat reflector of dimensions $2.5 \lambda \times 2.5 \lambda$. The enhancement factors relative to the free-space value and corresponding SARs are plotted in Figure 6. Also plotted in the figure are the values of E^2 that would be expected for a standing wave if the target were absent. By comparing Figures 5 and 6, one may note that the degree of enhancement of the SAR is given more accurately by antenna theory than by standing-wave theory. As predicted by antenna theory (Figure 5), a higher SAR is observed for $d = 0.125 \lambda$ than for 0.25λ because of coupling of the target to its image. Also, a maximum gain of 4.7 was observed experimentally. This value is in excellent agreement with antenna theory and is 17% higher than the value of 4.0 predicted on the basis of standing-wave theory.

Additional points to note in Figure 6 are: (a) Non-zero energy deposition at $d = 0.5 \lambda$, which may be ascribed to absorption due to magnetic fields at this setting, and (b) An enhancement factor of less than 4 at $d = 0.75 \lambda$, which may be due to insufficiency of the reflector's dimensions. From antenna theory, a reflector with a width larger than $4d$ (in the H plane) is recommended to simulate an infinite plane.

The important features of the above results have been confirmed by experiments that were performed with 100-g Wistar rats; the rats were placed at different locations in front of the flat reflector and were subjected to incident fields at their resonance frequency of 987 MHz. The details and the results of these experiments will be given elsewhere [Gandhi and Hunt, 1977].

The enhancement factor as a function of L/λ was measured (Figure 7) with different sizes of figurines at 987 and 2450 MHz. Because of the fairly broad lateral

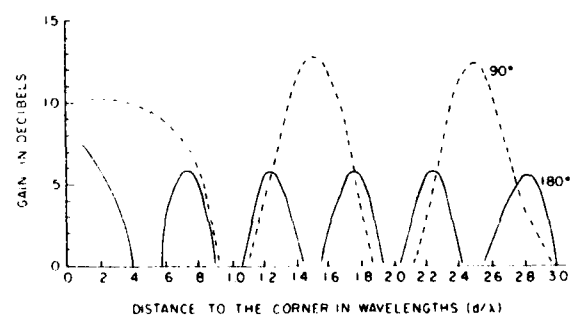


Fig. 5. Gain in rate of energy received by a half-wavelength antenna located at various distances from 90° -corner and 180° flat reflectors.

DEPOSITION OF EM ENERGY

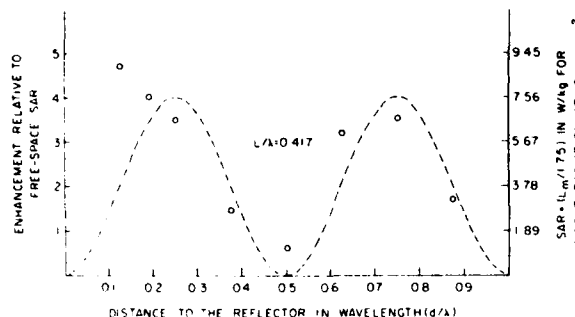


Fig. 6. The data points are measured values of whole-body averaged SARs of a model of a human being of height L (in meters) that is exposed near a flat reflector. The values of E^2 in the absence of the target are shown by the dashed line.

dimensions of the larger targets, a complete set of data was possible only for $d = 3\lambda/4$. The points to note in Figure 7 are: (a) The enhancement in SAR at frequencies above resonance diminishes and asymptotically approaches a value of about 2, (b) At frequencies below resonance, a higher gain in SARs from the corresponding free space values (Figure 1) is observed, and (c) For $d = 0.125\lambda$, a reduced enhancement factor is observed for smaller targets, which is reminiscent of the standing-wave point of view.

6. ENHANCED ABSORPTION CAUSED BY 90° CORNERS OF REFLECTING SURFACES

Using the near-resonant ($L/\lambda = 0.417$) saline-filled figurine, energy deposition rates were measured at

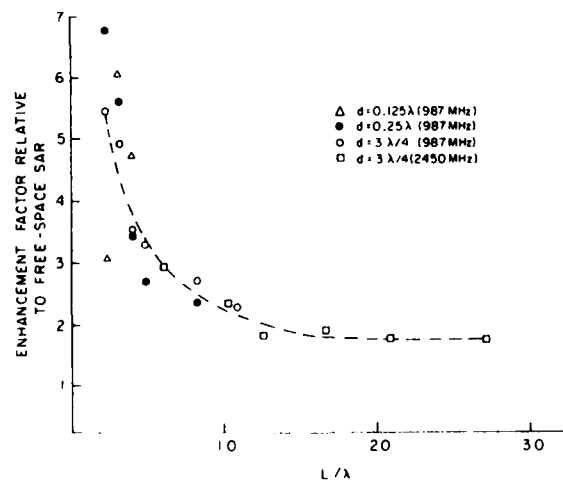


Fig. 7. Enhanced SARs of a body near a flat reflector as a function of the body's length in relation to wavelength of incident radiation.

different locations along the diagonal of the 90° corner of several reflectors, each of dimensions $3.5\lambda \times 2\lambda$ (in the E direction). The measured enhancement factors relative to the free-space value and the corresponding SARs for man are plotted in Figure 8. Also shown for comparison in the same figure are the values of E^2 as calculated from standing-wave theory (the kind of values that will be registered by a so-called power-density meter that is calibrated for free-space measurements). As with the flat reflector, the results here also conform to predictions based on antenna theory (Figure 5). Enhancement factors as large as 27 are observed for $d/\lambda = 1.5$. Another point of agreement with antenna theory is a plateau in the enhancement factor at a value of approximately 10.5 for $d/\lambda \leq 0.45$. Reduced gains of hot spots that are closer to the corner compared to $d = 1.5\lambda$ are predicted from antenna theory [Jasik, 1961] because of mutual-impedance effects.

A measured enhancement factor of 27 (Figure 8) in the SAR is considerably larger than the value of 16 that is predicted by standing-wave theory and is even higher than the value of 20 that is given by antenna theory for a 90° corner of a semi-infinite reflector. Gains higher than those for semi-infinite reflectors have previously been observed [Cottony and Wilson, 1958] for corner-reflector antennas of appropriate combinations of width and length. It turns out that our reflector's dimensions of $3.5\lambda \times 2\lambda$ are, fortuitously, the result of one of the super-gain combinations. There are many other combinations of width and length [Cottony and Wilson, 1958] that may also result in high SARs.

To confirm predictions of highly enhanced SARs, experiments were performed with male Wistar rats (104 ± 8.3 g) that were placed 0.44λ and 1.5λ from the corner of the reflectors. The $d = 0.44\lambda$ location was the minimum distance to the corner possible with the relatively microwave-transparent rat holder (Figure 9) that we used in our experiments. Also for the $d = 0.44\lambda$ experiments, 90° corner reflectors, each of dimensions $2\lambda \times 2\lambda$ (rather than $3.5\lambda \times 2\lambda$), were used. From antenna theory, reflectors of dimensions $2d$ ($= 0.88\lambda$)

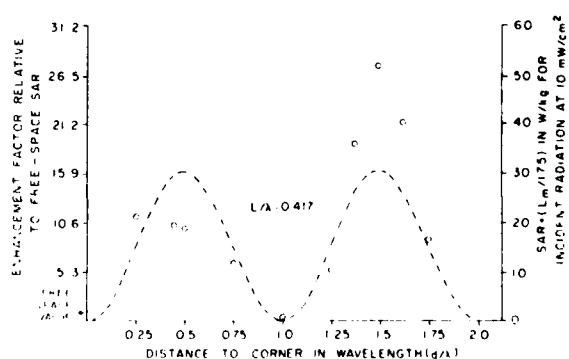


Fig. 8. Whole-body averaged SARs of a model of a human being near a 90°-corner reflector. The dashed line gives values of E^2 in the absence of the model.

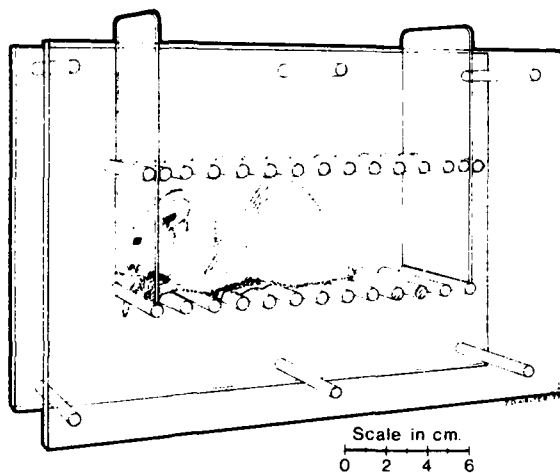


Fig. 9. Semischematic drawing of polycarbonate chamber that was used in irradiation of young rats.

$\times 0.6 \lambda$ would be quite adequate to simulate the semi-infinite sheets that would ideally be needed for 90° corners.

The mean times-to-convulsion together with the standard deviations for four animals for power densities of 3 to 20 mW/cm^2 are shown in Figure 10. For $d = 0.44 \lambda$, the mean time-to-convulsion of 225 seconds (for ~ 100 -g animals) during irradiation at 15 mW/cm^2 corresponds to the average of 260 seconds that was observed by Schrot and Hawkins [1975] for free-space irradiation at 150 mW/cm^2 . It is apparent, therefore, that the presence of a 90° -corner reflector causes an enhancement in the SAR by a factor of almost 11 as predicted from antenna theory [Jasik, 1961]. The rela-

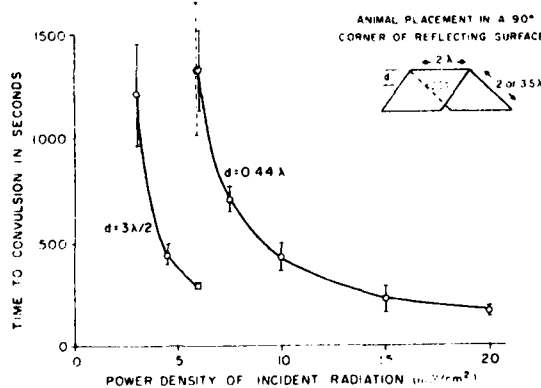


Fig. 10. Convulsive latencies ($\pm \text{SD}$) of rats (averaged mass near 100 g) as a function of measured power density of incident 987-MHz radiation for two distances of the animal from the corner of the reflector. (The dashed line and the data for $d = 3\lambda/2$ were obtained with a corner reflector of dimensions: $3.5\lambda \times 2.0\lambda$).

tive enhancements at the two locations may be compared by noting that, at power densities of 4.5 and 6 mW/cm^2 for $d = 1.5\lambda$, times-to-convulsion correspond, respectively, to 9.85 and 13.02 mW/cm^2 for $d = 0.44\lambda$. For a target-to-corner separation distance, d , of 1.5λ , a deposition rate larger by a factor of 2.18 as compared with $d = 0.44\lambda$ is consequently obtained from lethality experiments. This result is amazingly close to the relative enhancement of 2.15 observed between the two locations with man-shaped dolls (Figure 8).

The enhancement factors measured for different values of L/λ for a 90° -corner reflector are shown for $d/\lambda = 0.44, 1.5$, and 2.5 in Figure 11. As with a flat reflector, the enhancement in SAR at supraresonant frequencies diminishes and asymptotically approaches a value, in this case, of about 8. Also, for closer spacing to the corner, a reduction in the enhancement factor occurs for smaller values of L/λ . An asymptotic value of 9 would be projected from the simple-minded argument that for targets large compared to a wavelength, a three-sided rather than the four-sided exposure is more realistic. The wave that, for smaller targets, would bounce off the corner is largely masked for large values of L/λ .

From the point of view of standing-wave theory, the fields at different locations in the vicinity of a 90° -corner reflector can be written (see Figure 12) as:

$$E = E_1 + E_2 + E_3 + E_4 = E_{\text{inc}} \hat{E} \quad (5)$$

$$\cdot [1 + e^{-2jkd} - 2e^{-jkd} \cos ky]$$

where $k = 2\pi/\lambda$. Peaks of the E field are consequently anticipated not only for axial locations but also for several spots elsewhere (some of which are shown in Figure 12) in the region in front of the reflecting corner.

In order to verify the existence of hot spots elsewhere in the region of a 90° -corner reflector, whole-body

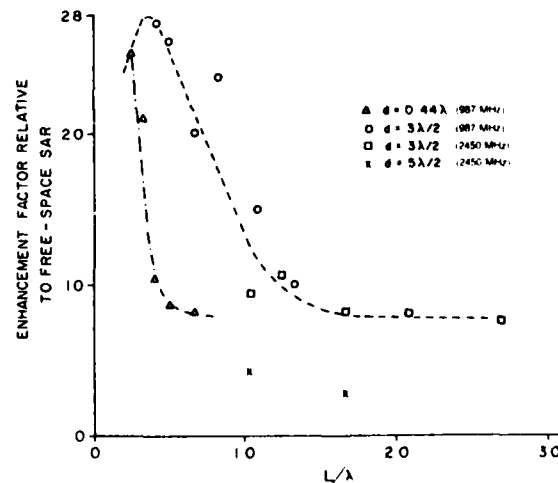


Fig. 11. Enhancement of SARs in a body near a 90° -corner reflector.

DEPOSITION OF EM ENERGY

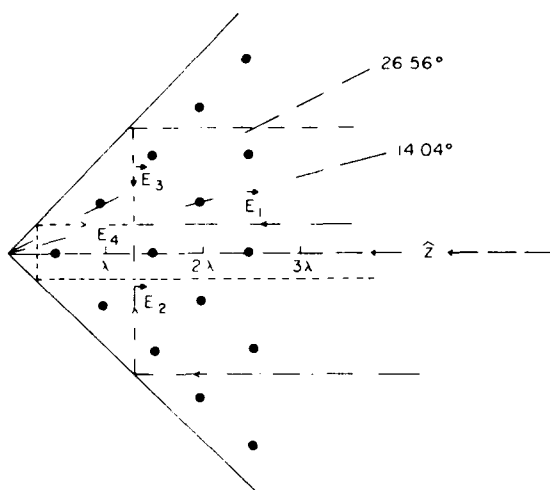


Fig. 12. E -field maxima near a 90° -corner reflector. Filled circles denote areas where a biological body will absorb maximal quantities of energy.

SARs were measured (see Figure 13) at $d/\lambda = 1.0$ with and without the 26.5° tilt of the reflectors around the E axis. The "cold" region without the tilt becomes a fairly "hot" region upon tilting. Another implication of this result is that regions associated with high rates of energy deposition are also strongly dependent on directionality of the incident field.

In view of these observations and also since the hot spots may shift rather readily upon placement of other targets in close proximity, the entire region may be considered as one that is potentially capable of creating large field enhancements.

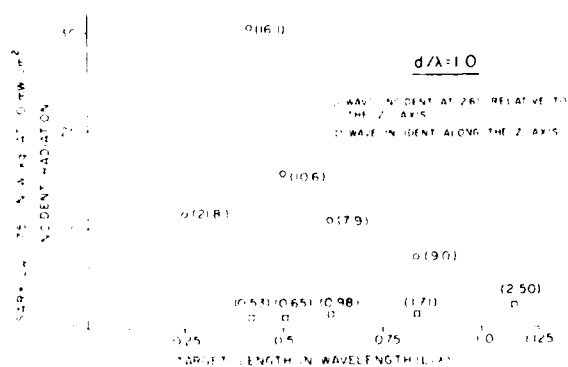


Fig. 13. Whole-body averaged SARs of models of human beings for an $E \parallel L$ orientation in a 90° -corner reflector. Numerical values in parentheses are enhancement factors relative to the free-field SAR.

Both for flat and for 90° -corner reflectors, targets placed in $k \parallel L$ and in $H \parallel L$ orientations gave SARs that were considerably enhanced as compared with their respective free-space values. In general, SAR enhancements commensurate with target-averaged E values were measured for L/λ on the order of 0.5 or less. For larger L/λ , enhancements lower than those predicted from a simple-minded E -averaged basis were measured and these are ascribed to significant perturbation of the fields by the targets.

7. CONDITIONS OF HIGHEST RATES OF ENERGY DEPOSITION IN MAN AND ANIMALS

As discussed above, some of the highest SARs in models of man and animals are observed for frequencies close to the region of resonance. Fairly strong enhancements are possible at higher frequencies in the presence of reflecting surfaces, but the enhancement of SARs here is considerably less than that which occurs at resonant frequencies. Enhancement factors just as large or somewhat larger are observed for frequencies below resonance, but the net SARs here, too, are not as large because of the rapid drop-off (see Figure 1) in the SAR on the low frequency side of the resonant curve.

In order to appreciate fully the reflector-caused enhancements of SARs, it should be mentioned that reflectors with dimensions $2d \times 1.2L$ (in the E direction) are considered adequate to simulate infinite planes. Furthermore, the reflecting surfaces need neither be good conductors nor solid in construction to cause enhancements. Indeed, surfaces of insulating material with conducting rods (oriented along E fields) that are spaced $\leq 0.1\lambda$ act quite effectively as solid conducting surfaces [Jasik, 1961].

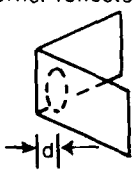
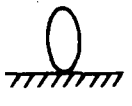
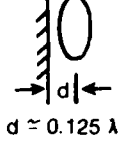
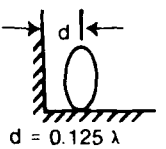
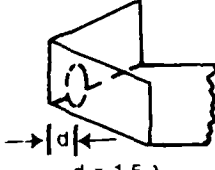
Whole-body rates of energy absorption for models of man and for animals subjected to 10 mW/cm^2 incident fields have been calculated for various exposure conditions and are tabulated in Table 1. The rates of energy deposition at resonant frequencies in the presence of a ground plane or a reflector markedly increase and, with grounding and reflection in combination they are truly staggering.

8. CONCLUSIONS

Generalized curves have been given for whole-body absorption of electromagnetic energy by models of human beings as a function of frequency for free space, for electrical contact with ground, and for the presence of reflecting surfaces. Based on these curves, generalized graphs for specific absorption rates for rats and mice are drawn and the results are shown to be in good agreement with experimental data. Tremendous enhancements in rates of energy deposition result for targets that are placed in proximity to reflecting surfaces. Energy deposition rates are given for models of man and for animals subjected to fields at a power density of 10 mW/cm^2 under various conditions of exposure; SAR values as high as 35 to 70 times the BMR are predicted for adult human beings at resonant fre-

GANDHI, HUNT, AND D'ANDREA

TABLE I. Rate of whole-body energy absorption in watts by man and animals at 10 mW/cm^2 .

70 kg Man (1.75 m Height)	100 g Rat (11.5 cm Length)	400 g Rat (18.9 cm Length)	70 kg Man (1.75 m Height)	100 g Rat (11.5 cm Length)	400 g Rat (18.9 cm Length)
38 Watts (no reflectance)	—	—	IV. At resonance for placement in a 90° corner reflector.	—	—
0.54 W/kg	—	—		—	—
19 Watts (50% reflectance)	—	—	$d = 1.5 \lambda$	—	—
0.27 W/kg	—	—	—	—	—
I. At resonance for free space.					
	—	—	—	—	—
151 Watts	0.8 Watts	2 Watts	27 \times 151 = 4077 Watts	21.6 Watts	54 Watts
2.16 W/kg	8 W/kg	5 W/kg	58.24 W/kg	216 W/kg	135 W/kg
$f \approx 62-68 \text{ MHz}$	$f \approx 987 \text{ MHz}$	$f \approx 600 \text{ MHz}$	$f \approx 62-68 \text{ MHz}$	$f \approx 987 \text{ MHz}$	$f \approx 600 \text{ MHz}$
II. At resonance for conditions of electrical contact with the ground plane.					
	—	—	—	—	—
2 \times 151 = 302 Watts	—	—	2 \times 710 = 1420 Watts	—	—
4.31 W/kg	—	—	20.28 W/kg	—	—
$f \approx 31-34 \text{ MHz}$	—	—	$f \approx 31-34 \text{ MHz}$	—	—
III. At resonance for placement in front of a flat reflector.					
	—	—	—	—	—
$d \approx 0.125 \lambda$	—	—	—	—	—
4.7 \times 151 = 710 Watts	3.8 Watts	9.4 Watts	2 \times 4077 = 8154 Watts	—	—
10.14 W/kg	38 W/kg	23.5 W/kg	116.48 W/kg	—	—
$f \approx 62-68 \text{ MHz}$	$f \approx 987 \text{ MHz}$	$f \approx 600 \text{ MHz}$	$f \approx 31-34 \text{ MHz}$	—	—
V. At resonance in electrical contact with ground plane, in front of a flat reflector.					
	—	—	—	—	—
$d = 0.125 \lambda$	—	—	—	—	—
2 \times 710 = 1420 Watts	—	—	—	—	—
20.28 W/kg	—	—	—	—	—
$f \approx 31-34 \text{ MHz}$	—	—	—	—	—
VI. At resonance in electrical contact with ground plane, in a 90° corner reflector.					
	—	—	—	—	—
$d = 1.5 \lambda$	—	—	—	—	—
2 \times 4077 = 8154 Watts	—	—	—	—	—
116.48 W/kg	—	—	—	—	—
$f \approx 31-34 \text{ MHz}$	—	—	—	—	—

quencies. The times-to-convulsion of ~ 100 -g rats for incident waves of power densities of 3 to 20 mW/cm^2 confirm some of the predictions of enhanced absorption in the presence of reflecting surfaces.

Acknowledgment. This work was supported by U. S. Army Medical Research and Development Command, Washington, D. C., under contract DAMD 17-74-C-4092.

The animals involved in this study were procured, maintained, and used in accordance with the Animal Welfare Act of 1970 and the "Guide for the Care and Use of Laboratory Animals" prepared by the Institute of Laboratory Animal Resources, National Research Council.

Cottony, H. V., and A. C. Wilson, (1958), gains of finite-size corner reflector antennas, *IRE Trans. Ant. Prop.* AP-6, 366-369.

Dreyfuss, H. (1967), *The Measure of Man, Human Factors in Design*, Whitney Library of Design, New York.

Gandhi, O. P. (1974), Polarization and frequency effects on whole animal absorption of RF energy, *Proc. IEEE*, 62, 1166-1168.

Gandhi, O. P. (1975), Conditions of strongest electromagnetic power deposition in man and animals, *IEEE Trans. Microwave Theory Tech.*, MTT-23, 1021-1029.

REFERENCES

DEPOSITION OF EM ENERGY

Gandhi, O. P., K. Sedigh, G. S. Beck, and E. L. Hunt (1976), Distribution of electromagnetic energy deposition in models of man with frequencies near resonance, in *Biological Effects of Electromagnetic Waves, Selected Papers of the USNC/URSI Annual Meeting, Boulder, Colorado, October 20-23, 1975, Vol. II, 44-67*, edited by C. C. Johnson and M. L. Shore, HEW Publ. (FDA) 77-8011, U. S. Government Printing Office, Washington, D.C. 20402.

Gandhi, O. P., and E. L. Hunt (1977), Enhancement in electromagnetic energy deposition for man and animals in the presence of reflecting surfaces, to be published.

Guyton, A. C. (1968), *Textbook of Medical Physiology*, pp. 978-983, W. B. Saunders, Philadelphia, Pennsylvania.

Jasik, H., (Ed.) (1961), *Antenna Engineering Handbook*, McGraw-Hill, New York, Chapter 11.

Massoudi, H., C. H. Durney, C. C. Johnson, and S. Allen (1976), Theoretical calculations of power absorbed by monkey and human prolate spheroidal phantoms in an irradiation chamber, in *Biological Effects of Electromagnetic Waves, Selected Papers of the USNC/URSI Annual Meeting, Boulder, Colorado, October 20-23, 1975, Vol. II, 135-157*, edited by C. C. Johnson and M. L. Shore, HEW Publ. (FDA) 77-8011, U. S. Government Printing Office, Washington, D.C. 20402.

Schrot, J., and T. D. Hawkins (1976), Interaction of microwave frequency and polarization with animal size, in *Biological Effects of Electromagnetic Waves, Selected Papers of the USNC/URSI Annual Meeting, Boulder, Colorado, October 20-23, 1975, Vol. II, 184-192*, edited by C. C. Johnson and M. L. Shore, HEW Publ. (FDA) 77-8011, U. S. Government Printing Office, Washington, D.C. 20402.

APPENDIX D

Radiators for microwave biological effects research – waveguide slot array with constant radiation intensity

Mark J. Hagmann and Om P. Gandhi

Departments of Electrical Engineering and Bioengineering, University of Utah, Salt Lake City, Utah 84112

A longitudinal-shunt slot array with reflectors has been designed, built, and tested. The antenna is easily matched near the design frequency. The radiation pattern has an intensity within ± 0.5 dB over a total angle of 15.6° in the H plane and 15.5° in the E plane. Gain is 19.7 dB which is 3.9 dB above that of a horn with a similar work area. By using energy-absorbing material, it is possible to produce a pattern in which the fields drop suddenly from the nearly constant values to nearly zero.

1. INTRODUCTION

Microwave biological studies with large targets or multiple targets require a large working area that provides near-uniform exposures to energy. At high microwave frequencies where high-power sources are not readily available, it is desirable to use a radiator that provides a constant intensity beam so the working area may receive almost all of the radiated energy.

A longitudinal-shunt slot array with reflectors has been designed, built, and tested, and has been found to have characteristics that are suitable for use in microwave biological studies. Design theory and characteristics are described in the following sections.

2. DESIGN THEORY

If finite width, thickness, and conductivity of the wall are neglected, then the radiation of a longitudinal resonant slot is identical to that of a half-wave dipole of same orientation if E and H fields are interchanged [Compton *et al.*, 1969]. A collinear array of half-wave dipoles may therefore be designed to obtain a desired pattern in the plane of the array, and the design parameters may then be used for a longitudinal-shunt slot array with a similar pattern of radiation intensity.

A half-wave dipole antenna that is located at the origin and oriented on the z axis will produce radiation with electric field intensity

$$E = \{j\eta I_m \cos[(\pi/2)\cos\theta]/(2\pi r_0 \sin\theta)\} \hat{\theta} \quad (1)$$

where η is the intrinsic impedance of free space, I_m is the peak current, ω is the angular frequency, k is the magnitude of the free-space propagation vector, r_0 is the distance from the point of origin to the point of observation, and θ is the angle from the positive z axis to the point of observation.

If a collinear array is formed with an odd number N of symmetrically fed half-wave dipoles that have center-to-center spacing d and peak current in the n th dipole I_n , then superposition using equation (1) gives the total E field

$$E_T = \frac{j\eta \cos[(\pi/2)\cos\theta]}{\pi r_0 \sin\theta} [\exp(j(\omega t - kr_0)) \cdot \sum_{n=0}^{(N-1)/2} I_n \cos(nkd \cos\theta)] \hat{\theta} \quad (2)$$

$$\cdot [\sum_{n=0}^{(N-1)/2} I_n \cos(nkd \cos\theta)] \hat{\theta}$$

Equation (2) was used to design a collinear array of half-wave dipoles having a radiation intensity that is nearly constant within a specified beam width and is nearly zero elsewhere. Weighted least squares were used to reduce the overshoot and ripple found in a Fourier synthesis of a discontinuous pattern.

Let the desired pattern be given by

$$f(\theta) = \begin{cases} \frac{j\eta A}{r_0} [\exp(j(\omega t - kr_0))] \hat{\theta} & \text{for } \frac{\pi - \xi}{2} < \theta < \frac{\pi + \xi}{2} \\ 0 & \text{elsewhere} \end{cases} \quad (3)$$

Define the weighting factor as

$$W(\theta) = \begin{cases} 1 & \text{for } \frac{\pi - \xi}{2} < \theta < \frac{\pi + \xi}{2} \\ \Delta & \text{elsewhere} \end{cases} \quad (4)$$

For weighted least squares, we wish to minimize the quantity:

$$\begin{aligned}
 S = & \int_0^{(\pi-\xi)/2} \left\{ \frac{\cos[(\pi/2)\cos\theta]}{\sin\theta} \sum_{n=0}^{(N-1)/2} I_n \cos(nkd \cos\theta) \right\}^2 d\theta \\
 & + \int_{(\pi-\xi)/2}^{(\pi+\xi)/2} \left\{ A - \frac{\cos[(\pi/2)\cos\theta]}{\sin\theta} \sum_{n=0}^{(N-1)/2} I_n \cos(nkd \cos\theta) \right\}^2 d\theta \quad (5) \\
 & + \int_{(\pi+\xi)/2}^{\pi} \left\{ \frac{\cos[(\pi/2)\cos\theta]}{\sin\theta} \sum_{n=0}^{(N-1)/2} I_n \cos(nkd \cos\theta) \right\}^2 d\theta
 \end{aligned}$$

Set $\partial S / \partial I_m = 0$ and use symmetry of the integrands in equation (5) about $\theta = \pi/2$ to obtain

$$\begin{aligned}
 & \int_0^{(\pi-\xi)/2} \left\{ \frac{\cos[(\pi/2)\cos\theta]}{\sin\theta} \right\}^2 \cos(mkd \cos\theta) \sum_{n=0}^{(N-1)/2} I_n \cos(nkd \cos\theta) d\theta \\
 & - \int_{(\pi-\xi)/2}^{\pi/2} \frac{A \cos[(\pi/2)\cos\theta]}{\sin\theta} \cos(mkd \cos\theta) d\theta \quad (6) \\
 & + \int_{(\pi-\xi)/2}^{\pi/2} \left\{ \frac{\cos[(\pi/2)\cos\theta]}{\sin\theta} \right\}^2 \cos(mkd \cos\theta) \sum_{n=0}^{(N-1)/2} I_n \cos(nkd \cos\theta) d\theta = 0
 \end{aligned}$$

Using all possible values of the index m in equation (6), there are $(N + 1)/2$ linear equations involving the $(N + 1)/2$ unknown currents. The system of equations may be written using matrix notation

$$M_{mn} I_n = B_m A \quad (7)$$

The matrix elements in equation (7) are given by

$$\begin{aligned}
 M_{mn} = & \int_0^{(\pi-\xi)/2} \left\{ \frac{\cos[(\pi/2)\cos\theta]}{\sin\theta} \right\}^2 \cos(mkd \cos\theta) \cos(nkd \cos\theta) d\theta \\
 & + \int_{(\pi-\xi)/2}^{\pi/2} \left\{ \frac{\cos[(\pi/2)\cos\theta]}{\sin\theta} \right\}^2 \cos(mkd \cos\theta) \cos(nkd \cos\theta) d\theta \quad (8)
 \end{aligned}$$

$$B_m = \int_{(\pi-\xi)/2}^{\pi/2} \frac{\cos[(\pi/2)\cos\theta]}{\sin\theta} \cos(mkd\cos\theta) d\theta \quad (9)$$

A FORTRAN program was written in which quadratures in equations (8) and (9) were performed using Simpson's rule with due respect for the indeterminant form of the integrand in equation (8) at $\theta = 0$. The matrix equation (7) is then solved with $L - U$ decomposition.

The beam width ξ was chosen as 12.5° to be small enough for the radiation to approximate a plane wave, yet give enough divergence for convenient chamber dimensions. For a resonant array the center-to-center spacing of slots should be an integral multiple of $\lambda_g/2$, so set $d = \lambda_g/2$, or $kd = 4.049$ for a design frequency of 10.4 GHz with an RG-52/U waveguide.

The ANPLOT [Gandhi, 1974] program was used to find the radiation pattern for a series of collinear dipole arrays with currents satisfying the matrix equation (7) with $\xi = 12.5^\circ$, $kd = 4.049$, and various values of N and Δ . A value of $\Delta = 0.002$ was found to provide a suitable compromise in reducing overshoot and ripple with fast rolloff outside the chosen beam width. The value $N = 11$ was found to be the minimum number of dipoles required to give a resonable approximation of the desired pattern. Table 1 gives the normalized currents found in the solution for 11 dipoles with $\Delta = 0.002$.

Next, a longitudinal-shunt slot array was designed that produces a pattern of radiation intensity similar to that of the optimized dipole array.

The normalized conductance of a longitudinal slot at a distance X from the axis of the broad face of a waveguide is given by [Ehrlich, 1961]:

$$g = 2.09(\lambda_g/\lambda)(a/b)\cos^2(\pi\lambda/2\lambda_g)\sin^2(\pi X/a) \quad (10)$$

The currents in the fourth pair of dipoles are inconveniently small, so slots were not used in those positions. Currents in the remaining slots have the same ratio as those in the dipole array if

$$g_0:g_1:g_2:g_3:g_5 = I_0^2:I_1^2:I_2^2:I_3^2:I_5^2 \quad (11)$$

For matching at the design frequency,

$$g_0 + 2g_1 + 2g_2 + 2g_3 + 2g_5 = 1 \quad (12)$$

The conductances g_n in Table 1 were found by solving the simultaneous equations given by equations (11) and (12). Knowing the g_n , the locations X_n are found from equation (10) and are given in Table 1. The slots are not collinear, but patterns found with ANPLOT suggest that radiation in the H plane of the slot array is not significantly altered from that for a collinear array. The slot lengths in Table 1 are for resonant slots with width of 0.0625 inches with the values of X_n [Ehrlich, 1961].

A sketch of the designed longitudinal-shunt slot array is given in Figure 1. A sliding short is used to allow tun-

TABLE 1. Current, conductance, location, and length of slots.

n	I_n	g_n	X_n Inches	l_n Inches
0	1.000000	0.244581	0.1781	0.5678
1	0.908742	0.201978	0.1598	0.5656
2	0.679020	0.112768	0.1165	0.5576
3	0.366270	0.032811	0.06159	0.5508
4	-0.0163023	--	--	--
5	-0.351113	0.030152	0.05900	0.5497

ing instead of using a fixed short at the theoretical location of $3\lambda_g/4$ from the center of the last slot.

The radiation pattern from the slot array just described is acceptable in the H plane but the pattern is slowly varying in the E plane. Reflectors are therefore used to improve the pattern in the E plane.

Reflectors may be attached to the sides of the waveguide as shown in Figure 2. Let a' be the distance between the reflectors in the plane of the aperture and ϕ be the angle from a normal to the plane of the array to the observation point in the E plane. If we consider only diffraction in the E plane, then from [Sherman, 1970] we can define

$$U = (\pi/a'/\lambda)\sin\phi \quad (13)$$

and the radiation intensity will follow

$$P \sim (\sin\phi/u)^2 \quad (14)$$

If we require the radiation intensity at $\phi = \pm 6^\circ$ to be down only ten percent from the peak value, then $a'/\lambda = 1.703$. The reflector design is shown in Figure 2. A photograph of the slot array with reflectors is given in Figure 3.

3. ANTENNA CHARACTERISTICS

Figure 4 gives the VSWR characteristics of the slot array without reflectors. The sliding short was adjusted for minimum reflection at each frequency of measurement. At the design frequency of 10.4 GHz, the minimum VSWR was found to be 1.01 with a short position 0.34 cm further from the center of the last slot than the theoretical value of $3\lambda_g/4$.

Figure 5 gives the VSWR characteristics of the slot array with reflectors. The bottom curve gives the VSWR with the short adjusted for minimum reflection at each frequency of measurement. At the design frequency of 10.4 GHz, the minimum VSWR was 1.16 with a short position 0.50 cm further from the center of the last slot than the theoretical value of $3\lambda_g/4$. Tuning with the sliding short is relatively sharp so that a VSWR of 2.36 was found using the theoretically shorted position. Figure 5 also gives the VSWR characteristics with the short fixed at positions for minimum reflection at 10.0,

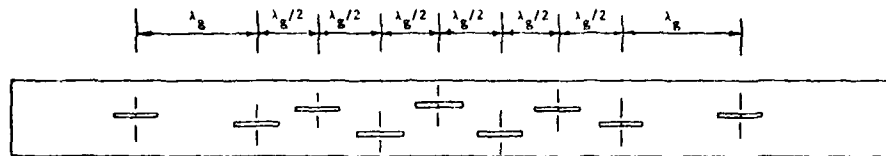


Fig. 1. Design of the longitudinal-shunt slot array.

10.2, 10.4, and 10.5 GHz. A sliding short with a set screw is recommended for use with the antenna. All of the pattern measurements that are described in the following were measured with the sliding short adjusted for minimum reflection.

All pattern measurements were made in a plane at a distance of 2 meters from the plane of the array in an anechoic chamber. The reflectors were used for all patterns.

Figure 6 shows both the theoretical and measured patterns in the plane of the array or in the *H* plane. The radiation intensity varied by less than ± 0.5 dB over an angle of 15.6° . The theoretical pattern was found by neglecting the reflectors and approximating the slots with half-wave dipoles as described in Section 2.

Figure 7 shows both the theoretical and measured patterns in the *E* plane. The radiation intensity varied by less than ± 0.5 dB over an angle of 15.5° . The theoretical pattern was found by assuming diffraction from an aperture having uniform irradiation as described in Section 2.

The gain was determined by a substitution method in which the same crystal detector was used to measure both transmitted and received values of power. An open-ended RG-52/U waveguide was used as the receiving antenna at a distance of 2 meters from the plane of the array. Attenuation was introduced so that the

two measurements of power were made within 1 dB. Gain of the array with reflectors was found to be 19.7 dB. The array with reflectors has radiation intensity down less than 1 dB from peak over a total angle of 15.6° in the *H* plane and 15.5° in the *E* plane. The two angles define the work area if we will tolerate only ± 0.5 dB variation in radiation intensity. An ideal radiator that produces a constant radiation intensity over a rectangle limited by the two angles and zero elsewhere would have a gain of 22.3 dB so the gain of the array with reflectors is 2.6 dB below ideal.

An optimal horn is defined as one where the dimensions of the aperture are adjusted to give maximum gain for given slant lengths of flare in the *H* and *E* planes [Jakes, 1961]. Using design curves given by Jakes, an optimal horn will produce a pattern with the same angles for ± 0.5 dB variation with $b/\lambda = 2.08$, $a/\lambda = 2.87$, and a gain of 15.8 dB. Gain of the array with reflectors is consequently 3.9 dB above the horn.

4. INCREASING CONTRAST WITH ENERGY-ABSORBING MATERIAL

There are biological applications in which it is desired to have a region of constant irradiation and a region of

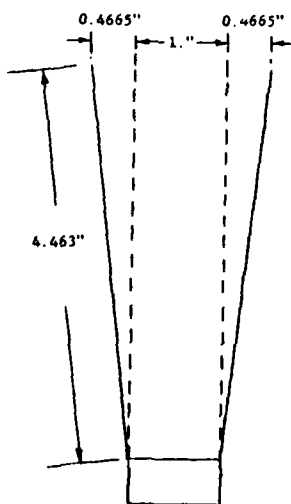


Fig. 2. Design of reflectors used with the slot array.

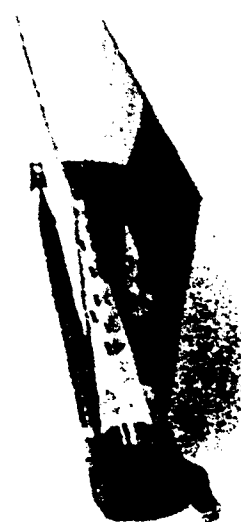


Fig. 3. Slot array with reflectors.

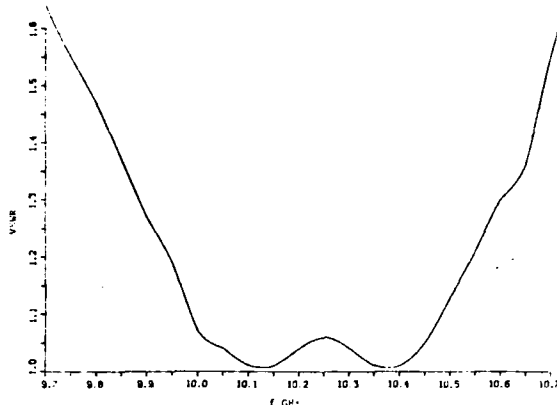


Fig. 4. Reflection characteristics of slot array without reflectors.

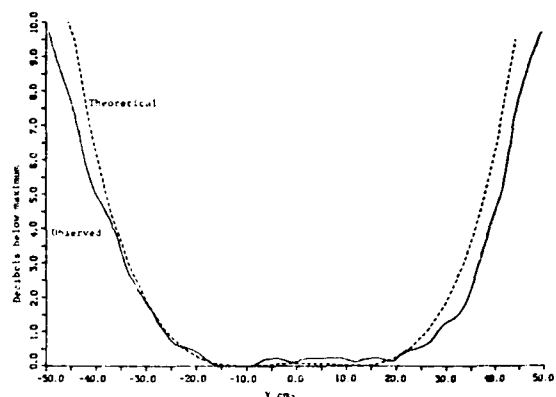


Fig. 6. *H*-plane pattern of slot array with reflectors at 10.4 GHz at a distance of 2 meters.

near zero irradiation with a sharp common boundary. Tests have been made in which a 4-inch thick sheet of energy-absorbing material is used to interrupt part of the beam from the slot array.

Figure 8 gives the *H*-plane pattern with and without interruption by a sheet of energy-absorbing material. Figure 9 gives the *E*-plane pattern found with and without interruption by a sheet of energy-absorbing material. In both figures diffraction effects broaden the boundary between the irradiated and nonirradiated regions to an inch or two. All measurements were made immediately behind the plane of the dark side of the sheet of energy-absorbing material.

5. CONCLUSIONS

A longitudinal-shunt slot array with reflectors has been designed, built, and tested. The antenna is easily matched with a sliding short at the design frequency and does not require an additional tuner. The antenna produces a pattern with a radiation intensity that is constant within ± 0.5 dB over a total angle of 15.6° in the *H* plane and 15.5° in the *E* plane. Gain is 3.9 dB above that of a typical horn with a similar work area.

All design parameters are given for the 10.4-GHz antenna but the design theory is readily applicable to other microwave frequencies.

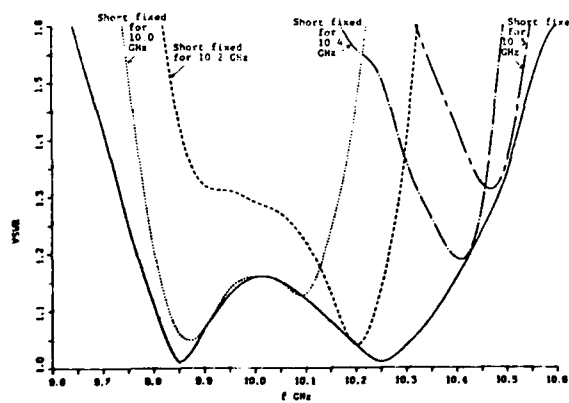


Fig. 5. Reflection characteristics of slot array with reflectors.

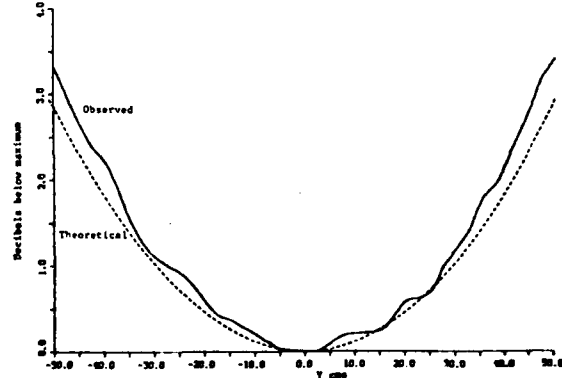


Fig. 7. *E*-plane pattern of slot array with reflectors at 10.4 GHz at a distance of 2 meters.

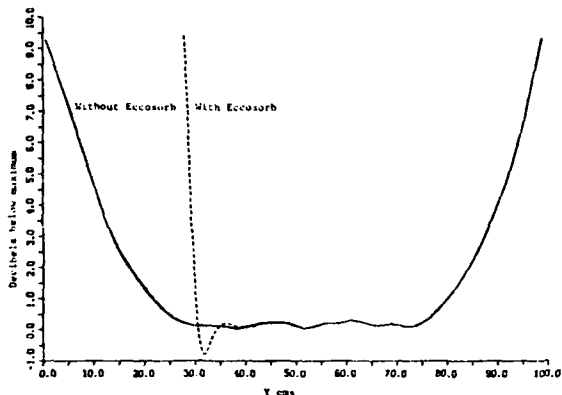


Fig. 8. *H*-plane pattern of slot array with reflectors at 10.4 GHz at a distance of 2 meters with and without Eccosorb.

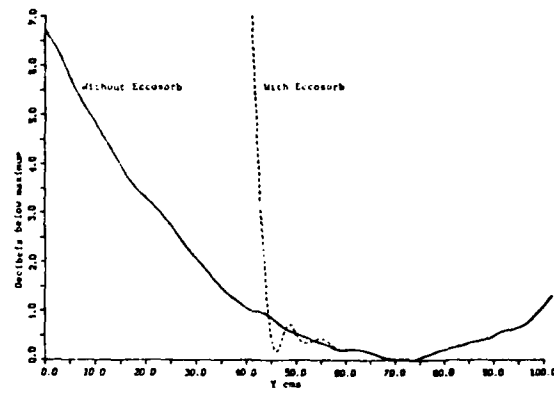


Fig. 9. *E*-plane pattern of the slot array with reflectors at 10.4 GHz at a distance of 2 meters with and without Eccosorb.

Acknowledgment. This work was supported by U. S. Army Medical Research and Development Command, Washington, D. C., under contract DAMD 17-74-C-4092.

REFERENCES

Compton, R. T., Jr., and R. E. Collin (1969), Slot antennas, in *Antenna Theory*, edited by R. E. Collin and F. J. Zucker, Part 1, pp. 560-620, McGraw-Hill, New York.

Ehrlich, M. J. (1961), Slot-antenna arrays, in *Antenna Engineering Handbook*, edited by H. Jasik, 9, pp. 1-18, McGraw-Hill, New York.
 Jakes, W. C., Jr. (1961), Horn antennas, in *Antenna Engineering Handbook*, edited by H. Jasik, 10, pp. 1-18, McGraw-Hill, New York.
 Gandhi, O. P. (1974), A computer program for calculating the radiation pattern of a general antenna array, *IEEE Trans. Educ.*, E-17, 124-126.
 Sherman, J. W., III (1970), Aperture-antenna analysis, in *Radar Handbook*, edited by M. K. Skolnik, 9, pp. 1-40, McGraw-Hill, New York.

Upper Bound on Cell Size for Moment-Method Solutions

MARK J. HAGMANN, STUDENT MEMBER, IEEE, OM P. GANDHI, SENIOR MEMBER, IEEE,
AND CARL H. DURNEY, MEMBER, IEEE

Abstract—When pulse functions are used in moment-method solutions, failure to allow for variation of the field within each cell limits the maximum usable electrical size of the cells. Appreciable error is expected for $|k|l \geq 2$ in one or two dimensions and $|k|l \geq \sqrt{6}$ in the three-dimensional problem where l is the side of a cell and k is the propagation constant in the material.

I. INTRODUCTION

IN ELECTROMAGNETICS, discretization of transformation of an integral equation to a matrix equation is often accomplished using pulse functions as a basis [1]–[4]. When using pulse functions, the scatterer is partitioned into a number of cells N , where N is large enough that complex permittivity and the complex time-independent electric field may be assumed constant within each subvolume.

In a given problem, it is common to estimate the maximum usable cell size and try several values of N to test for apparent convergence of the resulting solutions [5]. An approximate upper bound on cell size may be found from observation of the oscillatory nature of the kernel in the integral equation, which suggests that the cell size not exceed $\lambda_0/5$, where λ_0 is the free space wavelength [6]. It is the object of this paper to establish a significantly tighter upper bound on cell size in moment-method solutions with scatterers when pulse functions are used as the basis.

II. EVALUATION OF THE BOUND ON CELL SIZE

Consider a source-free region of space in which the dielectric properties are homogeneous, linear, and isotropic. All fields are assumed to have $\exp(j\omega t)$ time variation. We may set up a local Cartesian coordinate system at any point in the region and require that the homogeneous wave equation be satisfied:

$$\nabla^2 \vec{E} + k^2 \vec{E} = 0. \quad (1)$$

Six points are chosen a distance S from the origin on halves of each of the three local axes. f_i will represent the value of one component of \vec{E} , say E_x , at the i th point. Let

$$\delta f_i \equiv f_i - f_o \quad (2)$$

where f_o is the value of E_x at the origin.

If S is small enough so that there is little variation in E_x ,

Manuscript received November 29, 1976; revised April 4, 1977. This work was supported by the U.S. Army Medical Research and Development Command, Washington, DC, under Contract DAMD 17-74-C-4092.

The authors are with the Department of Electrical Engineering, University of Utah, Salt Lake City, UT 84112.

the difference equation approximation of (1) may be used with the result

$$\sum_{i=1}^6 \delta f_i + k^2 S^2 f_o = 0. \quad (3)$$

The greatest (in absolute value) of the δf_i must satisfy

$$\frac{|\delta f_i|}{|f_i|} \geq \frac{|k| S^2}{6}. \quad (4)$$

When (4) predicts large variations, we cannot expect the prediction to be quantitative, but we may safely infer that substantial variation of the fields will always occur within the volume of a cell containing the six points if the predicted fractional variation has a value of, say, one-half, for which

$$|k| S = \sqrt{3}. \quad (5)$$

Restricting our attention to cubical cells, we note that the smallest cube containing the six points has side

$$l = \sqrt{2} S \quad (6)$$

so large variations in the fields are expected for

$$|k| l \geq \sqrt{6}. \quad (7)$$

The corresponding result for square cells with side l in the two-dimensional problem or linear cells of length l in the one-dimensional problem is

$$|k| l \geq 2. \quad (8)$$

In an efficient moment-method solution such as in [1]–[4], variation of the Green's function within each cell is closely approximated so that the primary source of error is imperfect representation of the fields by the basis. If pulse functions are used, it is assumed that the fields are constant within each cell. Then appreciable error is expected if (8) is satisfied in a one- or two-dimensional problem or if (7) is satisfied in a three-dimensional problem. The smoothing property of the integral operator causes the error in the solution to be somewhat less than may be anticipated for a simple basis, but we may still expect that (7) and (8) give a reasonable upper bound for cell size.

III. EXAMPLES

The bound of (7) is tighter than that found from consideration of the oscillatory nature of the kernel for scatterers having a relative permittivity ϵ_r , such that $|\epsilon_r| > 3.8$. In order to illustrate this, a couple of biological applications using dielectric properties of muscle [7] will be considered

TABLE I
VALUES OF THE INDUCED ELECTRIC FIELD AT THE
CENTER OF MUSCLE CUBES AT 2450 MHz
AS GIVEN IN [4]: $\epsilon_1/\epsilon_0 = 47.0$, $\sigma = 2.21 \text{ mho/m}$

	Number of Cells	l/λ_e	$ k l$	l/λ_0	$ E _{\text{Center}} (\text{V/m})$
Cube one	1	1	6.37	0.144	0.0789
$a = \lambda$	27	1/3	2.12	0.0481	0.0922
Cube two	1	1/4	1.59	0.0361	0.0592
$a = \lambda/4$	27	1/12	0.531	0.0120	0.0556

TABLE II
ERRORS IN THE AVERAGE SPECIFIC ABSORBED POWER
DENSITY FOR AN INFINITE CYLINDER OF MUSCLE
WITH A 20- BY 20-cm CROSS SECTION AT 100 MHz:
 $\epsilon_1/\epsilon_0 = 68.0$, $\sigma = 0.890 \text{ mho/m}$

Number of Cells	l/λ_e	$ k l$	l/λ_0	Error
4	0.367	2.76	0.0334	-34.90%
9	0.245	1.84	0.0222	-16.40%
16	0.183	1.38	0.0167	-8.64%
25	0.147	1.11	0.0133	-4.96%

since the complex permittivity has a relatively large magnitude.

Table I uses the results given in [4] for two muscle cubes having sides of $a = \lambda_e$ and $\lambda_e/4$, respectively, at 2450 MHz, where λ_e is the wavelength in the material. No analytical solution is available for comparison, but variation of the calculated electric field with cell size suggests that there is significant error in the single-cell solution for the larger muscle cube. The small values of l/λ_0 suggest that the oscillatory nature of the kernel should contribute little error in the four calculations. Values of $|k|l$ and (7) suggest that significant error should be found using one cell with the larger cube, as is observed.

For the second example, Richmond's method [1] was used

to calculate the average specific absorbed power density in an infinite cylinder of muscle with a 20- \times 20-cm square cross section. A plane wave at 100 MHz with a power density of 1 mW/cm² incident normal to one of the four congruent flat surfaces was used for TM excitation. The average specific absorbed power density found using 100 cells is 0.05534 mW/cm³, which was used as a standard, differing by 0.39 percent from the value found using 81 cells. Table II gives the results found using fewer cells. Note that significant error is encountered when (8) is satisfied even though l/λ_0 is so small that the oscillatory nature of the kernel contributes negligible error.

IV. CONCLUSIONS

When pulse functions are used in moment-method solutions, failure to allow for variation of the field within each cell limits the maximum usable electrical size of the cells. Appreciable error is expected for $|k|l \geq 2$ in one or two dimensions, and $|k|l \geq \sqrt{6}$ in three-dimensional problems, where l is the side of a cell. The new upper bounds for cell size are significantly tighter than those found from the oscillatory nature of the kernel if the scatterer has a large relative permittivity. The new upper bounds have been demonstrated with two- and three-dimensional solutions.

REFERENCES

- [1] J. H. Richmond, "Scattering by a dielectric cylinder of arbitrary cross section shape," *IEEE Trans. Antennas Propagat.*, vol. AP-13, pp. 334-341, May 1965.
- [2] J. H. Richmond, "TE-wave scattering by a dielectric cylinder of arbitrary cross section shape," *IEEE Trans. Antennas Propagat.*, vol. AP-14, pp. 460-464, July 1966.
- [3] G. W. Hohmann, "Three-dimensional induced polarization and electromagnetic modeling," *Geophysics*, vol. 40, pp. 309-324, Apr. 1975.
- [4] D. E. Livesay and K. M. Chen, "Electromagnetic fields induced inside arbitrarily shaped biological bodies," *IEEE Trans. Microwave Theory Tech.*, vol. MTT-22, pp. 1273-1280, Dec. 1974.
- [5] R. H. T. Bates, "Analytic constraints on electromagnetic field computations," *IEEE Trans. Microwave Theory Tech.*, vol. MTT-23, pp. 605-623, Aug. 1975.
- [6] D. S. Jones, "Numerical methods for antenna problems," *Proc. Inst. Elec. Eng.*, vol. 121, pp. 573-582, July 1974.
- [7] C. C. Johnson and A. W. Guy, "Nonionizing electromagnetic wave effects in biological materials and systems," *Proc. IEEE*, vol. 60, pp. 692-718, June 1972.

APPENDIX F

PROCEDURES FOR IMPROVING CONVERGENCE OF MOMENT-METHOD SOLUTIONS IN ELECTROMAGNETICS*

M. J. Hagmann, O. P. Gandhi, and C. H. Durney
Department of Electrical Engineering
University of Utah
Salt Lake City, Utah 84112

ABSTRACT

Two new methods, termed "Plane Wave Correction" and "Cylindrical-Cell Correction", are presented for improving convergence of moment-method solutions in electromagnetics. Convergence is improved because the calculations include approximation for the variation of the field within each cell.

* This work was supported by U. S. Army Medical Research and Development Command, Washington, D. C., under Contract DAMD 17-74-C-4092.

Accepted for publication in *IEEE Transactions on Antennas and Propagation*

I. INTRODUCTION

In electromagnetics, discretization for transforming an integral equation to a matrix equation is commonly accomplished using pulse functions as a basis.¹⁻⁴ More elaborate bases such as modal fields may be justified in a particular problem but are avoided in the matrix formulation for the general scattering body.

Discretization with pulse functions requires that the scattering body be partitioned into a number N of cells, where N is large enough that complex permittivity and the complex time-independent electric field may be assumed constant within each subvolume. In a numerical solution the required storage is proportional to N^2 . With Gaussian elimination, solution of the matrix equation requires a number of operations that are proportional to N^3 . If N is large so that matrix storage and solution of the matrix equation are the dominant factors, the cost of computation is proportional to the product of storage and time, or N^5 . Procedures for improving convergence with the general scattering body are of interest since even a 13 percent reduction in the required number of cells would result in a cost savings of 50 percent when large N is required.

This paper describes two new procedures which have been found to improve convergence in solution of the two-dimensional problem of TM excitation of an infinite cylinder of arbitrary cross section shape. Convergence is improved because the calculations include part of the variation of the field within each cell.

II. REVIEW OF EARLIER SOLUTIONS USING PULSE FUNCTIONS

For TM excitation of an infinite cylinder, both incident and scattered fields have \vec{E} directed parallel to the infinite dimension (z axis). The electric field is described by a scalar integral equation:

$$E_z(x, y) = E_z^i(x, y) - \frac{jk_o^2}{4} \iint [e_r(x', y') - 1] E_z(x', y') H_o^{(2)}(k_o \rho) dx' dy' \quad (1)$$

where (x, y) and (x', y') are coordinates of the observation point and source point, respectively; ρ is the distance between the two points; E_z^i and E_z are incident and total electric field intensity, respectively, with $e^{j\omega t}$ time dependence; $e_r(x', y')$ is complex permittivity at the source point; $k_o \equiv \omega \sqrt{\mu_o \epsilon_o}$, and $H_o^{(2)}(k_o \rho)$ is the Hankel function of zero order.

The discrete analog of Eq. 1 consists of the N-by-N system of linear equations:

$$\sum_{n=1}^N A_{mn} E_{zn} = E_{zm}^i \quad m = 1, 2, \dots, N \quad (2)$$

Richmond performed the discretization using pulse functions.¹ Each square cell was approximated by a circle of radius a having an equal area to simplify integration of Bessel functions. His expressions for the matrix elements follow:

$$A_{mm} = 1 + (e_{rm} - 1) \left[1 + \frac{j\pi k_o a}{2} H_1^{(2)}(k_o a) \right] \quad (3)$$

$$A_{mn} = \frac{j\pi k_o a}{2} (\epsilon_{rn} - 1) J_1(k_o a) H_o^{(2)}(k_o \rho_{mn}) \quad m \neq n \quad (4)$$

In this method, the electric field intensity is considered to be constant over the area of a cell, an approximation that results in significant error if the cells are not very small. Larger cells can be used if the variation of the electric field is included in the calculations. A method of approximating the variation of the electric field called "plane wave correction" is described in the next section.

III. PLANE WAVE CORRECTION

Variation of E_z is initially unknown, but we may make the approximation of representing the fields within each cell by a superposition of plane waves. All member plane waves are required to have propagation vectors of magnitude k corresponding to the frequency of the incident wave and local complex permittivity of the dielectric body. If α_i and B_i represent orientation of propagation and amplitude of the i th component, respectively, the superposition of plane waves may be written as:

$$E_z(r', \theta') = \sum_i B_i e^{-jkr' \cos(\theta' - \alpha_i)} \quad (5)$$

For small cell size we may expand the exponential in Eq. 5 to obtain the approximation

$$E_z(r', \theta') = \sum_i B_i \left[1 - jkr' \cos(\theta' - \alpha_i) - \frac{1}{2} k^2 r'^2 \cos^2(\theta' - \alpha_i) \right] \quad (6)$$

If complex permittivity is constant within a cell and the approximation of circular cells is used in Eq. 1, then the diagonal matrix elements are:

$$A_{mm} = 1 + \frac{jk_o^2 (\epsilon_{rm} - 1)}{4 E_z(0, \theta')} \int_0^a r' dr' \int_0^{2\pi} E_z(r', \theta') H_o^{(2)}(k_o r') d\theta' \quad (7)$$

From Eqs. 6 and 7, after performing the θ' integrations,

$$A_{mm} = 1 + \frac{jk_o^2 (\epsilon_{rm} - 1)}{4 \sum_i B_i} \int_0^a \left[\sum_i B_i \left(2\pi - \frac{\pi}{2} k^2 r'^2 \right) \right] H_o^{(2)} (k_o r') r' dr' \quad (8)$$

The summation in the integrand in Eq. 8 has a factor that is independent of the summation index and may be removed from the summation. Consequently, the diagonal matrix elements have no dependence on the unknown coefficients in the expansion, a fortunate occurrence indeed. Using a dummy variable in Eq. 8,

$$A_{mm} = 1 + \frac{j\pi}{2} (\epsilon_{rm} - 1) \int_0^{k_o a} H_o^{(2)}(x) x dx - \frac{j\pi}{8} (\epsilon_{rm} - 1) \epsilon_{rm} \int_0^{k_o a} H_o^{(2)}(x) x^3 dx \quad (9)$$

Performing the integrations over the Hankel functions gives for the diagonal elements:

$$A_{mm} = 1 + (\epsilon_{rm} - 1) \left[(\epsilon_{rm} + 1) + \frac{j\pi k_o a}{2} \left(1 - \frac{\epsilon_{rm}}{4} (k_o a)^2 \right) H_1^{(2)} (k_o a) \right. \\ \left. + \frac{j\pi}{4} \epsilon_{rm} (k_o a)^2 H_2^{(2)} (k_o a) \right] \quad (10)$$

In evaluating the off-diagonal matrix elements, suppose that the source point P' is in the n th cell and the observation point P is at the center of the m th cell, as shown in Fig. 1. Let s_{mn} and r' be distances from the center of the n th cell to the observation point and source point, respectively. If the angle between s_{mn} and r' is θ' , then the distance between the source point and observation point is

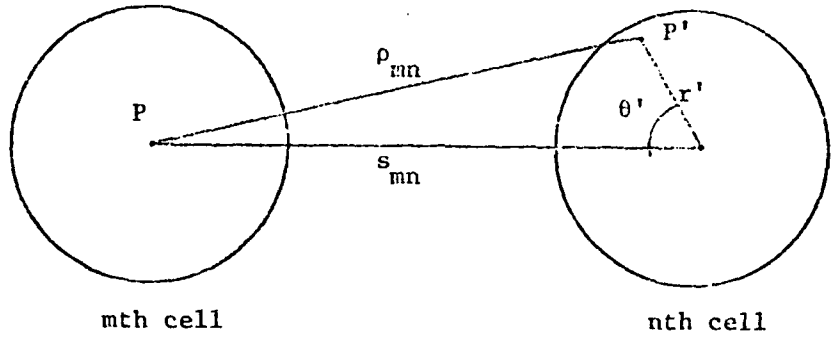


Fig. 1. Notation used in evaluation of off-diagonal matrix elements.

$$\rho_{mn} = \sqrt{r'^2 + s_{mn}^2 - 2r's_{mn} \cos \theta'} \quad (11)$$

If ϵ_r is constant within the nth cell and the approximation of circular cells is used in Eq. 1, then the off-diagonal matrix elements are:

$$A_{mn} = \frac{jk_o^2 (\epsilon_{rn} - 1)}{4 E_z(0,0')} \int_0^a r' dr' \int_0^{2\pi} E_z(r',\theta') H_o^{(2)}(k_o \rho_{mn}) d\theta' \quad (12)$$

From Graf's addition theorem,⁵

$$H_o^{(2)}(k_o \rho_{mn}) = \sum_{l=-\infty}^{\infty} H_l^{(2)}(k_o s_{mn}) J_l(k_o r') \cos l\theta' \quad (13)$$

From Eqs. 11, 12, and 13,

$$A_{mn} = \frac{jk_o^2 (\epsilon_{rn} - 1)}{4 E_z(0,0')} \sum_{l=-\infty}^{\infty} H_l^{(2)}(k_o s_{mn}) \int_0^a J_l(k_o r') r' dr' \int_0^{2\pi} E_z(r',\theta') \cos l\theta' d\theta' \quad (14)$$

From Eqs. 6 and 14,

$$A_{mn} = \frac{jk_o^2 (\epsilon_{rn} - 1) \sum_{l=-\infty}^{\infty} H_l^{(2)} (k_o s_{mn})}{4 \sum_i B_i} \int_0^a J_l (k_o r') r' dr' \\ \cdot \int_0^{2\pi} \sum_i B_i \left[1 - jkr' \cos(\theta' - \alpha_i) - \frac{1}{2} k^2 r'^2 \cos^2(\theta' - \alpha_i) \right] \cos l\theta' d\theta' \quad (15)$$

Performing the θ' integrations in Eq. 15,

$$A_{mn} = \frac{jk_o^2 (\epsilon_{rn} - 1) H_0^{(2)} (k_o s_{mn})}{4 \sum_i B_i} \int_0^a \left[\sum_i B_i 2\pi \right] J_0 (k_o r') r' dr' \\ - \frac{jk_o^2 (\epsilon_{rn} - 1) H_0^{(2)} (k_o s_{mn})}{4 \sum_i B_i} \int_0^a \left[\sum_i B_i \frac{\pi}{2} k^2 r'^2 \right] J_0 (k_o r') r' dr' \\ + \frac{2k_o^2 (\epsilon_{rn} - 1) H_1^{(2)} (k_o s_{mn})}{4 \sum_i B_i} \int_0^a \left[\sum_i B_i \pi kr' \cos \alpha_i \right] J_1 (k_o r') r' dr' \quad (16)$$

The summations in all three integrands of Eq. 16 contain factors independent of the summation index that may be removed from the summations. Also changing to a dummy variable,

$$A_{mn} = \frac{j\pi}{2} (\epsilon_{rn} - 1) H_0^{(2)} (k_o s_{mn}) \int_0^{k_o a} J_0(x) x dx$$

$$\begin{aligned}
& - j \frac{\pi}{8} (\epsilon_{rn} - 1) \epsilon_{rn} H_o^{(2)} (k_o s_{mn}) \int_0^{k_o a} J_o(x) x^3 dx \\
& + \frac{\pi}{2} (\epsilon_{rn} - 1) \sqrt{\epsilon_{rn}} H_1^{(2)} (k_o s_{mn}) \left[\frac{\sum_i B_i \cos \alpha_i}{\sum_i B_i} \right] \int_0^{k_o a} J_1(x) x^2 dx \quad (17)
\end{aligned}$$

Define

$$\gamma \equiv \frac{\sum_i B_i \cos \alpha_i}{\sum_i B_i} \quad (18)$$

Performing the integrations in Eq. 17 and using Eq. 18,

$$\begin{aligned}
A_{mn} &= \frac{j\pi}{2} (\epsilon_{rn} - 1) H_o^{(2)} (k_o s_{mn}) k_o a J_1(k_o a) \\
& + \frac{j\pi}{4} (\epsilon_{rn} - 1) \epsilon_{rn} H_o^{(2)} (k_o s_{mn}) (k_o a)^2 J_2 (k_o a) \\
& - \frac{j\pi}{8} (\epsilon_{rn} - 1) \epsilon_{rn} H_o^{(2)} (k_o s_{mn}) (k_o a)^3 J_1 (k_o a) \\
& + \frac{\pi}{2} (\epsilon_{rn} - 1) \sqrt{\epsilon_{rn}} \gamma H_1^{(2)} (k_o s_{mn}) (k_o a)^2 J_2 (k_o a) \quad (19)
\end{aligned}$$

Since only the last member in Eq. 19 is dependent on the unknown coefficients in the plane wave expansion, we wish to delete the term and use the first three members for the off-diagonal matrix elements:

$$A_{mn} = \frac{j\pi k_o a}{2} (\epsilon_{rn} - 1) H_o^{(2)}(k_o s_{mn}) \left[\left(1 - \frac{\epsilon_{rn}}{4} (k_o a)^2\right) J_1(k_o a) + \frac{\epsilon_{rn}}{2} k_o a J_2(k_o a) \right] \quad (20)$$

The use of Eq. 20 is justified only if the last member of Eq. 19 is small. Fractional error in A_{mn} due to neglecting the last member of Eq. 19 is:

$$\delta_{mn} = - \frac{j\gamma \sqrt{\epsilon_{rn}} H_1^{(2)}(k_o s_{mn}) k_o a J_2(k_o a)}{H_o^{(2)}(k_o s_{mn}) \left[\left(1 - \frac{\epsilon_{rn}}{4} (k_o a)^2\right) J_o(k_o a) + \frac{\epsilon_{rn}}{2} k_o a J_2(k_o a) \right]} \quad (21)$$

Since the magnitude of the ratio of the Hankel functions is greatest for small argument, we set $s_{mn} = \sqrt{\pi} a$ for adjacent cells.

Expanding the Bessel functions for small arguments gives:

$$|\gamma_{mn}| \leq \frac{|\sqrt{\epsilon_{rn}}| k_o a}{4\sqrt{\pi} \ln\left(\frac{2}{\Gamma\sqrt{\pi} k_o a}\right)} \quad (22)$$

where $\Gamma = e^\gamma \approx 1.78107$, with γ = Euler's constant.

In the plane wave correction method, Eqs. 10 and 20 are used for the matrix elements and the solution corresponds to the value of E_z at each cell center. Numerical considerations suggest that deletion of the last member in Eq. 19 is the primary source of error, so that it is possible to use Eq. 22 with the condition number of the matrix to give an error bound for the solution. Since no error bound is available in the method using pulse functions that is described in

Section II, the plane wave correction has the advantage of an expression for the error bound, in addition to improving convergence. A second method of approximating the variation of the electric field called "cylindrical-cell correction" is described in the next section.

IV. CYLINDRICAL-CELL CORRECTION

In the methods described in Sections II and III, the scattering body is divided into cells that are approximated by circular cylinders in calculation of the matrix elements. The method of cylindrical-cell correction, which is presented for the first time in this paper, emphasizes the properties of such a model of the original body.

Let the cross section of the scatterer be divided into square cells, each having side s . For the model, replace each cell with a circular cylinder having radius a , and assume properties of free space between the cylinders. For the chosen geometry⁶ the effective relative complex permittivity ϵ_{eff} of the model and the complex permittivity ϵ_r' of each cylinder are related by

$$\epsilon_{\text{eff}} = 1 + \frac{\pi a^2}{s^2} (\epsilon_r' - 1) \quad (23)$$

If we require that the effective relative complex permittivity of the model equal that of the original scatterer, then

$$\epsilon_r' = 1 + \frac{s^2}{\pi a^2} (\epsilon_{\text{eff}} - 1) \quad (24)$$

If the electrical size of the cylinders is sufficiently small, the inhomogeneities of the model will have no significant effect, so that scattering from the model satisfying Eq. 24 will duplicate that of the physical scatterer. The model is useful since we may approximate the variation of the electric field within each cylinder. A

circular cylinder with TM excitation will have internal fields given by

$$E_z = \sum_{n=0}^{\infty} b_n J_n(kr) \cos(n\theta + c_n) \quad (25)$$

where the b_n and c_n are determined by the excitation. If the cylinder is sufficiently small, the zero order term will dominate, so we may use the approximation

$$E_z = b_0 J_0(kr) \quad (26)$$

From Eqs. 7 and 26 the diagonal matrix elements are given by:

$$A_{mm} = 1 + \frac{jk_o^2 (\epsilon'_{rm} - 1)}{4} \int_0^a J_0(k'r') H_o^{(2)}(k_o r') r' dr' \int_0^{2\pi} d\theta' \quad (27)$$

where $k' \equiv \sqrt{\epsilon'_{r'}} k_o$.

Performing the θ' integration and using a relationship from Ref. 7 for the r' integration, we obtain the following expression used to calculate the diagonal matrix elements:

$$A_{mm} = \frac{j\pi}{2} \left[k' a J_1(k'a) H_o^{(2)}(k_o a) - k_o a J_0(k'a) H_1^{(2)}(k_o a) \right] \quad (28)$$

From Eqs. 12 and 26 the off-diagonal matrix elements are given by:

$$A_{mn} = \frac{jk_o^2 (\epsilon'_{rn} - 1)}{4} \int_0^a r' dr' \int_0^{2\pi} J_0(k'r') H_o^{(2)}(k_o r_{mn}) d\theta' \quad (29)$$

Using Graf's addition theorem⁵ and notation of Fig. 1:

$$A_{mn} = \frac{jk_o^2}{4} (\epsilon'_{rn} - 1) \sum_{\ell=-\infty}^{\infty} H_{\ell}^{(2)}(k_o s_{mn}) \int_0^a J_{\ell}(k_o r') J_o(k' r') r' dr' \int_0^{2\pi} \cos \ell \theta' d\theta' \quad (30)$$

Performing the θ' integration, which collapses the summation, we get

$$A_{mn} = \frac{j\pi}{2} k_o^2 (\epsilon'_{rn} - 1) H_o^{(2)}(k_o s_{mn}) \int_0^a J_o(k' r') J_o(k_o r') r' dr' \quad (31)$$

Using a relationship from Ref. 6 for the r' integration, we obtain the following expression used to calculate the off-diagonal matrix elements:

$$A_{mn} = \frac{j\pi}{2} H_o^{(2)}(k_o s_{mn}) [k' a J_1(k' a) J_o(k_o a) - k_o a J_o(k' a) J_1(k_o a)] \quad (32)$$

$$m \neq n$$

In the cylindrical-cell correction method, Eqs. 28 and 32 are used for the matrix elements and the solution corresponds to the value of E_z at each cell center. A solution is defined for any ratio of a/s , but only two cases have been studied:

$$\text{Tangent cylindrical cells: } a = \frac{s}{2} \quad \epsilon'_{r'} = 1 + \frac{4}{\pi} (\epsilon_r - 1)$$

$$\text{Overlapping cylindrical cells: } a = \frac{s}{\sqrt{\pi}} \quad \epsilon'_{r'} = \epsilon_r$$

For very large or very small values of a/s , the structure of the model

differs significantly from that of the scatterer so that the solution, which actually corresponds to scattering from the composite of circular cylinders, will differ from that for the desired scatterer. Advantages of the method will be seen in the example in Section VI.

V. CALCULATION OF POWER ABSORPTION

With both plane wave correction and cylindrical-cell correction, the solution corresponds to the value of E_z at each cell center. The plane wave correction leaves the variation of E_z within each cell undefined, but with cylindrical-cell correction Eq. 26 describes the approximate variation of E_z within each circular cylinder of the model.

If the value of power absorption is desired, then $1/2 \sigma E_z E_z^*$ may be computed within each cell using the values of E_z found using pulse functions or plane wave corrections. In this section the approximate variation of E_z within each cell is used for an improved expression for power absorption if cylindrical-cell correction is used.

Total power absorption in one circular cylinder is given by:

$$P = \int_0^a \int_0^{2\pi} \frac{1}{2} \sigma' E_z E_z^* r dr d\theta \quad (33)$$

From Eq. 24 the conductivity of the cylinder is related to that of the scatterer by

$$\sigma' = \frac{s^2}{\pi a^2} \sigma \quad (34)$$

Substituting Eqs. 26 and 34 in Eq. 33 gives:

$$P = \frac{s^2 \sigma}{a^2} b_o b_o^* \int_0^a J_0(k'r) J_0^*(k'r) r dr \quad (35)$$

Using a relationship from Ref. 6 for the r' integration:

$$P = \frac{s^2 \sigma b_o b_o^* \left[k'a J_0(k'^*a) J_1(k'a) - k'^*a J_0(k'a) J_1(k'^*a) \right]}{a^2 \left[(k')^2 - (k'^*)^2 \right]} \quad (36)$$

Then the average absorbed power density within the cell is given by:

$$P_d = \frac{\sigma b_o b_o^* \left[k'a J_0(k'^*a) J_1(k'a) - k'^*a J_0(k'a) J_1(k'^*a) \right]}{\left[(k'a)^2 - (k'^*a)^2 \right]} \quad (37)$$

Simplifying Eq. 37 we obtain the result

$$P_d = \frac{\sigma}{2} b_o b_o^* \left[\frac{\text{Im} \left[k'a J_0^*(k'a) J_1(k'a) \right]}{\text{Re}(k'a) \text{Im}(k'a)} \right] \quad (38)$$

where b_o is the calculated value of E_z found using cylindrical-cell correction.

VI. NUMERICAL EXAMPLE: THE INFINITE CYLINDER MODEL OF MAN

The infinite cylinder has been suggested for use as a model for body extremities or the chest cavity in evaluation of biological hazards from electromagnetic radiation.⁸ Approximation of an extremity or the whole body by an infinite cylinder may be made using the ratio of volume to length for the cross-sectional area.

The model considered in this example is an infinitely long cylinder with square cross section of 20 by 20 cm, having TM excitation by a plane wave incident perpendicular to one of the four congruent faces. The body is homogeneous with values of permittivity and conductivity that are typical for muscle, skin, and other tissues having high water content.⁹

The methods described in this paper have been used to calculate average specific absorbed power for the model. Suitability of the model can only be justified at high frequencies where end effects may be neglected, but calculations have been made over a wide range of frequencies to allow comparison of convergence with the different methods.

Figure 2 illustrates the frequency dependence of average specific absorption rate (SAR) for the model. The values obtained using the accepted method of pulse functions with 100 cells are the standard for comparison. Values obtained using pulse functions with 81 cells were found to differ from those with 100 cells by less than 1 percent for frequencies up to 200 MHz. Values found using 9 cells with pulse functions, plane wave correction, and cylindrical-cell

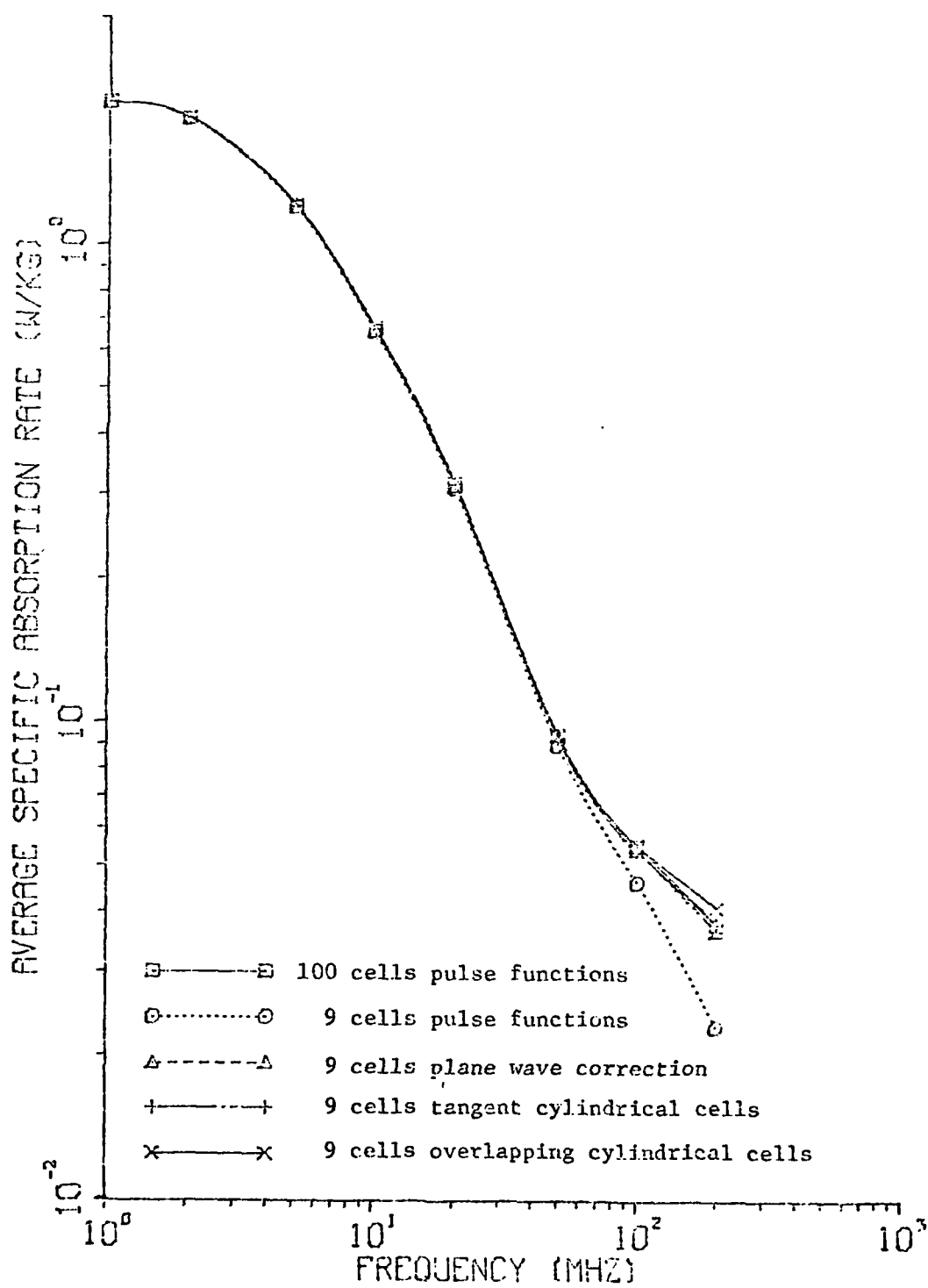


Fig. 2. Variation of average specific absorption rate with frequency for the infinite cylinder model of man.

correction with tangent and overlapping cells are also given in the figure. For 9 cells all four calculations are in good agreement with the standard at low frequencies, where the cells have small electrical size. Calculations with the new methods appear to have comparable accuracy and appear to offer a significant improvement in convergence when compared to pulse functions.

From Eq. 22, $|\delta_{mn}| \leq 3.3, 7.0, \text{ or } 18.1$ percent with 9 cells at 50, 100, or 200 MHz, respectively. Then significant error in the calculations with plane wave corrections is not predicted until the frequency is about 200 MHz, at which the curve deviates from the standard in Fig. 2. It appears that Eq. 22 is usable for determining maximum usable cell size for calculations at a given frequency.

VII. CONCLUSIONS

Two methods have been found which improve convergence in solution of the two-dimensional problem of TM excitation of an infinite cylinder of arbitrary cross section shape. The extension to the three-dimensional problem has not yet been completed.

Convergence is improved because the calculations include approximation for the variation of the field within each cell. The new methods give expressions for the matrix elements that are different from those found using pulse functions, but values of the matrix elements are in good agreement for electrically small cells.

The matrix elements found with the new methods do not require a substantial increase in computational effort. For a homogeneous scatterer, if equal size cells are used, the new methods require one time computation of several additional Bessel functions, but time for calculation of the matrix elements is dominated by recalculation of the zero-order Hankel function which is needed with or without the corrections made in the new methods. If the scatterer is not homogeneous or if different cell sizes are used, then time for calculation of each matrix element is approximately doubled in the new methods. Time spent in calculation of the matrix elements is proportional to N^2 , whereas time spent in solving the matrix equation is proportional to N^3 , so for large numbers of cells there is still no significant increase in computation time with the new methods.

REFERENCES

1. J. H. Richmond, "Scattering by a Dielectric Cylinder of Arbitrary Cross Section Shape", *IEEE Transactions on Antennas and Propagation*, Vol. AP-13, May 1965, pp. 334-341.
2. J. H. Richmond, "TE-Wave Scattering by a Dielectric Cylinder of Arbitrary Cross Section Shape", *IEEE Transactions on Antennas and Propagation*, Vol. AP-14, July 1966, pp. 460-464.
3. G. W. Hohmann, "Three-Dimensional Induced Polarization and Electromagnetic Modeling", *Geophysics*, Vol. 40, April 1975, pp. 309-324.
4. D. E. Livesay and K. M. Chen, "Electromagnetic Fields Induced Inside Arbitrarily Shaped Biological Bodies", *IEEE Transactions on Microwave Theory and Techniques*, Vol. MTT-22, December 1974, pp. 1273-1280.
5. M. Abramowitz and I. A. Stegun, Eds., *Handbook of Mathematical Functions*, National Bureau of Standards, 1964.
6. L. K. H. Van Beek, "Dielectric Behaviour of Heterogeneous Systems", *Progress in Dielectrics*, Vol. 7, 1967, pp. 69-114.
7. P. M. Morse and H. Feshbach, *Methods of Theoretical Physics*, McGraw-Hill, New York, 1953.
8. T. K. Wu and L. L. Tsai, "Numerical Analysis of Electromagnetic Fields in Biological Tissues", *Proceedings of the IEEE*, Vol. 62, August 1974, pp. 1167-1168.
9. C. C. Johnson and A. W. Guy, "Nonionizing Electromagnetic Wave Effects in Biological Materials and Systems", *Proceedings of the IEEE*, Vol. 60, June 1972, pp. 692-718.

APPENDIX G

Behavioral and thermal effects of microwave radiation at resonant and nonresonant wavelengths

J. A. D'Andrea, O. P. Gandhi

Departments of Electrical Engineering and Bioengineering, University of Utah, Salt Lake City, Utah 84112

J. L. Lords

Departments of Biology and Electrical Engineering, University of Utah, Salt Lake City, Utah 84112

Behavioral and thermal effects of radiating an animal with differing wavelengths of microwave energy at the same power density were investigated in the first of two studies. Five Long-Evans rats were trained to perform a lever-pressing task and were rewarded with food on a variable interval schedule of reinforcement. Rats were individually exposed in random order to 400-, 500-, 600-, and 700-MHz CW radiation at a power density of 20 mW/cm^2 with the long axis of the rat's body parallel to the vector of the electric field. Radiation at all wavelengths produced rises of body temperature and stoppage of lever pressing. The averaged rise in body temperature was greatest and work stoppage was most rapid during exposures at 600 MHz. In the second study, six rats were exposed in random order to 600-MHz CW radiation at power densities of 5, 7.5, 10, and 20 mW/cm^2 while performing the same behavioral task. Exposures at 10 and 20 mW/cm^2 resulted in work stoppage, while exposures at 5 and 7.5 mW/cm^2 did not. In addition, three of the rats were subsequently exposed while responding to 600-MHz pulsed radiation (1000 pps, 3- or $30\text{-}\mu\text{s}$ pulse durations at a peak power density of 170 mW/cm^2 (averaged 0.51 and 5.1 mW/cm^2). No work stoppage occurred to pulsed radiation. Taken in sum, the data show that the mature Long-Evans rat is resonant at a frequency near 600 MHz while work stoppage during short-term exposures to 600-MHz radiation occurs at a power density between 7.5 and 10 mW/cm^2 .

1. INTRODUCTION

Biological effects of microwave radiation have generated considerable interest in recent years. Much of this interest has focused on variables that control the amount of energy absorbed by the living animal. Recent investigations have shown that such variables as the animal's mass and geometry and the wavelength of radiation are potent determiners in production of differential absorption of microwave energy [Justesen and King, 1970; Gandhi, 1974; Githens *et al.*, 1975; Schrot and Hawkins, 1976; D'Andrea *et al.*, 1976]. The peak of a differential curve of microwave absorption has been termed resonance. A clear demonstration of resonance would require nonmonotonic rates of absorption across a range of frequencies, the maximum occurring, by definition, at the resonant frequency. Recently, D'Andrea *et al.* [1976] demonstrated an increasingly larger rise of body temperature and an increasing tendency for behavioral disruption to occur in animals as frequency of radiation was increased from 200 to 500 MHz. However, 500 MHz is below the resonant frequency of the rat. The present study is part of a program to delineate a predicted disruption of behavior at a frequency near 600 MHz, which approximates the resonant wavelength of the long axis of the mature rat.

2. METHOD AND MATERIALS

2.1. *Rationale.*

Eleven rats were trained to perform a lever-pressing task. The task was performed in a radiation chamber for

a reward -- a Noyes food pellet -- on a variable interval (30-second average) schedule of reinforcement. Over many sessions one group of five rats was exposed in random order to 400-, 500-, 600-, and 700-MHz CW radiation at a power density of 20 mW/cm^2 . In addition, the remaining rats were exposed in random order to 600-MHz CW radiation at 20, 10, 7.5, and 5 mW/cm^2 to determine latencies of work stoppage. Subsequently, three animals of this group were exposed to pulsed 600-MHz radiation at 3- and 30-microsecond pulse durations and 170 mW/cm^2 peak power density.

2.2. *Subjects.*

Eleven male Long-Evans rats were obtained from Simonsen of California and, at commencement of study, had body masses ranging from 420 to 450 grams. All of the rats had been partially deprived of food until their averaged body mass stabilized at 85 percent of that before deprivation. All of the rats were maintained at this level of Noyes 45-mg pellets and carefully metered supplemental feeding one hour after each session with Simonsen 4.5 rat chow. Each animal was housed separately in a 35 by 30 by 16 cm cage. Each rat was given free access to water in the home cage and was kept on a 12/12-hour light/dark cycle (on, 0700 hours; off, 1900 hours). Ambient temperature and relative humidity in the colony were maintained at $23 \pm 1^\circ\text{C}$ and 10 to 30% respectively. The averaged length from snout to base of tail of the animals was 19 cm.

2.3. *Apparatus.*

The microwave radiation chamber (Figure 1) consisted

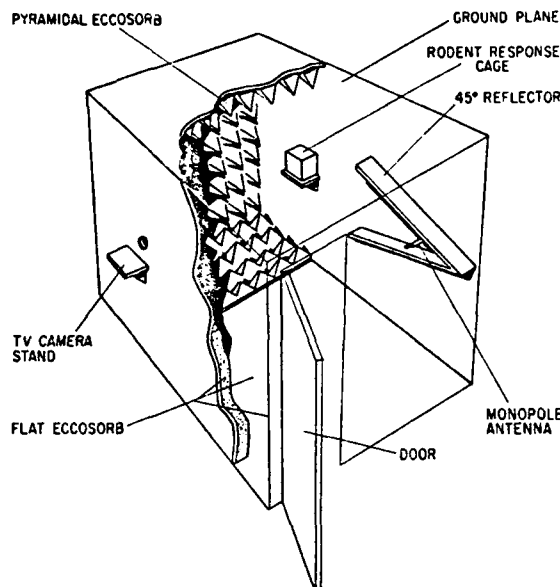


Fig. 1. Monopole-above-ground radiation chamber.

of a Filshield grounded Faraday cage (3 by 3 by 3 meters). The interior of the cage was partially lined with Eccosorb AN-79 material. One wall and one half of the floor and ceiling of the chamber opposite a radiating antenna were covered with Eccosorb VHP-18 pyramidal material. The remaining wall was covered by a 2-mm thick copper sheet to form a ground plane. A single brass monopole antenna (1/4 λ length, 1.2-cm diameter) was inserted through the copper sheet. A copper sheet (3 m by 0.5 m by 2 mm thick) was formed into a 45° reflector and was mounted on the copper wall 33 cm behind the antenna. An animal-response cage (Figure 2) that was constructed of Plexiglas was located 143 cm from the antenna. The cage was held on the vertical wall by a Styrofoam support that was constructed of 2.5-cm thick Styrofoam sheet.

The chamber was equipped with a 50-watt spotlight and a sensitive RCA television camera that was coupled to an external video monitor. A ventilation fan was mounted on top of the chamber and circulated air from the room through the chamber at a rate of approximately eight cubic meters per minute.

Since standard metallic caging and behavioral operanda cannot be used in a microwave field, an alternate system of monitoring and reinforcing lever-pressing behavior within the radiation chamber was devised. A plastic response cage (Figure 2) was constructed using two, 24 by 16 cm, 2-cm thick Plexiglas panels. The panels were joined at top and bottom by 32 rods (5-mm dia by 13.3-cm long) of Plexiglas equally spaced to form a grid floor and top. Two pieces of Plexiglas sheet (12.7 by 15.2 cm) were used, one as an end panel and one as a sliding guillotine door for the response cage. A plastic lever was mounted on a Plexiglas rod (5 mm by 13 cm) at one end of the cage. One end of the rod was

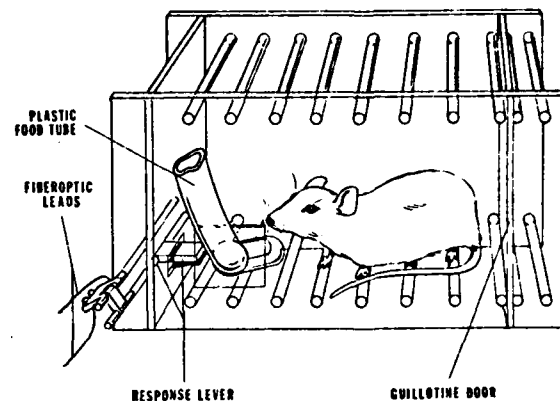


Fig. 2. Plastic cage in which a rat worked for food during exposure to sham or microwave radiation.

cemented to the cage, while the other end was free to move. Depression of the lever was detected remotely by its interruption of a beam of light that normally passed via Dupont Crofon fiber optic material to and from the plastic response cage. A sensitive photocell relay in conjunction with timing circuitry, digital printing counters, and cumulative-response recorders served to detect, to program and to record events of the experiments. A BRS/LVE pellet feeder was mounted outside the chamber. A Noyes food pellet (45 mg) was delivered, when programmed, to the response cage by a tube of flexible Tygon plastic (1.27 cm dia by 1.5 m length).

The microwave source used was an Epsco tunable signal generator (200 to 750 MHz) with a minimum power output of 100 watts. For the exposures to pulsed radiation, an MCL-1114 one-kilowatt linear amplifier (400 to 800 MHz) was used in conjunction with the Epsco source. A Hewlett-Packard No. 214A pulse generator was used to drive the signal source at 1000 pulses per second. Radiation frequency was monitored by a DANA 7580 frequency counter. A Sierra Philco 168B power meter was used to monitor the forward and reverse powers at the monopole antenna. A Weinschell double-stub tuner was used to match the signal source to an antenna (1/4 λ for each frequency used) and to reduce reflected power to a minimum. The power density of the microwave field within the plastic response cage in the radiation chamber at the position normally occupied by the rat was measured in mW/cm² by a General Microwave Corporation Raham Model 1 (300 to 18,000 MHz) probe. The probe was inserted into the radiation chamber from the top with the length of the probe perpendicular to the *E*-field vector and was remotely monitored outside of the radiation chamber before and after each exposure of a rat.

2.4. Procedure.

All rats were trained to press the lever for food pellets on a variable interval schedule of reinforcement. The clock time used for the schedule was three seconds, with a probability of 0.10 of delivery of a food pellet. With this arrangement a food pellet could be delivered at in-

tervals of three seconds or longer, the averaged time of delivery being 30 seconds. Each rat was scheduled daily for a one-hour session of lever pressing, until a stable rate of responding was achieved. Lever-pressing behavior was considered stable when the total number of lever presses during a session differed by less than 15% from the total of a previous session. On the average, approximately 14 sessions were required to achieve stable responding.

Once stable responding was observed the animals were randomly divided into two groups. Each of the animals of the first group ($n = 5$) was individually exposed in random order to 400-, 500-, 600-, and 700-MHz CW radiation at a power density of 20 mW/cm^2 while responding in the radiation chamber. Each of the animals of the second group ($n = 6$), also while responding in the radiation chamber, was individually exposed in random order to CW radiation at 600 MHz at 20, 10, 7.5, and 5 mW/cm^2 . In addition, three of the animals in the second group were subsequently exposed to 600-MHz pulsed radiation (1000 pulses per second at 3- and at 30- μs pulse durations; 170 mW/cm^2 peak power density, 0.51 and 5.10 mW/cm^2 averaged. The long axis of the rat's body in each exposure was parallel to the vector of the electric field.

Four to six retraining sessions were conducted for each rat after each exposure to microwaves to maintain stable rates of responding and to check for possible carry-over of behavioral effects from sessions of prior exposure. Exposures to microwaves began after the fifth minute of each session and were terminated at the end of the first one-minute period during which responding fell below one-third of the rat's normal rate of responding, as determined by data from the previous daily session. If a rat responded consistently throughout the session, as defined, irradiation was continuous for 55 minutes. The primary measure was time to work stoppage after onset of irradiation until the 60th second of the minute during which responding fell below the 33% criterion. Each rat was removed from the response cage and radiation chamber at stoppage of work or at session's end, whichever occurred first.

Measurements of colonic temperature were made with a BAT-8 digital electronic thermometer, first at the beginning of a radiation session and again at the time of work stoppage (or at session's end) to determine the amount of microwave-induced heating. Measurement of colonic temperature was also made before and after several training and retraining sessions on a random basis. Ambient temperature of the radiation chamber was controlled by room temperature (21° to 22°C) as monitored on the BAT-8 thermometer. Relative humidity of the radiation chamber and surrounding room was monitored by a Mason hygrometer during radiation sessions (27% mean, 2.7% SE). During all training and radiation sessions, each animal was monitored on the closed-circuit television.

3. RESULTS

Frequency of microwave radiation proved to be an important variable in heating of the rat and consequent

stoppage of work. For the rats exposed to 400-, 500-, 600-, and 700-MHz CW radiation at 20 mW/cm^2 , the most rapid stoppage of work (Figure 3) and the highest elevations of body temperature (Figure 4) occurred at 600 MHz. Averages of both the rise in temperature and the time to work stoppage reflect a nonmonotonic relation to frequency of radiation. In other words, the rate of absorption of energy increased as did the likelihood of behavioral disruption as frequency increased to 600 MHz and then declined at the highest frequency of 700 MHz.

Irrespective of frequency, animals exposed to radiation at 20 mW/cm^2 exhibited evidence of vasodilation, became immobilized, and were prone upon removal from the radiation chamber. The animals were clearly stressed by heat. However, as reported earlier [Justesen and King, 1970; D'Andrea *et al.*, 1976], the animals quickly regained an upright posture and mobility within minutes after removal from the radiation chamber. At the time of work stoppage, nearly all animals engaged in licking behavior, possibly to induce evaporative cooling, which continued after the animal was removed from the radiation chamber and was placed in its home cage.

A repeated-measures analysis of variance [Kirk, 1968] was used to evaluate the effects of the treatments. The analysis revealed a significant difference among the radiation frequencies with respect to time to work stoppage ($F = 16.41, df = 3/12, P < 0.01$). A Newman-Keuls test on the ordered means indicated a significant difference in times to work stoppage between 600 MHz and 500 MHz ($P < 0.05$), between 600 MHz and 700 MHz ($P < 0.05$), and between 400 MHz and all other frequencies ($P < 0.01$). The difference between exposures at 500 and 700 MHz was not significant ($P > 0.05$).

As an indicant of energy dosing, the rise of body temperature of the exposed animal was divided by the duration of exposure in minutes. Moderate rises of body temperatures were also observed during training sessions. These data are presented in Figure 4 with the

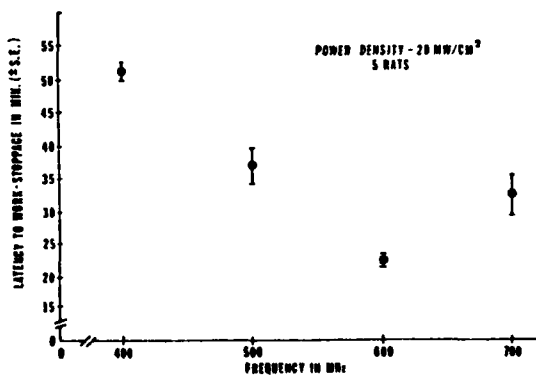


Fig. 3. Mean latencies (\pm SE) of time to work stoppage as a function of radiation frequency at 20 mW/cm^2 power density.

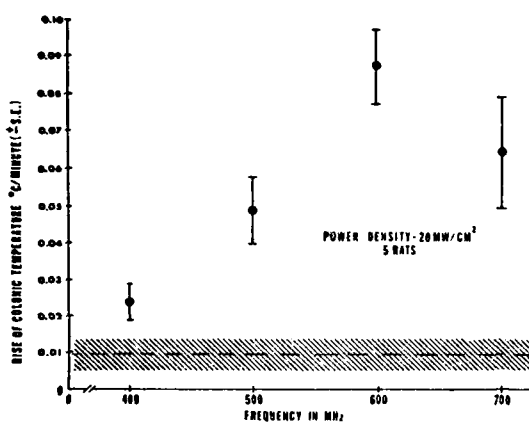


Fig. 4. Rise of colonic temperature (\pm SE) per unit of time as a function of frequency of radiation at 20-mW/cm² power density. Shaded area represents averaged increment of body temperature (\pm SE) of rats that responded during training sessions in the absence of radiation.

shaded area representing averaged increases of body temperature during training. A repeated-measures analysis of variance revealed significant differences across radiation frequencies with respect to heating ($F = 6.06, df = 3/12, P < 0.01$). A Newman-Keuls test of ordered means revealed significant differences of temperature increments for all possible comparisons ($P_s < 0.01$).

The measures of time to work stoppage and body heating followed each other very closely and, of course, inversely. As body temperature increased, time to work stoppage became shorter. The coefficient of the product-moment correlation between time to work stoppage and rise of body temperature for all radiation exposures is -0.78 (at $df = 18, P < 0.001$).

A comparison was made between the total of responses during a session before and that after exposure of the rats to radiation. This was done to determine if a session of radiation influenced the animals' responding during the subsequent session of retraining, as compared to responding during the training session prior to exposure. A repeated-measures factorial analysis of variance [Kirk, 1968] revealed no differences between the average of total responses for the session before and that after the exposure to radiation ($F = 0.01, df = 1/28, P > 0.05$).

A comparison was also made between the time to work stoppage for each rat as a function of the order in which treatments were given. This was done to determine if the order (which was putatively random) of the radiation sessions may have introduced an avoidance contingency, i.e., may have resulted in a rat's learning to stop working in order to avoid radiation. An analysis of variance [Kirk, 1968] revealed but chance differences between the variable of ordering and that of work-stoppage latency ($F = 0.30, df = 3/16, P > 0.05$).

For the rats exposed to 600-MHz CW radiation at

power densities of 20 and 10 mW/cm², stoppage of work invariably occurred. As shown in Figure 5, the averaged time to work stoppage and variability (i.e., magnitude of standard errors) both tended to increase as power density decreased. The earliest work stoppage was observed in animals exposed to radiation at 20 mW/cm². Exposures at 10 mW/cm² required nearly twice the averaged duration to reduce the animals' response rate to the work-stoppage criterion. Exposures to 5 and 7.5 mW/cm² produced little evidence of work stoppage. A repeated-measures analysis of variance [Kirk, 1968] was used to evaluate the work-stoppage variable as a function of power density. The analysis revealed a highly significant difference ($F = 35.29, df = 3/15, P < 0.01$). A Newman-Keuls test on the ordered means of time to work stoppage revealed a significant difference in time to work stoppage between 20 mW/cm² and all other exposures ($P_s < 0.01$), between 10 mW/cm² and 7.5 mW/cm² ($P < 0.05$), and between 10 mW/cm² and 5 mW/cm² ($P < 0.05$). There was little difference between exposures at 7.5 mW/cm² and 5 mW/cm² ($P > 0.05$).

The body heating induced by the exposures to 600-MHz radiation at different power densities (Figure 6) also followed a nearly monotonic function. The temperature differential was greatest at 20 mW/cm² and decreased by nearly one half at 10 mW/cm². Body temperatures at 5 and 7.5 mW/cm² were only slightly higher than those of baseline measures (shaded area, Figure 6). A repeated-measures analysis of variance revealed a significant difference in body temperature as a function of power density ($F = 5.89, df = 3/15, P < 0.01$). A Newman-Keuls test on the ordered means of body temperature revealed a significant difference in increase of body temperature as a function of power densities between 20 mW/cm² and lower power densities of ($P < 0.05$). All other comparisons were not significant. The coefficient of the product-moment correlation between times to work stoppage and temperatures across power densities is -0.83 (at $df = 22, P < 0.01$).

A comparison was again made between the total

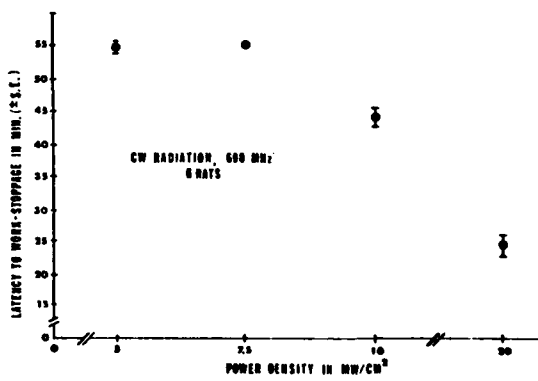


Fig. 5. Mean latency (\pm SE) of time to work stoppage as a function of power density at 600 mHz.

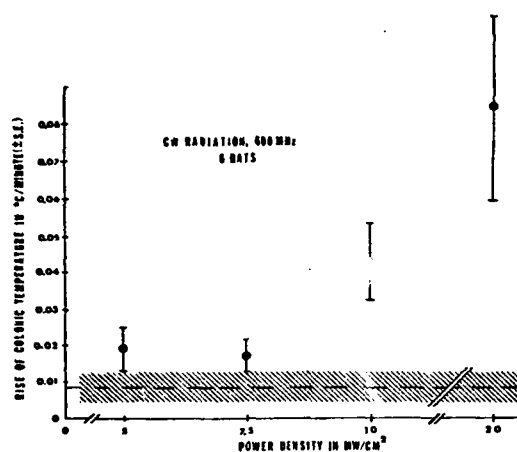


Fig. 6. Rise of colonic temperature (\pm SE) per unit of time as a function of power density. Frequency of radiation = 600 MHz. Shaded area represents average and increment of body temperatures, (\pm SE) of rats that responded during training sessions in the absence of radiation.

number of responses that were recorded during the session before and that after exposures to radiation to determine if a session of radiation influenced the animals' responding during subsequent retraining. A repeated-measures factorial analysis of variance [Kirk, 1968] revealed no differences between the average of total responses for a session before and that after the radiation sessions ($F = 0.07$, $df = 1/35$, $P > 0.05$).

There was no reliable effect of pulsed radiation (1000 pps, 170 mW/cm² peak power) on suppression of lever-pressing behavior at either 3- or 30-microsecond pulse durations. All three of the animals exposed under these conditions responded at near normal rates throughout the radiation session. One animal stopped responding near the end of a session of pulsed radiation at 3 microseconds. The data on body heating for these exposures, however, indicate but little elevation of body temperatures.

4. DISCUSSION

Our study was conducted, first, to investigate the contribution of radiation frequency on the rate of heating of the living, active rat and, second, to investigate the effects that such radiation may have in altering a well-trained behavior. Considering the four frequencies of radiation that were studied, our data indicate that 600 MHz approximates the resonant frequency of the adult rat with a body mass of 380-400 grams and averaged length (less the tail) of 19 to 20 cm for the long axis - and with this long axis oriented parallel to the vector of the electric field. The proximity to resonance is reflected both by the time to work stoppage and by measures of body heating, both of which yielded nonmonotonic functions. Our findings of resonance near 600 MHz are

in good agreement with previous work on the calculated resonant frequency of this animal [Gandhi, 1975; Johnson *et al.*, 1976]. It was of some interest to us that the tail of the rat did not seem to contribute to the factor of resonance.

Our use of the rise of colonic temperature (ΔT) in the behaving animal was only as an indicant of energy dosing. Not only will the intact mammal dissipate thermal energy, emotional reactions to the environment can produce psychogenic "fever" [cf. Justesen *et al.*, 1974 with Lu *et al.*, 1977]. We have previously observed (unpublished) that the active alert animal as compared with the anesthetized animal has a much higher body temperature. The indexing of absorbed microwave energy by body temperature, as described in this report, should only be construed, therefore, as a relative measure.

Radiation at a frequency of 600 MHz, given a 55-minute maximum period of radiation, produced disruption of lever-pressing behavior. As measured by the work-stoppage criterion, disruption occurred at power densities of 20 and 10 mW/cm². Disruption of behavior was not evident at lower power densities at 7.5 and 5 mW/cm². However, our data do not infirm the possibility that biological effects can occur at power densities below 10 mW/cm².

The use of pulsed energy, albeit at an averaged power density of 5 mW/cm², showed no reliable effect on time to work stoppage. This is not surprising since CW radiation at the same power density did not disrupt behavior. The "package" (dose) of energy per radiated pulse was about half that found by Guy *et al.* [1975] to be necessary for threshold stimulation of an acoustic response. Given full resonance, which may not have been observed by us, and given the use of higher peak values of power density than used by us, it is possible that behavioral disruption will occur to pulsed radiation at lower averaged power densities. Too, the greater sensitivity of other behavioral tests - such as conditional suppression - is much more likely to reveal effects of radiation at low power densities [King *et al.*, 1971].

As noted earlier [D'Andrea *et al.*, 1976], no reliable carry-over of behavioral effects was observed from one radiation session to the next. Visual observation of the animals during responding in subsequent retraining sessions did not indicate any attempts to escape from the response cage, as one might see with rats upon their return to an operant chamber where electric foot shock has previously been administered. The lack of carry-over suggests that the most reliable effect of the radiation was sufficient heating of the animal to suppress behavior but the radiation was not intense enough or of sufficient duration to produce noticeable physical damage.

Acknowledgment. We wish to thank Janice Hansen for her aid in completion of our experiments, and Doris Bartsch for her help in preparation of the manuscript. Our work was supported by U. S. Army Medical Research and Development Command, Washington, D. C., under contract DAMD 17-74-C-4092.

REFERENCES

D'Andrea, J. A., O. P. Gandhi, and R. P. Kesner (1976), Behavioral effects of resonant electromagnetic power absorption in rats, in *Biological Effects of Electromagnetic Waves, Selected Papers of the USNC/URSI Annual Meeting, Boulder, Colorado, October 20-23, 1975, Vol. I*, edited by C. C. Johnson and M. L. Shore, 257-273, *HEW Publ. (FDA) 77-8010*, U. S. Government Printing Office, Washington, D. C., 20402.

Gandhi, O. P. (1974), Polarization and frequency effects on whole animal absorption of RF energy, *Proc. IEEE*, 62(8), 1171-1175.

Gandhi, O. P. (1975), Conditions of strongest electromagnetic power deposition in man and animals, *IEEE Trans. Microwave Theory Tech.*, MTT-23(12), 1021-1029.

Githens, S. H., T. D. Hawkins, and J. Schrot (1975), Colonic temperature changes during microwave exposure (abstract only) *Technical Program Booklet, USNC/URSI Annual Meeting, October 20-23, 1975, Boulder, Colorado*, p. 232 (USNC/URSI National Academy of Sciences, Washington, D. C.).

Guy, A. W., C. K. Chou, J. C. Lin, and D. Christensen (1975), Microwave induced acoustic effects in mammalian auditory systems and physical materials, *Ann. N. Y. Acad. Sci.*, 247, 194-218.

Johnson, C. C., C. H. Durney, P. W. Barber, H. Massoudi, S. J. Allen, and J. C. Mitchell (1975), *Radiofrequency Radiation Dosimetry Handbook, Rep. SAM-TR-76-35*, pp. 100-101, Interim report under contract F41609-76-C-0025, USAF School of Aerospace Medicine, Brooks Air Force Base, Texas.

Justesen, D. R., and N. W. King (1970), Behavioral effects of low-level microwave irradiation in the closed space situation, in *Biological Effects and Health Implications of Microwave Radiation - Symposium Proceedings*, edited by S. F. Cleary, U. S. Public Health Service Publication No. BRH/DBE 70-2, Washington, D. C., pp. 154-179.

Justesen, D. R., D. M. Levinson, and L. R. Justesen (1974), Psychogenic stressors are potent mediators of the thermal response to microwave irradiation, in *Biologic Effects and Health Hazards of Microwave Radiation*, edited by P. Czerski, pp. 134-140, Polish Medical Publishers, Warsaw.

King, N. W., D. R. Justesen, and R. L. Clarke (1971), Behavioral sensitivity to microwave radiation, *Science*, 172, 398-401.

Kirk, R. E. (1968), *Experimental Design Procedures for the Behavioral Sciences*, Brooks Cole, California, 577 pp.

Lu, S.-T., N. Lebda, S. M. Michaelson, S. Pettit, and D. Rivera [1977], Thermal and endocrinological effects of protracted irradiation of rats by 2450-MHz microwaves, *Radio Sci.*, this issue.

Schrot, J., and T. D. Hawkins (1976), Interaction of microwave frequency and polarization with animal size, in *Biological Effects of Electromagnetic Waves, Selected Papers of the USNC/URSI Annual Meeting, Boulder, Colorado, October 20-23, 1975, Vol. II*, 184-192, edited by C. C. Johnson and M. L. Shore, *HEW Publ. (FDA) 77-8011*, U. S. Government Printing Office, Washington, D. C., 20402.

DISTRIBUTION LIST

USAMRDC (SGRD-RMS)
Fort Detrick
Frederick, MD 21701

Defense Technical Information Center (DTIC)
ATTN: DTIC-DDA
Cameron Station
Alexandria, VA 22314

DATE
ILME